FAULT DIAGNOSIS OF MECHANICAL SYSTEMS BASED ON ELECTRICAL SUPPLY CHARACTERISTICS

by

Mohamed. Issa. M. Assaeh

A thesis submitted to the University of Huddersfield in partial fulfilment of the requirements for the degree of Doctor of Philosophy

UK

(April 2019)

COPYRIGHT STATEMENT

ABSTRACT

Induction motors are the main workhorses of industry. Condition monitoring (CM) of motor based systems plays an important role in the early detection of possible defects, averting adverse operational and financial effects caused by unexpected breakdowns. Limited information has been found which explores the diagnostic abilities of voltage and motor current signals from motors with variable speed drives (VSDs), which are increasingly used in industry to obtain better dynamic response, higher efficiency and lower energy consumption. This study addresses the gap identified by carrying out a systematic review of the monitoring of mechanical systems using induction motors with sensorless VSDs. Specifically, existing techniques often prove ineffective for common internal and external faults that develop in Induction motors. The primary aim is to extract accurate diagnostic information from the power supply parameters of a VSD to monitor IM driven systems for early diagnosis of both mechanical and electrical faults. This thesis examines the effectiveness of both motor current and voltage signals using spectrum analysis for detecting broken rotor bar(s) and/or shaft misalignment and gear oil viscosity changes with different degrees of severities under sensorless control (close) modes. The results are obtained from common spectrum analysis applied to signals from a laboratory experimental setup operating under different speeds and loads. Evaluation of the results shows that the faults cause an increase in sideband amplitudes, which can be observed in both the current and voltage signals under the sensorless control mode. In addition, combined faults cause an additional increase in the sideband amplitudes and this increase can be observed in both the current and voltage signals. The voltage signals show greater change compared with the current signals because the VSD adapts the voltage supply source to compensate for changes in the system dynamics. Furthermore, this study also presents a model of an Induction motor fed by a variable speed drive (VSD), as an approach to simulate broken rotor bars and shaft misalignments to give an in-depth understanding of fault signatures. The model was validated with experimental results in both current and voltage signals, with good agreement. The model confirmed that BRB causes a shift and increase in the amplitudes of the sidebands with the amplitudes of the rotor frequency components increased due to shaft misalignment.

ACKNOWLEDGEMENTS

First and foremost, thanks to Allah Almighty who has enabled and given me the power to finish this piece of work.

I would like to thank Prof. Andrew Ball for his unwavering support, help and insights provided to me throughout the entire period of my research. Additionally, I am deeply indebted for his motivation, patience and skills which have greatly enriched my graduate experience.

I would also like to extend my gratitude to my co-supervisor, Dr. Fengshou Gu for his expertise, direction and encouragement accorded to me which has enabled me to complete my research and write this thesis successfully. Furthermore, through his understanding, kindness and patience I was able to develop strong theoretical frameworks in my thesis which have been presented in a logical and consistent manner. Dr Gu was also very instrumental in guiding my experimental work and ensured that it achieved the highest of standards, for this I am deeply indebted and words not convey my deepest appreciation and gratitude.

Special thanks also go to my colleagues as well as all staff members for their unwavering support, encouragement and time which has helped in my research being a success and has also helped me grow professionally and socially.

Lastly, many thanks and appreciation go to my wonderful family: my wife, children (Marbrouka, Issa, Abdulghaffar, Bissan) for their firm support. Their love and encouragement gave me strength and determination during my research and writing of this thesis, consequently, I dedicate this thesis to them. Moreover, I would like to extend my thanks to my mother and soul of my father as well as my sisters and brothers for their support and belief in me.

DEDICATION

"Allah will raise those who have believed among you and those who were given knowledge, by degrees, and Allah is aware of what you do" (Al-Mujadilah ayat 11)

- *I would like to dedicate this Doctoral thesis to my mother "Mabrouka" and soul of my father "Issa" my beloved wife "Fatmah", my dear sons "Issa, Abdulghaffar" and gorgeous daughters "Mabrouka, Bissan" for the ultimate and boundless love who have been an endless source of support, encouragement and love during the challenges of postgraduate study and life. I am truly thankful for having you all in my life.*
- *I dedicate this work to my dear sisters and brothers for an ultimate help and support since the early stages of my study.*
- *I will not forget to extend my sincere thanks to my family in law especially my brothers and sisters in law for their encouragement and support.*

TO ALL OF YOU I DEDICATE THIS DOCTORAL THESIS

LIST OF CONTENTS

LIST OF FIGURES

LIST OF TABLES

LIST OF ABBREVIATIONS

AC	Alternating Current
ACIM	Alternating Current Induction Motor
AE	Acoustic Emission
AIS	Artificial Intelligent System
BRB	Broken Rotor Bar
BL	Base Line
CBM	Condition Based Monitoring
CM	Condition Monitoring
CSI	Current Source Inverter
DAS	Data Acquisition System
DC	Direct Current
EMF	Electro-Motive Force
FFT	Fast Fourier Transforms
FLBC	Fuzzy Logic Based Control
FOC	Field Oriented Control
HOS	Higher Order Spectra
Hz	Hertz
IAS	Instantaneous Angular Speed
IGBT	Insulated Gate Bipolar Transistor
IMs	Induction Machines
kW	Kilo-Watt
Ls	Left Sideband

LRT	Locked Rotor Torque
MA	Shaft Misalignment
MBFD	Model Based Fault Detection
MCSA	Motor Current Signature Analysis
MVSA	Motor Voltage Signature Analysis
MMF	Magneto Motive Force
MRAS	Model Reference Adaptive System
MSB	Modulation Signal Bispectrum
PID	Proportional Integral Derivative Controller
PLC	Programmable Logic Controller
PM	Preventive Maintenance
PS	Power Spectrum
PWM	Pulse Width Modulation
RMS	Root Mean Square
RPM	Revolution Per minute
Rs	Right Sideband
SFOC	Sensorless Field Oriented Control
SL	Sensorless
TMD	Time Domain Analysis
SCADA	Supervision Control and Data Acquisition
VFD	Variable Frequency Drive
VSD	Variable Speed Drive
VSI	Voltage Source Inverter

LIST OF NOTATION

f_r	Rotor Frequency
f_s	Fundamental Supply Frequency
L_{ms}	Magnetising Inductance for a Stator Winding
n_r	Rotor speed
n_s	Synchronous Speed
p	Number of Pole Pairs
R_r	Resistance of Rotor Phase Winding
s	Motor Slip
μo	Permeability of Air=4π×10-7 H/m
θ_r	Angular Position of the Rotor with Respect to the Stator Reference
u_{sd}	The d Axis Stator Phase Voltage
u_{sq}	The q Axis Stator Phase Voltage
i_{sd}	The d Axis Stator Phase Current
i_{sq}	The q Axis Stator Phase Current
R_s	Stator Resistance
R_r	Rotor Resistance
ψ_s	Stator Flux
ψ_r	Rotor Flux
L_{ls}	Stator Leakage Inductance
L_{lr}	Rotor leakage Inductance
L_s	Stator Inductance
L_r	Rotor Inductance
L_a	Stator Leakage
L_b	Mutual Inductance

T_e	Electromagnetic Torque
T_l	Load Torque
J	Load and Motor Total Inertia
B_m	System Viscous Friction Coefficient
L_m	Motor Mutual Inductance
e_{ss}	Steady State Error
Subscripts d and q	Represent the d-q Reference Frame Coordinates
Subscripts α and β	Represent the Stationery Reference Frame Coordinates
ω_e, ω_s	Motor Synchronous (Electrical) Angular Frequency
ω_r, ω_m	Rotor Angular Mechanical Frequency
r_b	Represents the Rotor Bar Resistances,
$\Delta r_{ra,b,c}$	Represent Rotor Resistance Changes in Phase a, b and c
N_b	Number of total Rotor Bars
N_s	Equivalent Stator Winding Turns.
ω_M^*	Set point Speed (Reference)
ω_M	Feedback Speed (Estimated)
α_I	The Phase Angle between Voltage and Current
α_ψ	The Phase Angle between Stator Flux and Voltage
PID	Proportional, Integral, and Derivative Controller
n_{bb}	Number of broken rotor bars

Chapter 1 Introduction

In this chapter, a brief discussion and review of the basic condition monitoring technique of mechanical systems are provided. The motor current signature analysis technique is chosen as the method for facilitating the detection and diagnosis of faults associated with motors. Additionally, this chapter also provides a fully detailed explanation of the aims and objectives of the study, the layout of the thesis and the content.

1.1 Introduction

Condition monitoring and diagnosis is becoming a necessary practice to ensure safe and efficient operation of modern industries with very high levels of automation [1]. Particularly, the early detection of faults allows preventive maintenance actions to be taken in a timely manner to improve economical operation and avoid any unexpected breakdowns that can cause high economical losses and major disasters. Motors are the most common reason for breakdowns. Not only are there a large number of motors in an industrial process, motor's operation involves high speed, high temperature, high voltage and current processes that could cause various unpredicted failure modes and lead to severe consequences such as catching fire and electrical shocks.

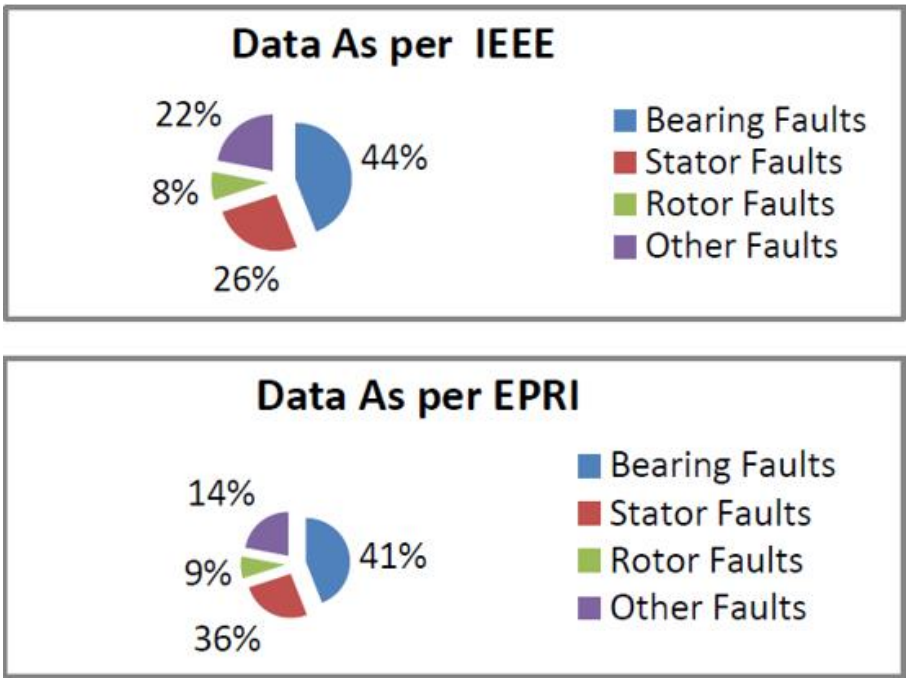

Figure 1-1 Percentage (%) component of AC induction motor failure(IEEE & EPRI)[2]

According to general construction, faults on induction machines can happen on rotors, stators and bearings which are regarded as the three main groups [3]. Approximately 30% and 40 % of failures of induction machine[4] are as a result of faults linked with bearing and stator in such machines. As demonstrated in Figure 1-1, the failures linked with rotors

comprise around 10% of failures of induction machines[4, 5]. However, the rotor assembly, consisting of both the rotor and bearings attribute to more than half of breakdowns.

As reported in Complete Plant Maintenance (CPM) Engineering Ltd. Only 1% of costs are attributable to the maintenance spend throughout the lifecycle of an electric motor. From information obtained from a recent document produced by the Motor Summit in Zurich, it is suggested that only 1% of the total lifecycle costs of an electric motor are attributable to maintenance and repair, 2% represents the initial purchase price and 97% of the cost is for energy to power the machine [6]

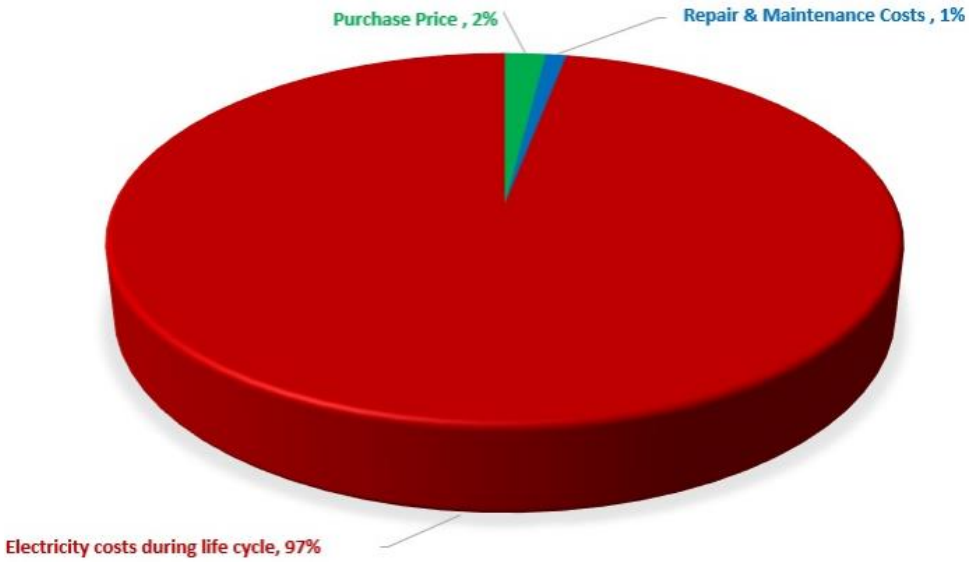

Figure 1-2 Lifetime costing in electrical machines[6].

It is estimated that the Global Electric Motor Market could reach $173 billion by 2024; with an annual CAGR compound growth rate of 5.7% from 2016 to 2024. An electric motor is a device driven by magnetic force which transforms electric into mechanical energy, this being one of the biggest advancements in the field of technology and engineering. This has attracted an era of research and new innovations being developed. Many types of motors have been developed from basic to more complex with features such as Stepper Motor and Linear Induction Motor (LIM) and many others which have been designed to accommodate the needs of the industry. Motors have a wide variety of

uses both in domestic and industrial settings, for example hairdryers, fridges, water pumps and fork lift trucks to name but a few. [7].

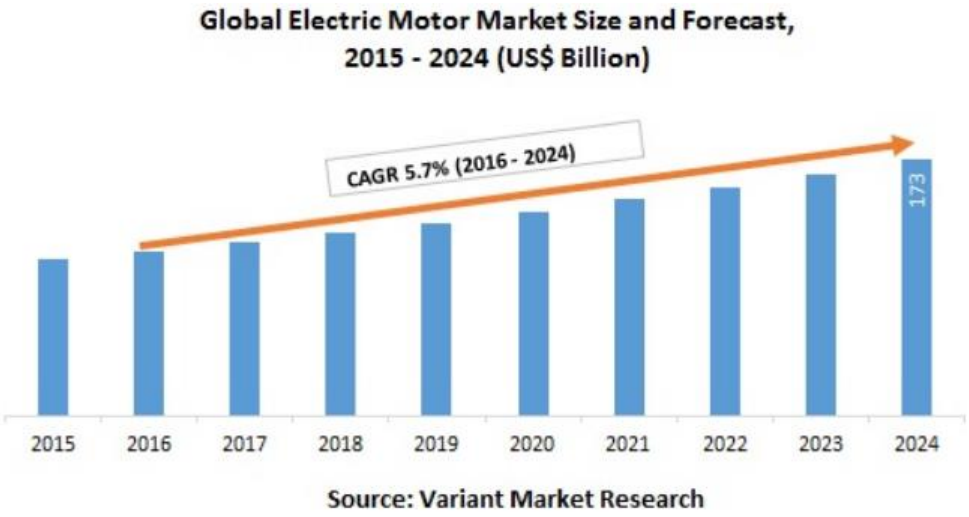

Figure 1-3 Market costing (US$ Billion) in electrical machines [7]

Given that condition monitoring covers a broad spectrum, a solid understanding of various aspects is key to succeed in this area and includes having thorough knowledge of construction of the machine to be monitored, comprehensively understanding how the monitored machines fail; signal analysis; and comprehensive presentation of such signals [8-10].

Many companies, especially those in energy management, view condition monitoring as being extremely important [11]. It is vital that the seamless operation of electrical equipment in power stations is achieved as any operational breakdown could be the source of accidents and financial loss for a company. As such, energy management companies have to devise ways to minimize downtime, avoid failures, reduce the cost of maintenance and prolong equipment service life. This can be effectively achieved using accurate and reliable condition monitoring.

Whilst time-based maintenance of equipment or machines be helpful, this can be viewed as being inefficient as the breakdown of machines often occur before their scheduled maintenance time or maintenance may be undertaken early when there is no need [12]. This can be avoided using condition-based maintenance or predictive maintenance [13].

Condition monitoring can be defined as the process where parameters or variables which are associated with certain performance characteristics of machines are monitored to facilitate the identification of changes that predict faulty conditions. These parameters include temperature, vibration and electrical supply. Condition based monitoring is a key element of predictive maintenance [14].

For many years, AC induction motor (ACIM) has gained a reputation for its wide use in both domestic and industrial applications. Since the end of the 19th Century it has been regarded as the workhorse of industry. Nikola Tesla put forward the idea of ACIM, a polyphase structure that consists of two stators that are orthogonally related [15]. ACIM has since undergone major modifications and now works on three phases which is more balanced with regard to voltages and currents [16].

The induction motor has been improved over time. Electrical motors today are significantly smaller and more compact than those of the early 1900's. Engineers can now make motors smaller and lighter whilst producing the same power output. However, some early motors are still in use today at historic factories and power plants. Through the course of development and invention of the cast aluminium squirrel-cage winding, improvements in magnetic steel and insulation, and the progressive reduction of the dimensions for a given horsepower rating, today a 100-hp motor has the same mounting dimensions as the 75-hp motor of 1897[15, 16].

As noted in the paragraph above, ACIMs are the most commonly used motors both in households and industries and this is associated with their simple and rugged design. Advantages of ACIM motors include low cost, low maintenance, high reliability, long lifespan, energy efficiency, and can be directly connected to AC power supply. In the market today, one can purchase different types of ACIM based on their use and field of application. Additionally, the ease of design of AC motors is higher than that of DC motors, but speed control of ACIM is more challenging as it requires a thorough understanding of the design and characteristics of ACIMs [17-20].

Despite the advantages that come with ACIMs, they can experience failure modes which are associated with failure of the various components of the motor such as the rotor,

bearings, and the stator. Other components that have a significant impact on the performance of the motor are coupling, gearboxes and the motor drive [21].

Given that ACIMs are very important and may be associated with high costs upon their failure, condition monitoring is needed for the early detection of faults and therefore prevent any unplanned breakdown and maximize the performance and service life of the ACIM whilst impacting positively on reliability[9, 17, 20, 22]. Without affecting production activities, the operating condition of ACIM can be monitored under open loop condition using Motor Current Signature Analysis technique(MCSA).

MCSA can be used to monitor operating conditions of both mechanical systems and electrical systems as there is an interaction between faults arising from these two types of faults.

1.2 Background and Motivation

The condition of machines has been monitored using a variety of methods and techniques. The approach or technique for monitoring the condition of a machine is limited by the kind of machine and the condition to be monitored. Types of monitoring techniques include MCSA, acoustic monitoring, vibration analysis (machinery vibration), performance monitoring, and temperature monitoring (thermal measurements). These are some of the most common monitoring techniques employed by industries in machine monitoring, with the aim of improving the reliability of condition monitoring systems and reduce the cost of implementation [23, 24].

A typical effective and efficient condition monitoring process is characterised by minimal data collection and instrumentation and with a perfect analytical and processing scheme that is not only fast, but also accurate. According to Seera. M (2014) [25] several studies and developers have attempted to achieve these requirements however further study is required to improve the accurate collection of this data. There continues to be further development required to identify issues.

In sensorless VSD driven systems, control systems constantly vary the supply parameters of the motors and change their value with the aim of maintaining the stable motor speed in reference to a set speed [26]. For example, mechanical faults may cause system oscillations, which are considered by the VSD as disturbances and alter the motor power

supply to compensate for the oscillation leading to the systems stability. The increase in the magnitude of the fault can lead to an increase in the power fed to the motor by the VSD, and this may result in catastrophic failure. Furthermore, sensorless VSDs have control systems that include regulators, state observers and estimators which make the diagnostic process more complex. Power supply characteristics such as current, voltage and frequency are manipulated by the drive to achieve speed adjustment for the induction motor, resulting in changes in the features that are key to fault detection and diagnosis. For this reason, techniques used for the detection of faults in open loop or line-fed ACIMs should be adjusted when used for closed loop VSDs. Consideration needs to be given to the nonlinearity of the machine model, uncertainties related to non-stationary signals, power estimation accuracy, and parameter tuning of regulators and observers in addition to controlling process actions [21, 27-29].

The field of condition monitoring and fault detection has been significantly impacted by the rapid development in technology and control systems, and as of today, advanced monitoring techniques have been developed for condition monitoring of complex systems. This advance has seen the development of advanced techniques meant for VSD driven systems to detect faults that may arise in an ACIM. One of these methods is the observer-based fault detection. In the last few years, observer-based fault detection has been widely researched and has shown effective results [28, 30].

Additionally, sensorless VSDs have control systems that include regulators, state observers, and estimators which make the diagnostic process of ACIMs more complex, unpredictable, and therefore requires one to take into consideration influences of drive controllers and estimators, nonlinearity of the machine model, uncertainties related to non-stationary signals, accuracy of the machine parameters, and observers and controller parameter tuning [31-33].

The majority of condition monitoring techniques studied and used are those that are well known including lubricant Analysis, acoustic, temperature, vibration, pressure and motor current signature analysis (MCSA). Additionally, conventional diagnostic and conditional monitoring technique needs additional devices for data acquisition,

processing and analysis. This additional requirement makes implementation of these conventional condition monitoring systems considerably more expensive [28, 34].

Other limitations include accessibility that presents challenges in the mounting of sensors and transducers, the location of the sensor, and the interference from environmental factors [35]. The availability of the VSD also means that conventional techniques may not work because the VSD masks the faults of the system by the producing a high level of noise through the regulators.

With this issue, it is necessary to conduct an exploration of supply parameters in a supply system having a closed-loop VSD to develop a fault detection and diagnosis system that is not only reliable but cost-effective [16]. For speed regulation, the terminal signals are passed through the drive regulators, therefore the drive systems, including the regulator's output and error signals, should provide information on the systems health [29, 35].

Currently, limited studies have been conducted on fault detection of the ACIMs driven by a sensorless VSD. Furthermore, the majority of existing studies have only looked into detection of faults that occur either outside or inside the motor having open-loop operations such as faults from the stator, rotor, bearing, lubrication oil or the shaft misalignment. Little research appears to have been conducted into the study of faults that occur inside or outside the motor, especially on the mechanical parts that are driven by the motor which is connected to a sensorless VSD by using the motor voltage signature analysis (MVSA) and motor current signature analysis(MCSA). Likewise, no former studies have been carried out to detect and diagnose the influence of BRB with shaft misalignment under a sensorless mode. This is something that needs to be researched further and the results of BRB shaft misalignment to be analysed

without the need for additional resource or complex calculation using the characteristic of current and voltage from a VSD by means of motor current signature analysis and motor voltage signature analysis. For this reason, this research is aimed at filling this gap through implementing both MCSA and MVSA to detect both electrical and/or mechanical faults in sensorless VSD based mechanical systems and develop accurate diagnostic information.

1.3 Research Scope

This study presents comparative outcomes among the performance of current and voltage spectra in detecting ACIM faults with various degrees of severity under sensorless modes. The results are gotten from common spectrum analysis applied to signals from a laboratory empirical setup operating under various loads and speeds. Experimental tests are undertaken based on a 4 kW and 15 kW transmission system to replicate real common faults with different degrees of severity; broken rotor bar, misalignment, and a combination of faults as well as gear oil viscosity changes with different degrees of severities and under sensorless mode. This study as well examines the influence of misalignment on the diagnosis of broken rotor bar faults under sensorless mode. It examines the effectiveness of conventional diagnostic features in both motor current and voltage signals analysis using power spectrum.

1.4 Aim and Objectives

1.4.1 Study Logical Aim

The aim of this research is to examine the detection and diagnosis of electrical and mechanical faults of mechanical systems based on electrical supply parameters from a VSD based system. The tasks were performed to facilitate this aim with different levels of severity and two different types of faults were used. For benchmarking and comparison purposes, the vibrational analysis was used in parallel with MCSA and MVSA.

1.4.2 Objectives of the Study

The objectives of this study were attentive to ACIM condition monitoring with a sensorless VSD system. The achievement of this research objective was facilitated by the following specific objectives:

Objective 1. To perform a study and literature review of condition monitoring in rotating machinery as well as performing a literature review of theory and application of condition

monitoring systems to electrical and mechanical machines using sensorless modes and identifying gaps in the knowledge.

Objective 2. To review the literature and explain the most common techniques utilized for condition monitoring of electrical and mechanical system under sensorless VSDs and speed control schemes, as well as describe the principles of ACIM and control systems, including field oriented control (FOC).

Objective 3. To describe the principles of motor faults, including electrical and mechanical faults and parameters under healthy and faulty conditions.

Objective 4. In this objective, experiments were designed and performed with the aim of testing the performance of a mechanical system, together with the control system, under healthy conditions for different applied loads and speeds, to facilitate the set up characteristics and baseline evaluation.

Objective 5. To allow the experiments to reproduce common mechanical and electrical faults with varying severities, under different load operating conditions and speed.

The ACIM faults were to include both mechanical and electrical under VSD, such as shaft misalignment and/or broken rotor bar and also to investigate the effects of gear lubrication oil viscosity.

Objective 6. To analyse the influence of an external fault on the diagnosis of an internal fault, and perform successful data analysis to investigate the possibility of detecting the examined faults under a VSD system without requiring more resources than normally needed when the advanced and complex analysis is undertaken. Conventional spectrum analysis will be applied to the dynamic data.

Objective 7. To develop mathematical models and simulations to help better understand the behaviour of the AC induction motor with sensorless VSD for healthy and faulty conditions, when operating under different speed and load conditions.

Objective 8. To perform an analysis of the response exhibited by sensorless VSD driven systems under varying fault conditions as well as perform an investigation on the capabilities of detecting and diagnosing faults under this mode of operation.

Objective 9. To implement experiments to replicate common mechanical faults in the gear transmission, based on different degrees of severities and under different operating conditions of speed and load.

Objective 10. To provide suggestions and recommendations for further research in this area of study.

1.5 Structure of Research

In this thesis, the researcher presents the topic of study and declares its objectives with the aim of fulfilling the research aims. The paper has eight main chapters.

Chapter 2: Literature review on condition monitoring and techniques used for detection of a fault in mechanical systems driven by ACIM and ACIM with VSDs is provided. Additionally, the main advantages of condition monitoring systems and the conventional fault detection techniques commonly used are provided. In the latter sections of the chapter, the researcher also reviews the techniques used for condition monitoring and why it is considered the best industrial application. In the final part of the chapter a description of both mechanical and electrical faults is given.

Chapter 3: In this chapter, the construction of ACIM is described in addition to their working principles, control system concepts and theory as well as ACIM control using sensorless VSD. The working principle of sensorless drives is also provided. Based on this theory, the researcher then presented the concept of field oriented control (FOC).

Chapter 4: In this chapter, the author presents an analysis of the various electrical and mechanical faults as well as reviewing the behaviour of the electrical parameter in ACIM under both healthy and faulty conditions. Additionally, the physical phenomena of faulty

ACIM with various faults such as stator faults, broken rotor bars, shaft misalignment and air-gap eccentricity motor bearing faults is also presented.

Chapter 5: In this chapter, the researcher uses Simulink/MATLAB to present a mathematical model of the ACIM in the d-q domain and the orientation of a VSD. Ready to use models available in the Simulink library are used for the creation of the model after modification to suit the test rig ACIM. A description of the three-phase ACIM model is first provided followed by an introduction of FOC modelling equations. Additionally, an investigation is also made into the impacts of load oscillations on sensorless VSD response characteristics. An analysis of the FOC scheme results is provided and validated with the rig data.

Chapter 6: The general specifications of the test rig facility used in this study is provided in this chapter. The specifications include control systems, mechanical systems, and the faults (electrical and mechanical) used in the study of the electrical signals of the induction motor. Additionally, the instrumentation systems, equipment and sensors used in the acquisition of data are also provided. Furthermore, repeatability checks are performed for the various signals.

Chapter 7: Experimental results are presented in this chapter. The results are used for electrical and mechanical signal identification and analysis. The influence of a broken rotor and three degrees of severity on the electric supply parameters on sensorless VSD is performed. This is followed by an examination on the influence of shaft misalignments with three degrees of severities on supply power parameters under a sensorless VSD associated with the mechanical fluctuations. Also, under a sensorless mode of operation together with MA and BRB, the response of the system is provided and analysed.

Chapter 8: A study on oils with different viscosities using electrical supply analysis is provided in this chapter. The impact of the faults due to lubricants is provided as well as test rig facility and operations. Lastly, different feature frequencies due to their dynamic features are used to investigate the results for all the cases under test.

Chapter 9: The achievements of the research work are summarized in this chapter in addition to explaining the way in which the research objectives stated in section 1.4.2 were achieved. The key conclusion of the study is provided. The key contributions of the author to the topic of study are also summarised, in addition to describing the novel concepts put forward by this research. A conclusion on condition monitoring of ACIM using motor current signature analysis under sensorless operational mode is also provided. Recommendations of further investigation required on future studies is also presented. Figure 1-1 illustration flowchart of research work.

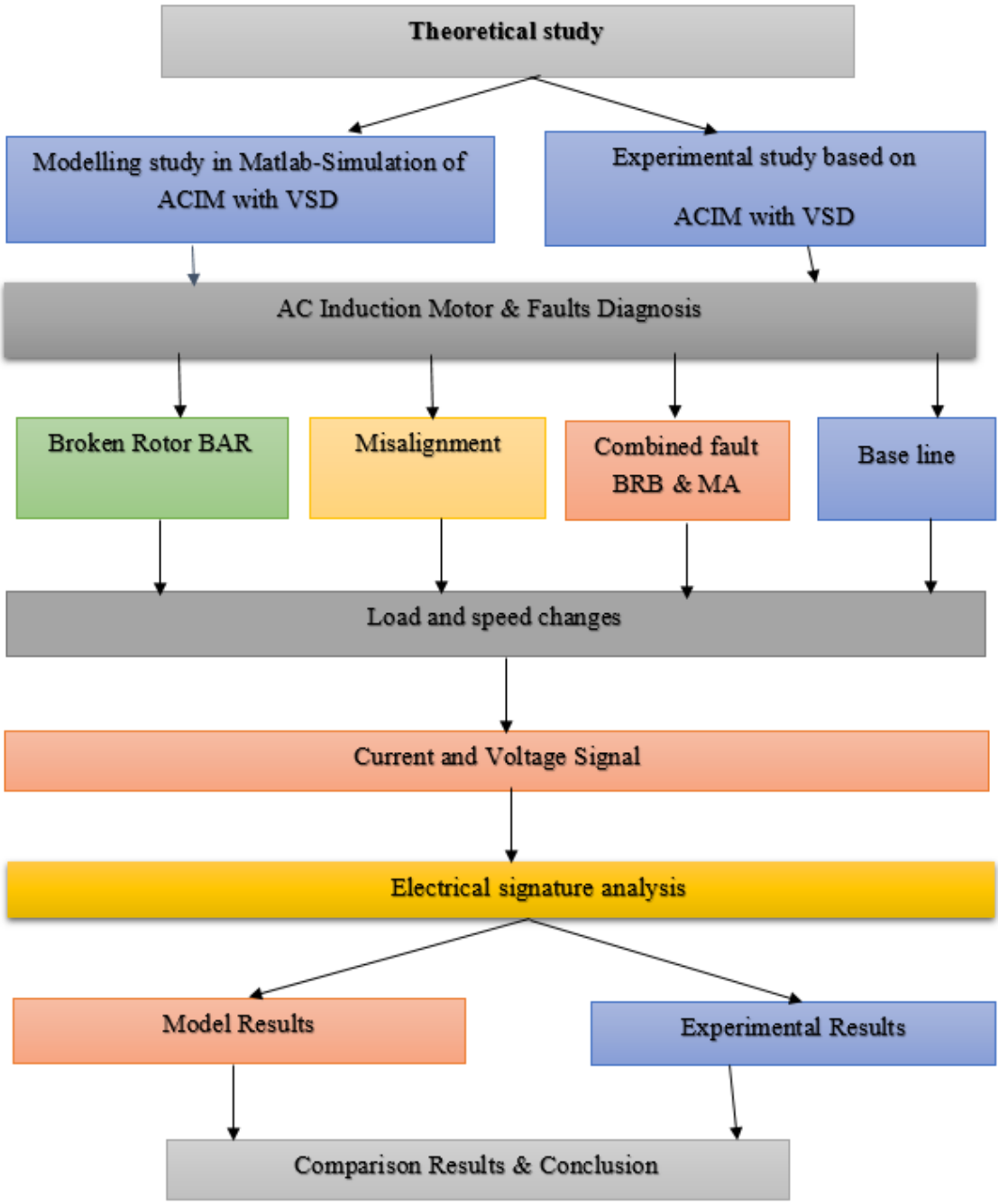

Figure 1-4 The flowchart of research context

Chapter 2 Literature Review

This chapter overviews previous studies on maintenance procedures within current and industrial fault detection and condition tracking methods used for mechanical and electrical systems that use ACIM drives. It features a recap of the key benefits of using the condition tracking system and outlines the common conventionally applied schemes. Condition tracking method and the rationale for its selection as the most ideal within industrial use is also reviewed. Finally, a description of mechanical and electrical faults is presented.

2.1 Introduction

One major economic benefit within the industrial field pertains to effectively maintaining mechanical and electrical systems. Schedules of maintenance for long and medium term can be considered an effective operation for many types of machinery and plants; there are various factors influencing maintenance schedules, such as investment, production continuity and effective operation of the plant. A strategy for effective maintenance can play a crucial role in protecting any machine malfunction through diagnosis and detection of machine faults and timely prediction of failure[31].

2.1.1 Condition-Based Maintenance (CBM)

Condition-Based Maintenance (CBM) could be considered a manufacturing on-line tracking system where the key concern is operational security. CBM would reduce the breakdown of machines through anticipation of a breakdown, locating components of machine faults and machine condition approximation. The data is gathered accurately from tracked parameters including process parameters, vibration, temperature, voltage, and current. CBM allows maintenance employees to attain the required corrective measures at the appropriate time prior to the occurrence of a failure. Besides, online tracking of machines could be undertaken when the machine is operational; this not only reduces lost time of the machine but also utilises employees' time efficiently through the timely arrangement of spare parts, thus enabling maintenance to be undertaken at the appropriate time. All the aforementioned constitute essential factors in decreasing the costs of lost production [36, 37].

2.1.2 Fault Diagnosis and Condition Monitoring in Machines

Notably, condition monitoring refers to the consistent equipment and plant condition assessment in its entire serviceable life. The creation of CM is intended for assessment of the physical properties which differentiate the existing conditions of the machine and employ such measures to recognize and anticipate possible deficiencies. Nevertheless, CM might be tested to incorporate protection, but its main important capacity should regularly distinguish any changes in machine behaviour and anticipate drawbacks in the

initial stages. Such process would generate a progressive caution, which can be used for perceiving the need for maintenance in the initial phase and gives support specialists sufficient time to schedule repairs accordingly, thus leading to less downtime and reduced costs [21, 23, 38]. CM is capable of identifying and tracking any major changes that express an emerging fault for reduction of cost over-runs, avoidance of consequences, and prevention of failure.

2.1.3 Condition Tracking Benefits

The key objectives and benefits of CM within industrial machinery pertain to prompt anticipation of machine failure. These benefits include [25]:

- Maximizing machine productivity
- Improving the performance of machines
- Decreasing spare part inventory and improving repair time
- Improving manufacturing effectiveness and enhancing the safety of the product
- Increasing the equipment and operators' safety
- Safely expanding overhaul intervals
- Improving the quality of products
- Reducing the quantity of repairs, inspections and checking
- Decreasing overall maintenance costs and production costs
- Minimizing unscheduled downtime and unplanned breakdown
- Ensuring longer periods of operation, safely extending overhaul durations, and increasing machine productivity

A CM system should be able to offer accurate data regarding the machines, anticipating the need for maintenance before breakdown, failure, or severe damage. It would be undertaken through the incorporation of fault diagnosis, identification and detection with the estimated lifespan of the machine [21, 25]. Notably, specialists could conduct a condition monitoring system interpretation and analysis offline; additionally, advanced skills and technologies could be used for performing online CM system interpretation and analysis [39].

2.2 Condition Monitoring of Induction Machine

Traditional condition methods are complex and have been utilised for tracking the machine conditions; however, they are characterised by merits and demerits [40]. The techniques include Electrical Signature Analysis (ESA), lubricant analysis, thermal measurements (temperature monitoring), ultrasound function, acoustic emission method, vibration analysis, aural and visual inspections, all of which constitute current signature analysis (MCSA). Choosing the ideal CM method depends mainly on the support maintenance targets, elements under observation, cost, machine, and process. For example, visual investigation could be enough for exploring the machine's validity when it is almost failing; however, in contrast, progressive condition monitoring approaches should be attained for a more complex and advanced course of action. Nevertheless, both monitoring targets and expenses are considered while choosing the condition monitoring technique [31] In contrast, advanced condition monitoring methods should be conducted as a more complex and sophisticated course of action. Monitoring targets and costs are considered while choosing the CM method. A brief description of the Condition Monitoring Techniques are as follows [25, 41].

2.3 Condition Monitoring Techniques

2.3.1 Aural and Visual Inspections

Visual inspection constitutes the main evaluation and examination process of components within the systems. The process of inspection must be used by experts with extensive skills or knowledge within a system. Visual inspection constitutes the most widely utilised CM method. The process could be undertaken using actions including twisting, shaking, smelling, and looking [42]. IA visual investigation assessment can detect possible changes in appearance, damage, and degradation. Visual inspection offers immediate data regarding the machine's condition validity. To get more reliable and accurate outcomes, inspections might be complemented using hand-held equipment such as infrared detectors and stroboscopes, simple tools, and instrumentation [10, 43].

Nevertheless, the major limitation with the technique pertains to its insufficiency and its irrelevancy in the initial phases of detecting a fault [44].

The main demerit of visual inspection involves [42, 43]: individual base testing, different inspectors or persons that check machines could produce different reports or notes for one machine because of people's varying knowledge, background and skills. Additionally, the technique is restricted to apparent components and parts [41].

2.3.2 Temperature Monitoring (Thermal Measurements)

The temperature measurement or thermal monitoring method is conducted using thermal sensors within specified sites including bearings, drive winding, and stator; the method is ideal for locating electrical and mechanical faults. Thermal monitoring effectively shows the system changes. Additionally, the efficiency of thermal monitoring depends on the site of the fitted sensor. For example, vibration measurements and temperature of bearings are traditionally measured as a single unit to offer a standardised mechanism that could be utilised for approximating the condition of the machine [21]. The thermal measurement effect on the parameters of machines is cited by [21], and [45]. Nevertheless, the measurement of temperature also constitutes the main setback in ascertaining the difference between the sensor point of temperature, which can be measured easily but only yields local data, and the entire thermal measurement that is complex and is at risk of interference from local information. Moreover, the technique controls vital and active parts' temperature such as rotor winding and core parts [21, 28, 45]. This form of measurement is undertaken with various thermal sensor types including thermal cameras, thermometers, and thermocouples [10, 41].

2.3.3 Acoustic Emission Monitoring

In previous years the focus of research has been on employing acoustic emissions (AE) for CM. Acoustic emission emanates from damages within the mechanical components of an oscillating machine.

Detection of acoustic emissions could be undertaken when the acoustic signal's spectrum frequency or amplitude is altered [46]. The identification of acoustic emissions could be

made based on frequencies ranging between 20kHz and 1MHz and have been found in frequencies of 100MHz. Acoustic emission constitutes an efficient mechanism for monitoring motors, tools, bearings, and gearboxes. Additionally, even though the acoustics are triggered at Nano and micro levels, the energy released ranges between 1 kHz and 1 MHz

Rapid stress-emitting events produce stress wave spectrums from 0Hz and fluctuating at different MHz [47]. Nevertheless, the major limitation of acoustic emission monitoring is that the ratio of noise to signal is negligible, and general noise level increases with time, thus making comprehension of the signal complex. Moreover, effects include noise emanating from other sources of sound including reflecting surfaces, driving motor, loading generator and cooling fan [48].

2.3.4 Lubricant Analysis

One common and predictive maintenance technology for oscillating machine currently being used is the lubrication oil for additive elements, contaminants, and worn metals. Lubricating oil directly affects the overall machine lifespan, emission, efficiency, performance, and operation. In view of this, the monitoring of lubricating oil assists in maintaining the health of the machine through the prediction of machine conditions as well as taking precautionary measures to avert catastrophic failures [49]. The lubricant provides insightful data from the internal towards the external of functioning machines in the form of changed viscosity, chemical contaminants, and wear particles. The equipment condition is determined through wear-particle analysis on the basis of the lubricant's wear particles. The condition of oil is restricted to the lubricating systems' circulating oil. While other analysis could be conducted on grease lubricants, debris detection analysis can be used on oscillating equipment including turbines, bearings and gearboxes to track oil parameters that include moisture content and viscosity, wear and tear and level of oil. Such parameters are measured through oil analysis and measurement of the engine lubricant's electrical, optical, chemical, and physical-mechanical properties, and can offer detailed information concerning the condition of the machine under measurement. It is possible to identify faults earlier prior to the occurrence of catastrophic

failure through the acquisition of accurate information from the wreckage formed within the lubricating oil [28, 50].

2.3.5 Vibration Monitoring

Vibration monitoring constitutes one commonly and extensively utilised method to specific CM and it is used for detecting faults within oscillating machines.

Vibration method constitutes a powerful method which could be used for condition monitoring of many industrial types of machinery, including incorrect eccentric clearance shafts, misaligned component bearing, and gearboxes [47]. During the operation of the machine, it produces motion and forces, which produce structural vibrations that are transferred from one machine part to another. The oscillating machine's vibration signal carries the fault signature within the machinethus early detection of faults could be actualised by assessing vibration signals with different methods of processing signals. It offers insightful information concerning the condition of the parts within the machine –oriented chain [21, 51]. A baseline for levels of machine vibration is obtained to ascertain the condition of the machine in order to contrast the present level of vibration with a previous vibration baseline. Many methods for processing and analysing signals that demonstrate efficiency at identifying issues within any equipment and components have become sophisticated [21]. Numerous vibration-based methods including cepstrum analysis, joint frequency-time domain analysis, also frequency and time domain analysis exists [52].

Additionally, vibration-based methods can be considered redundant or lack the diagnostic ability to detect faults in the initial phases [21].

Challenges have emerged from several causes that include advanced signal processing, which is needed for acquisition of accurate information, transducer locations or sensor, transfer function impact between transducers and vibration sources, presence of dynamic phenomena, and the presence of different types of vibration as well as sources of noise [31, 53, 54] Due to such demerits characterising the vibration tracking method, it is not an ideal method of choice.

2.3.6 Electrical Signature Analysis (ESA)

Many CM methods including oil, thermal analysis, acoustic monitoring, and vibration monitoring are expensive and require special tools [31, 41]. The high costs of implementing and operating such methods are often limited to use within critical machines in the manufacturing factory. Whilst voltage and current tracking do not need extra gadgets due to the main electrical volume with system plants including both voltage and current, this can be more easily measured by present voltage and current transformers which are often fitted as the main part of protection systems [55].

Therefore, ESA constitutes a method for assessing the condition of transformers, generators, and motors among other electrical equipment. The technology could offer assessment for functioning electrical equipment and could locate several mechanical and electrical issues. To overcome issues associated with traditional fault detection techniques, MVSA and MCSA are suggested for detecting different induction motor issues. The measurement of electrical signals is usually undertaken for purposes of control, thus eliminating the need for more measurements [56].

As illustrated in [57, 58] extensive research in the past few years that explore the CM for induction motor drives over many approaches has existed. Studies [59-61] have shown that faults emerging within downstream-based equipment could be identified using the changes within the induction motor's current signal. Extensive research examines the CM methods sophistication for driven physical-mechanical systems and induction motors. For instance, [62-65], which offer a thorough overview on analysis and detection schemes of faults and methods of signal processing, as well as the ideal method that is proposed for different faults, which often occur within induction driven motor systems. They are based mainly on the assessment of induction motor supply measurement and analyses.

There is extensive published literature examining some methods of motor current signature analysis. A review of the studies was undertaken with many revealing viable preferences for electrical signal analysis methods. Furthermore, investigators have found that electrical supply signals of induction motors possess considerable information and parts associated with the condition of driven physical-mechanical equipment including

conveyors, pumps, mixers and gearboxes. In particular, the component of rotation frequency within induction motor could be detected using electrical signal spectra that use electrical supply signal for detection of fault characteristics such as those of gearboxes, bearing and shaft misalignments [60, 66]. For purposes of simplicity, the MCSA method has many benefits compared to other monitoring methods. MCSA is premised on the notion that torsional vibration within the system will influence the current signal's frequency spectra [67].

The main benefit of MCSA, unlike other CM methods, is that it constitutes a strong method with the capacity of monitoring non-intrusive and remotely located faults, and can be used in ordinary and hostile settings. Additionally, MSCA is not impacted by current transducer and location, it can be considered an active and safe tool for induction motor monitoring. Furthermore, the method is inexpensive and simple, therefore convenient and cost-effective.

Different analysis techniques and approaches are suggested for extraction of fault features and frequency components. For example, in 2015, Ahmed Alwodai [61] examined studies that have utilised the induction motor current bi-spectrum analysis to detect and diagnose motor bearing and rotor bar fault. In the study, the outcome revealed that diagnostic results for broken rotor bar are affected by supply frequency amplitude implying the sensitivity of the outcomes to the load conditions. The results revealed that faults of motor bearings trigger tiny modulations to components of current supply with significant levels of noise, thus using modulation signal bi-spectrum could address such concerns enabling the detection of motor bearing faults.

Mohamed Benbouzid et al. (1999, 2000) [56, 68] investigated several sophisticated analysis methods on the motor current signal for the detection of various induction motor faults. Tested faults included the eccentricity of supply voltage imbalance, bearings failure and broken rotor bars. Nevertheless, there is a need for a high resolution analysis to obtain clear and pure information from the signal of the stator current.

Research has revealed that the MCSA could be utilised for detecting downstream equipment including a gear transmission system. In (2012) Haram et al. [69] examined

the measured current signals from ACIM, identifying faults within the mechanical gear transmission system through a novel modulation signal bi-spectrum technique(MSB). By using this technique gear faults and shaft misalignment were identified.

Kar, C. and A Mohanty (2006) [70] proposed that the traditional vibration monitoring technique for mechanical transmission systems could be substituted through motor current analysis. The sophisticated technique has been subjected to tests on multi-phase gearbox transmission systems. The current signal was decomposed using a discrete wavelet transform (DWT), and the extraction of sidebands under high frequencies was undertaken through Fast Fourier transform analysis. The outcomes indicate that MCSA with DWT could be utilised by substituting the traditional vibration monitoring technique.

Zhang et al. (2015) in [71] have asserted that current measurement properties could be utilised for detecting faults in planetary gearboxes. The proposed method analyses the spectra sites around the frequency of resonance within the motor current signals for extraction of feature components linked to faults of planetary gearboxes.

In conclusion, MCSA has attracted significant attention in many recent studies. However, it remains pertinent and considerable work is required to examine the suggested methods and test whether their applicability is relevant for actual applications. Moreover, future research is necessary to acquire suitable information, decrease or eliminate noise from the resultant current signal using simple calculations and fewer resources. Furthermore, a large portion of the reviewed literature used and focused upon directly fed induction motor or open loop controller mode [41].

The motor will not work with its specified performance when there are any faults occurring in the system. However, as the interested faults are very small and cannot easily be seen by the drive the intention is to detect very small and developing faults in the early stages to prevent further detrimental consequences.

It is worth noting that when the fault is small, the drive regulator actions and the noise from the PWM switches masks the fault features in the current signal, making it difficult to detect them. Meanwhile, in closed-loop systems, the voltage signals are likely to be

more sensitive to such faults than the current signals. This is because the VSD regulates the voltage to adapt to changes in the electromagnetic torque caused by the faults[41].

2.4 Control Systems Based Condition Monitoring

The focus of the previous section was on traditional CM methods; these methods still require the fitting of additional tools including data acquisition systems, sensors and transducers to gather and observe any information relating to the machines that are under surveillance. Moreover, trained and qualified human resources are paramount to the performance of different tasks, including physical processes such as detectors installed on gadgets and linked to data interpretation, analysis and collection of the gadget. Such methods are expensive, complex and advanced.

To conduct efficient monitoring, the drives should estimate, compute and measure the quantity of parameters, which influence the speed of the induction motor. Through measurement of supply current and supply voltage at the drive terminals, the signals are used for regulating the force (torque) and speed through specific calculations. Despite the AC drive using control methods, many closed loop systems require the signals for implementation of effective control and determination for the desired performance.

The actions of the control system with regard to any differences could reflect the regulation and performance of the system's health. Any signal, which is processed within the controller, could signal a particular fault. Simply put, any variation or change within the driven physical/mechanical system would alter the system in terms of time constant and the stability conditions of the system that emerge in response to the control systems which could be seen on transient responses or steady-state responses.

2.4.1 Diagnostic Techniques Applied for Induction Motor Drive

A large number of published articles examine various methods and techniques for detecting electrical and mechanical faults which occur within an AC induction motor drive. Most of these publications were focused on an open loop mode system, in which the AC induction motor is directly connected to the power line supply. However,

detecting these faults with variable speed drives (closed-loop) was limited. There is little literature that explores the capacity of diagnosis by electrical supply parameters both current and voltage[41].

Abusaad, S.,(2015) [28] have investigated how control affects the behaviour of a faulty induction machine. These faults lead to small variations in related parameters, for example, Id and Iq. The authors utilised the model-based method to represent the data from a gearbox under different conditions, concluding that it is possible to utilise any of the torque linked variables for observing MA. It was confirmed that it can also utilise static data for fault detection.

Lane et al., [72] have debated the effect of variable speed drives through unbalanced windings faults in ACIM. It was found there is a slight rise in stator resistances when comparing healthy and faulty cases which can be sensed by voltage and current signals. The change also led to small growth in efficiency of the motor. The writers decided that additional tests are essential under both open and closed modes to validate this result.

Benghozzi et al., [73] study investigates the detection of gearbox transmission faults under sensorless mode by using the data from control systems. The study established that it is capable of using present control data for detecting gearbox fault systems.

Ben-Ghozzi, (2016)[74], has debated the effect of VSD on theoretical and experimental studies and also how control affects the behaviour of a faulted induction machine by developing a hybrid model to monitor several faults occurring in the motor which could be used effectively for monitoring and diagnosing the machine conditions.

Shaeboub, A. (2018)[41] study investigates the detection of stator and rotor faults using electrical signals (current and voltage) under different conditions. It was carried out under both an open and close loop mode. This study proved that it is possible to use existing control data for observing electrical faults in an induction motor.

Cunha, C.C.M., et al. (2007) [75], has debated the effect of variable speed drives through control of torque and feedback on the behaviour of asymmetric rotor cage-based induction machines. The method indicates that stator d-q components for the stator

current signals (iqs) and (ids) that already exist at the drives have features which could be used effectively for monitoring and diagnosing the machine conditions.

Additionally, the method indicated that torque current (iqs) cannot be considered as a strong indicator for diagnosis, because it is considerably affected by the frequency, control gain and load variations. Moreover, the sideband component amplitude that the rotor asymmetries introduced generally depend on the bandwidth of the speed control loop. In contrast, besides the (iqs) error and current loop error signals (ids) error of the drive, the magnetising current component ids do not essentially depend on the conditions of operation. The technique was premised on the current signature analysis and the (iqs) and (ids) error signal analysis using a band-pass digital filter.

Bellini, A., et al.[76], have investigated how control affects the behaviour of a faulted induction machine. The authors utilised two dynamic models, one representing fragmented rotor bars, the other represented a short-circuited motor stator.

The diagnostic index for closed-loop operation is used for investigating components of torque current and field current when the field based induction motor drive is available.

The work confirmed that correct features could be identified from the component of field current within a field-oriented regulated machine, which could be efficient for CM and diagnosis. It indicates that the spectra components under 2sf and 2f frequencies do not depend on the control parameters but to a certain extent depend on the faults.

Parlos, Kim and Bharadwaj (2001) [77], designed a high-speed sensor-less fault diagnostic system for induction motors, using Fourier-based or multi-resolution signal processing and recurrent dynamic neural networks for quasi-steady state or transient operations. The suggested mechanism of diagnosing faults solely employs motor terminal currents and voltages that can be obtained from the motor nameplate data and drives.

The reviewed articles indicate the existence of several techniques used to acquire information from the frequency speed drive for diagnosis and detection of faults. Notably, current signal analysis, artificial neural network, and motor model-based methods constitute the most extensive methods in the detection of ACIM drive faults.

The research findings from the study of Kołodziejek and Bogalecka (2009)[78], were used by Kołodziejek and Bogalecka (2012) [79] for investigating the effect of rotor fault signal amplitudes within variables of a sensorless and state control system. The identified properties were then utilised for designing a diagnosis technique.

The variables, which exhibit sensitivity towards rotor defects initially identified, next to the symptoms within such variables, which when combined, indicate the aggregation of some rotor faults irrespective of the mode of control system used or the kinds of estimators for the state variable.

Ochoa and Pacas (2012) [80] have designed mathematical models, which detect fragmented rotor bars within induction motors regulated by a field-based method. The algorithms of detection tested successfully on sensor-less and sensor-based systems.

The study undertaken by Kral, C. et al. [81] used the Vienna Monitoring technique in the detection of inverter-fed drive rotor cage asymmetries. Through input signals that exist within the variable speed drives, where a field-based control drive was used, the real condition of the machine determined and contrasted against the voltage model and current model's output and any variations within the frame of a rotor fixed was referenced. The suggested method was solely investigated on faults of one rotor bar.

Studies on fault detection and diagnosis within Field Oriented Controlled (FOC) induction machines have been increasing in the past few years. For instance, Cruz and Cardoso(2007) [82] proposed different pathways for diagnosing rotor faults within FOC-oriented induction motors, that is, the current controller output, d-q current component error signals and approximated rotor flux. The methods were analysed to determine the correlation between faults of the motor rotor, drive and control parameters.

Because of the increasing popularity of sensor-less variable speed drives, the necessity for studies in areas including diagnosis application technique, fault symptoms, reliability, and stable operation is increasing significantly.

The study undertaken by Kołodziejek and Bogalecka (2009) [78] examined the impact of faulty rotors within induction machines on sensor-less control systems for diagnostic and

monitoring purposes. On the basis of machine model and chosen state observer structures, which are utilised for the synthesis of sensor-less drives, the compensating effect of machine asymmetry caused by fragmented bars with closed-loop control system coupled with the speed sensor feedback within the parameters of the control system are determined. Moreover, the components of frequency linked to rotor asymmetry for chosen state observers are contrasted in open-loop and closed-loop operations. The methods used include cepstrum analysis, frequency domain and time domain. In time domain, evaluation of waveform data constitutes a common CM method. The overall signal level root mean square or peak amplitude values constitutes the common time-domain method utilised for fault detection within oscillating machines. The method has been improved through the integration of skewness, kurtosis, crest factor, and peak-to-peak value. Furthermore, usage of time synchronous averages has increased the effectiveness of time-domain analysis in locating gearbox faults through vibration analysis. In this method, the signal's time history could be utilised for determining the parameters being analysed for fault signs. In the frequency domain analysis, a time domain signal is converted into the frequency domain to enhance information existing within the time signals. The frequency spectrum divides the determined signals into different segments, which are investigated for a single or discrete frequency indicating unwanted excitation. Frequency domain analysis constitutes an extensively utilised technique for analysing signals from oscillating machines and enables the detection of amplitude and frequency modulation occurrence and the monitoring and detection of single frequency components[41].

2.5 Summary of Chapter 2

A brief review is given of industrial maintenance processes for induction machines, including the application of condition monitoring to the diagnostics of mechanical faults, electrical faults and also a combination of the two; condition monitoring features for induction motors and diagnostic methods was presented in the chapter.

The conclusion drawn from the reviewed literature shows that there are many techniques applicable to obtain processes' health information, which includes vibration monitoring,

lubricant analysis, acoustic emission tracking, temperature monitoring, visual and aural inspections. However, most of them are less satisfied by industries because of the low accuracy and cost-intensity.

The literature also indicated that the use of current and voltage signals from ACIM with VSDs, which are increasingly utilised in industry owing to their effectiveness and lower energy consumption and are readily available at the motor terminals has been relatively neglected because of high demands of signal process in extracting the diagnostic information from the noisy signals.

Signature analysis of motor electrical signals in induction motor drive systems has attracted significant attention because it is readily available at the motor terminals. The benefits of detecting such faults using electrical signals means it is not necessary to carry out further device measurement within the non-invasive tracking technique.

Limited publication is available on the detection of BRBs and/or misalignment for VSD systems. Developments of fewer studies that detect faults within VSD have been undertaken. Moreover, many developed mechanisms are premised on the identification of faults, which are those taking place within the induction motor, including current or speed sensor faults, bearing, stator, and rotor faults under open loop mode. Very few studies have been conducted on the identification of external and internal motor faults, which develop within the induction motor based mechanical system components in sensor-less modes.

No work has been found describing in detail the effectiveness of MCSA and MVSA for detection and diagnosis of BRB under sensorless mode. Too, no formerly published work has reported investigating the potential for detecting and diagnosing the effect of asymmetry in a BRB with misalignment under sensorless mode.

The aim of this research is examine the detection and diagnosis of electrical and mechanical faults of mechanical systems based on electrical supply parameters from a VSD. The tasks were performed to facilitate this aim with different levels of severity and two different types of faults were used. For benchmarking and comparison purposes, the vibrational analysis was used in parallel with MCSA and MVSA.

This study seeks to provide information and develop accurate diagnostics for detecting electrical and mechanical faults, such as BRB, MA and combined faults by using electrical signals obtained from induction motors with VSDs.

Chapter 3 AC Induction Motor and Drives

In this chapter the author looks at the working principle of ACIM, the construction features and the concept and theory of control systems of the motors driven by a sensorless VSD system. The author also discusses the concept of field oriented control (FOC) based on the discussed theories. The working principle of sensorless VSD systems is also described as well as the impact that electrical and mechanical faults have with power supply parameters and VSD response.

3.1 Introduction

In most of the industrial applications, AC induction motors have to receive wide applications due to their characteristics such as high reliability, simple structures, affordable prices, the stability of operations, longer lifespan, direct connection to AC power supply, high energy efficiency [26, 31, 41]

Efficient operation of ACIM is achieved at low slip, the speed of the ACIM is dependent on the frequency of supply and the number of poles of the motor. However, for the wide range of speed adjustability, variable frequency supply systems are needed. The wide range of speed is usually attained by using a VSD or inverter drives. [28, 61, 83].

3.2 AC Motors: Construction and Work Principle

AC induction motors are types of electric motors that are driven using alternating current (AC). ACIM has two main parts, the stator and the rotor. The stator is stationary and is found on the outside of the motor and its coils are supplied by an AC current that produces a rotating magnetic field. The rotor is the inside part of the motor and has a shaft that is a source of the second rotating magnetic field. The magnetic field of the rotor may be produced by AC or DC electrical windings, permanent magnets or reluctance saliency. From the stator, currents are induced into the rotor via the air gap. Both rotor and stator have a core sheet of highly magnetisable materials which provides low eddy current and hysteresis losses. Less commonly, the operating principle of linear AC motors is the same as that of rotating motors with the difference arising from the arrangement of the stationary and moving parts which have a straight-line configuration and therefore produces a linear motion [26, 61].

Figure 3-1 shows the typical ACIM.

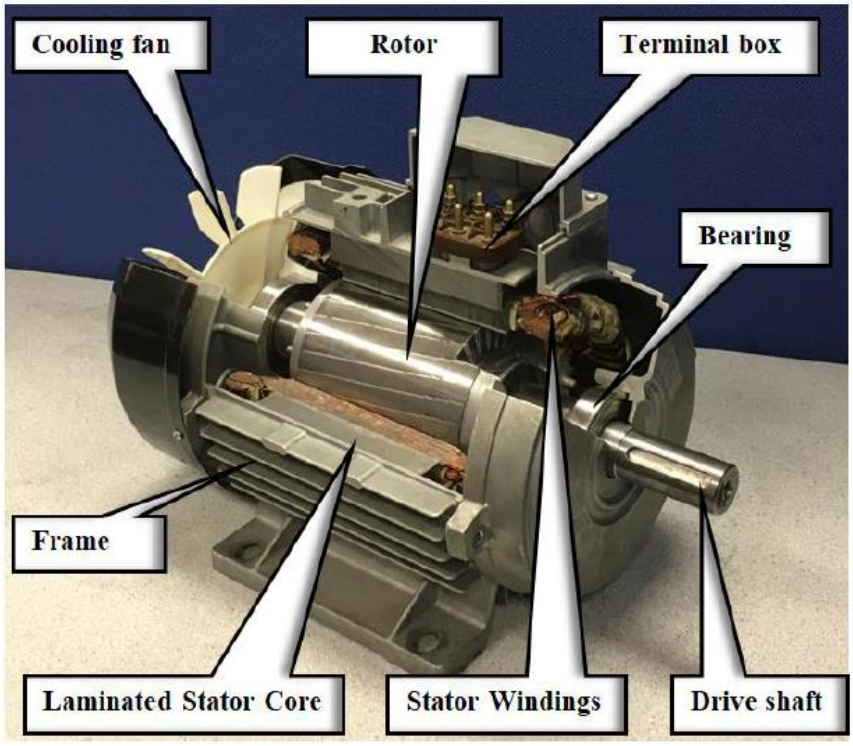

Figure 3-1 Typical AC induction motor [41]

3.2.1 The AC Induction Motor Stator (Stationary Part)

The stator is constructed using stacks of steel laminations. The laminations have slots that open to the stator inside diameter, holding the windings (coils) of the stator and further supported to form a rigid structure. The magnetic flux is carried by the teeth which separate the slots and transfers it to the air gap separating the rotor and the stator [61, 84].

3.2.2 The AC Induction Motor Rotor (Rotating Part)

The rotor consists of the shaft and the cage conductors. The shaft consists of a cylindrical cast iron core. Heavy straight copper or cast aluminium bars form the bulk of the material of the squirrel cage rotor windings with a regular circulation about the periphery, with the ends connected using end rings. The rotor conductors are accommodated in the slots and have a skewed design which helps in minimising magnetic hum and magnetic locking to avoid torque pulsation. The end rings have blades attached to them for cooling purposes [17, 61]

3.2.3 Other Parts of ACIM

Figure 3.1 shows other parts of a three-phase ACIM. It includes the fan, fan cover, motor end shields, terminal box, spring washers, assembly screws, and bearings. There is also the air gap which is the space between the stator and the rotor [28]. This space must be as minimal as possible, and this is achieved by using a short and rigid shaft to prevent it from deflecting to prevent air gap irregularities that are a cause of the unbalanced magnetic field. Asymmetries are avoided by using accurate centring bearings

A laminated core form envelope the iron core concentrating the magnetic flux of stator to the rotor windings. This lamination provides mechanical support for the shaft of the rotor. The free spinning of the rotor shaft inside the stator is made possible by the bearings on both sides of the shaft [17, 28].

3.3 Principles of ACIM Operation

Figure 3-2 shows Three-Phase ACIM currents in stator windings. All phases are induced by a magnetic field, the difference between phases being 120 degrees.

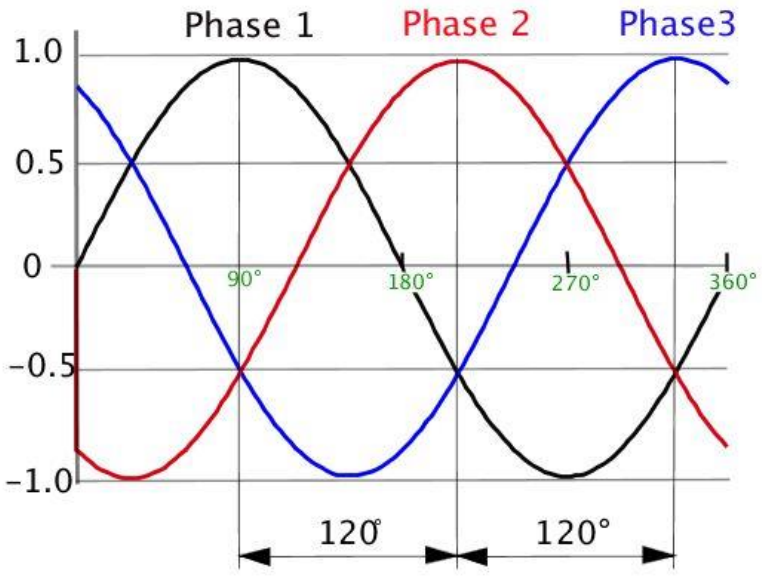

Figure 3-2 Three-Phase ACIM currents [45]

The interaction between the stator radial magnetic field and the rotor axial currents is the source of generation of the motor torque by ACIM. The rotor and the stator have no physical connection. The rotating magnetic fields from the stator are induced into the rotor of the motor through the air gap. Based on Lenz law, the electromagnetic field created by the stator is induced into the rotor, inducing a voltage into the bars of the rotor, generating a second magnetic field which creates a current flow. The flow of current in the rotor generates a field that networks with the stator generating an electromagnetic field. This interaction generates a twisting force (torque) that causes the rotation of the motor in the resultant direction of the torque [18, 85, 86].

3.3.1 Speed, Slip and Efficiency

The synchronous speed of the motor or the speed due to the field, is calculated using the following general formula [86]

$$n_s = \frac{120 * f_s}{P} \qquad (3.1)$$

Where: n_s is synchronous speed, P is the pole number (integer number), f_s is the supply frequency (fifty Hz in the United Kingdom). From Equation 3.1, it is evident that the motor speed could be adjusted by varying the source frequency. The rotor can never achieve a synchronous speed because rotation at this speed implies that there will be no field and no EMF which would be induced into the bars of the rotor and therefore the rotor will not have any torque [86].

The slip, ***s***, is defined as [26]:

$$S = \frac{n_s - n_r}{n_s} \qquad (3.2)$$

Where: n_s *:* synchronous speed; n_r *:* rotor speed

Efficiency is the ratio of input power, subtract power losses and then divide the result with the input power. Therefore, higher values of efficiency can be achieved by decreasing the power losses [85]

3.3.2 Load and Torque of ACIM Rotor Current

The interaction between the axial currents and the radial flux wave in the rotor generates the torque of the motor. The torque is in the same direction as the rotation and drags the rotor along with the field. As mentioned previously, the rotor can never rotate at synchronous speed. Figure 3-3 shows a typical current and torque curves characteristic for induction motor [41, 86].

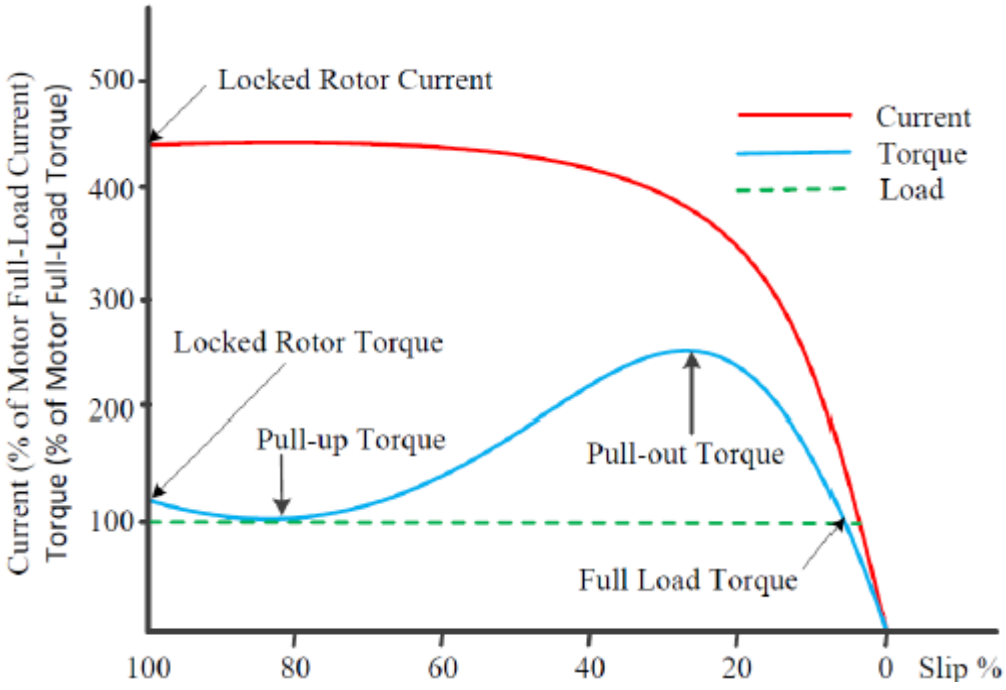

Figure 3-3 Torque and current curves versus slip (%)[41]

When the ACIM starting with a full supply voltage, “Locked Rotor Current (LRC)” sees the induction of an extremely high starting current into the rotor of ACIM, this current will cause a significant amount of EMF to be induced into the rotor, generating the “Starting” or “Locked-rotor torque” (LRT). However, with the adjustment of the rotor speed, there is the adjustment of current and the acceleration of the rotor torque, and with

a constant voltage, the torque is expected to reach a minimum value known as the pull-out torque. As the speed of the rotor increase and approaches its full speed, it approaches its extreme value which is alluded to as the breakdown or the pull-out torque. It is associated with a small drop in the current. Further acceleration of the rotor to values near the speed of the motor not under any load, the torque and the current of the motor falls to minimal values. When loaded to the full load torque, the motor finally achieves stability. The motor speed during normal operating conditions is determined by the stator poles and the motor runs at low slip [18, 28, 86].

3.3.3 Rotating Magnetic Field

An electromagnet can be created by winding a conductor with a coil and applying a DC voltage to it. The flow of current through the conductor creates the lines of flux which, when combined, produces a magnetic field that is larger and stronger. The core is the centre of the coil. Electromagnet created in this way has an air core with iron having a higher conductivity of magnetic flux as compared to air. Winding an insulated conductor around the iron core produces an even stronger magnetic field using the same amount of current. Additionally, using the same level of current and increasing the number of coils, a stronger magnetic field is generated [17, 87-90].

3.3.4 Induction Motor Field Weakening

In certain conditions, the range of speed control of a motor can be extended beyond a nominal speed by up to four times. There is a gradual escalation of mechanical power linearly as a function of motor speed which is equal to the nominal power of the motor under nominal load, with the flux remaining constant. Assuming torque times speed is proportional to mechanical power and that the nominal value of the power has been attained when the nominal speed is reached, in this scenario, if the application needs a higher speed than the nominal value, then there must be a reduction in the production of torque [91].

The operating range has two areas where the field weakens. The first region is the base speed and stops at the point where the current limit is unreachable as a result of the

voltage limit. The second point of weakness starts where the first region ends with the current limit being overridden by the voltage limit leading to a reduction of the stator current below the current limit Imax [92].

In applications such as spindle drives and electric vehicle, constant power operation plays a key role. The use of field-oriented induction motor drive in these applications is suitable as there is an easy weakening of the flux of the induction machine. In this application, there is a close operation between the voltage limit and the drive and therefore a sensible selection of the reference flux has to be made. ACIM control with weakened flux has been studied by various authors [93]

3.4 Theory of AC Drives and Conventional VSD

Generally, by adjusting both frequency and voltage, the speed of an ACIM can be varied [26, 85]. Expressions 3.1 and 3.2 describe synchronous speed and slip respectively. Supplying a three-phase ACIM using a sinusoidal three-phase voltage and assuming no drop in the windings of the stator, during the steady state of the voltage magnitude can be estimated as [81]:

$$u \approx \omega_s \psi \tag{3.3}$$

$$\psi_s \approx \frac{u}{\omega_s} = \frac{u}{2\pi f_s} \tag{3.4}$$

The motor speed as illustrated in formula 3.2 is influenced by the frequency of the supply, while formula 3.3 indicates that when the voltage per frequency ratio is maintained constant, the stator flux remains constant [26, 94]. However, a considerable drop in voltage occurs across the windings of the stator at low frequency and hence low V/Hz ratio, therefore compensation must be provided. High voltage is additionally required for consistent V/Hz proportionally constant at high speeds. However, high voltage can also be problematic if it exceeds the rated value of the motor as this could result in the burning of the windings of the motor. In such a case, it is necessary not to maintain the ratio of V/Hz constant by adjusting the voltage to ensure that damage does not occur. The motor rated voltage must not be exceeded [94].

The working principle of an AC drive is that it changes the frequency and the voltage of supply from being fixed to being variable. The motor speed is determined by output frequency whilst the electromagnetic torque that the motor generates is regulated by the V/Hz ratio [85].

The interaction between the axial currents and the radial flux wave in the rotor generates the torque of the motor. The torque is in the same direction as the rotation and drags the rotor along with the field. As mentioned previously, the rotor can never rotate at synchronous speed. Figure 3-4 illustrates electromagnetic torque and speed for ACIM in which was feeding with various values including: frequency and voltage. On the other hand, to identify a fixed current value, the electromagnetic torque of the motor should be constant as far as the speed of the motor usually indicated as less than the rated speed. This is particularly being represented as the constant torque region. Nevertheless, in this region the voltage and hence the power, increases linearly with speed and the breakdown torque is constant for the entire region. When the motor speed reaches the level of rated value, both current and voltage level are off. Consequently, the electrical supply goes in the constant power region. When the voltage reaches the rated value, the breakdown torque value is reached and torque will decrease as the speed increases [74].

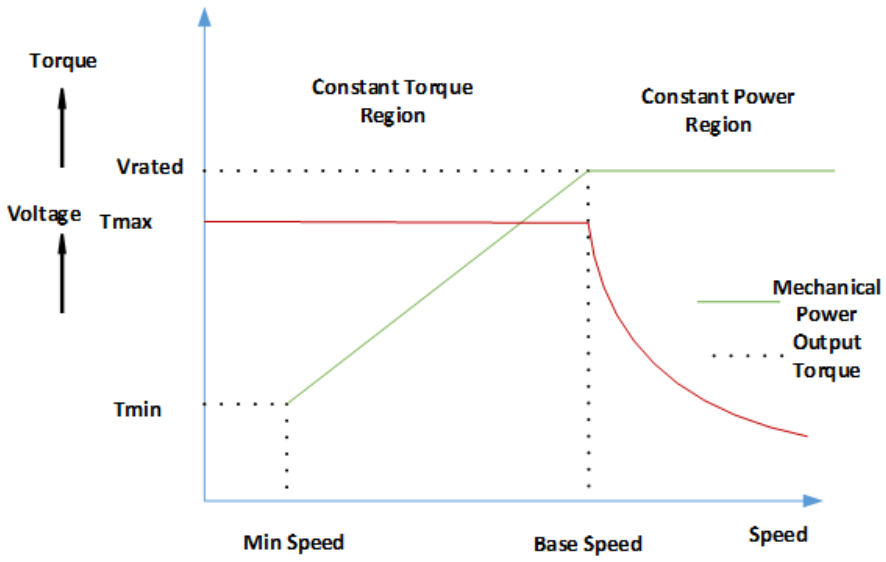

Figure 3-4 Motor torque-power curve vs speed [74]

Every frequency has a torque-speed curve; these curves have the same breakdown torque value. In the constant torque region, as shown in Figure 3-5, the operating points can be established at torque-speed curves at 100% of the torque level [28, 41].

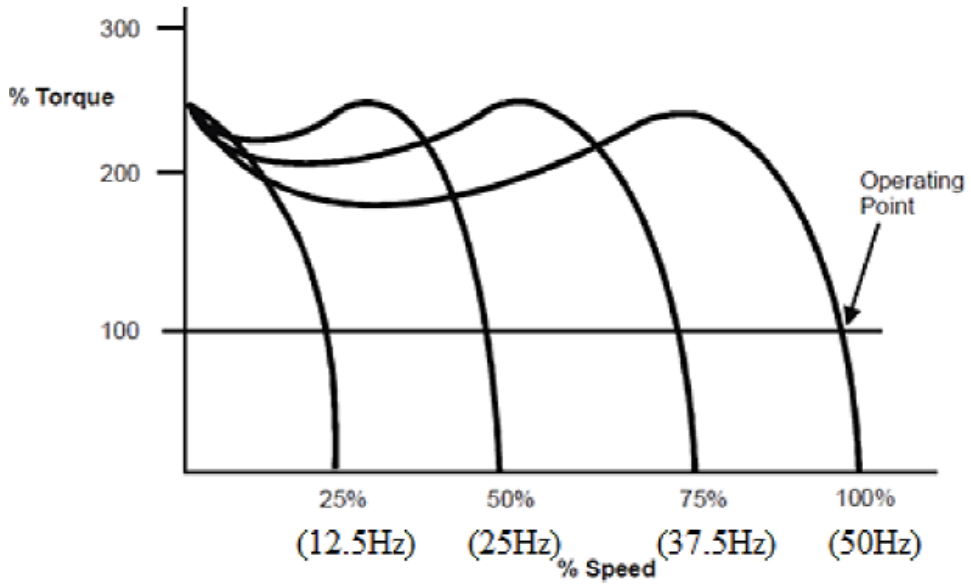

Figure 3-5 Motor torque vs supply frequency[28]

3.4.1 Principles of Control Systems

A control system is a term utilised to describe a system used for maintaining variables at required levels within acceptable limits. The set-point or the desired value is delivered to the controller by the operator. The control signal to the control process to stimulate the desired behaviour is provided by the control system [95].

3.4.2 AC Drive

A three-phase variable speed drive has three main parts namely, the rectifier, DC link, inverter and the control circuits. The rectifier performs the conversion of AC into DC while the DC link filters and smoothens the rectifier output. The inverter then converts the DC power into AC with controllable and variable frequency and voltage. The control circuits are used for controlling either the rectifier bridges or the inverter to output the

needed frequency and voltage levels. Currently, inverter and rectifier circuits make use of high-frequency self-controlled power switches [18, 96], ACIM Fed by VSD as shown in Figure 3-6.

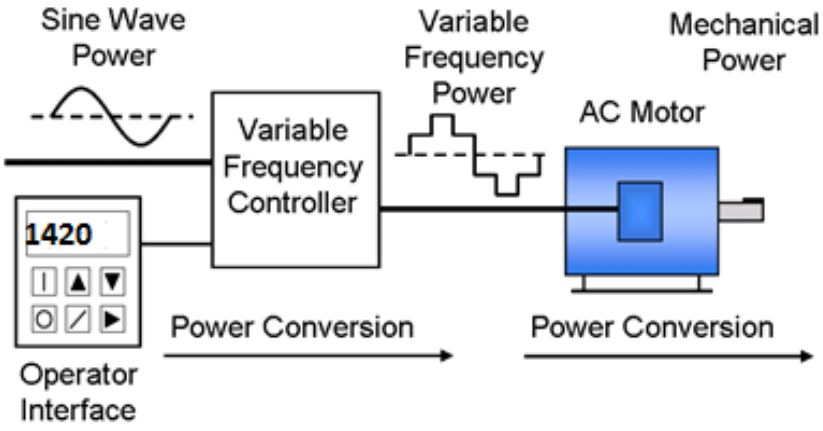

Figure 3-6 ACIM fed by VSD [61]

Three main types of inverters are mainly used in AC drives. These are: [61, 85, 96, 97].

a) *Variable Voltage Inverter (VVI).*

b) *Current Source Inverter (CSI).*

c) *Pulse Width Modulation Inverter (PWM).*

3.4.3 General Structure of Variable Speed Drives

The state of operation of AC motors is generally on/off. The design of VSD caters for this requirement and other extra features. According to Munoz, O. D [98] VSDs have the following advantages including providing multiple motor speeds and increases in the efficiency of the systems because only the needed amount of power is supplied. Additionally, VSD allows a gradual increase of motor speed and therefore eliminating the high start-up current that can damage the motor [98].

The three main parts of a VSD drive are exemplified in following Figures 3-7 and 3-8:

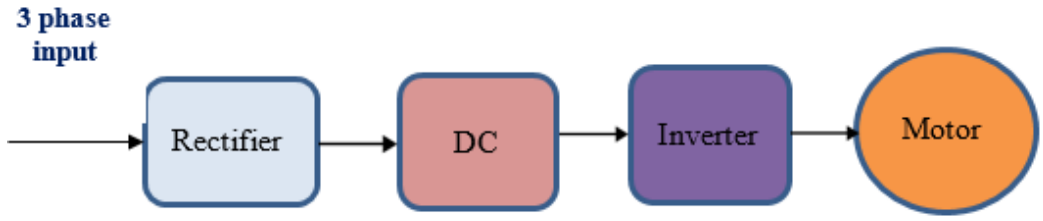

Figure 3-7 AC variable speed drive main parts[98]

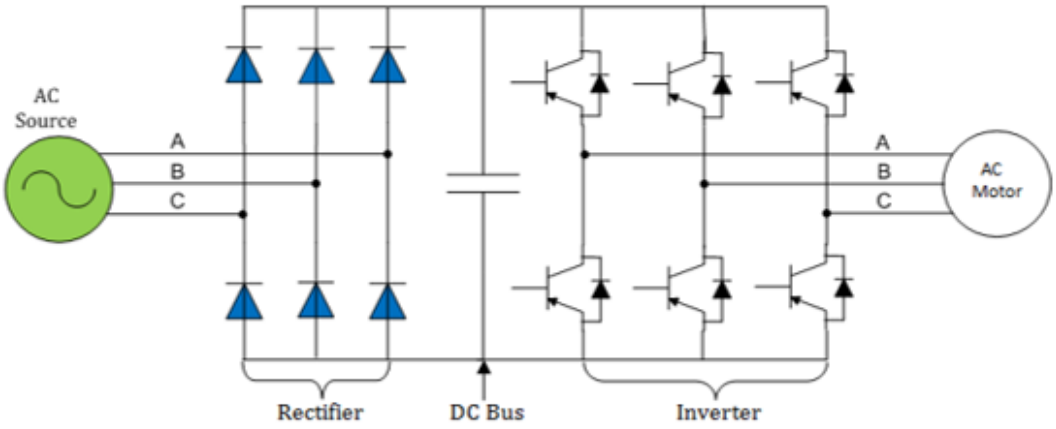

Figure 3-8 Structure of variable speed drive[61]

3.4.3.1 Rectifier:

The rectifier performs the conversion of AC into DC and feeds the DC link elements. [99].

$$V_{peak} = \sqrt{2} \times V_{rms} \tag{3.5}$$

3.4.3.2 DC Bus:

Receives the output of the rectifier and stores it on the DC bus which comprises several capacitors [99, 100].

3.4.3.3 Inverter:

Comprising various capacitors that act as a distribution point of power to the ACIM. Additionally, the inverter makes use of insulated gate bi-polar transistors (IGBTs) that regulate the voltage of the DC at a specific interval to create a frequency and voltage that is variable. IGBTs are switched ON & OFF on a needs basis at specific intervals thereby producing voltage pulses with a constant magnitude as shown in Figure 3.9. [96].

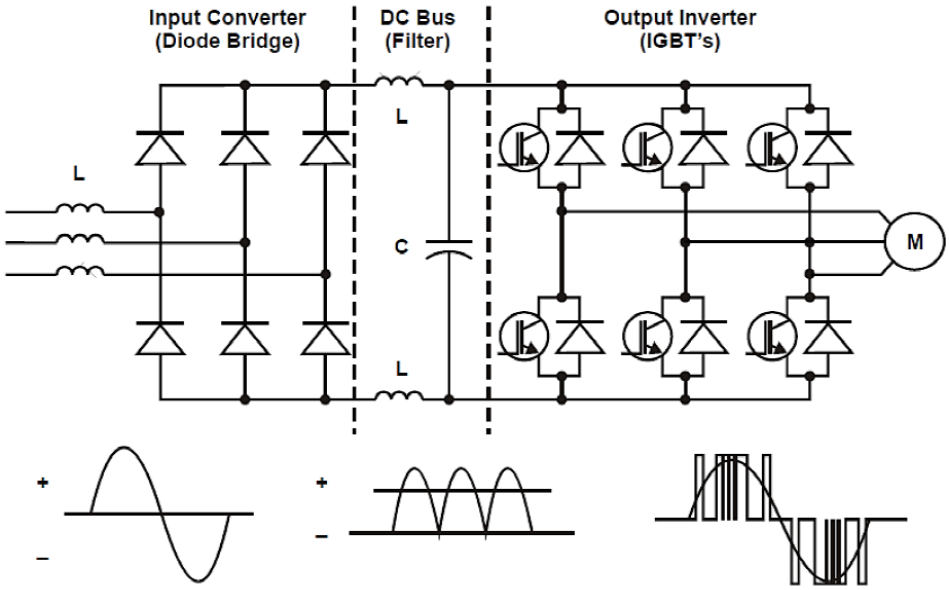

Figure 3-9 Block diagram exemplifying a PWM VSD[85]

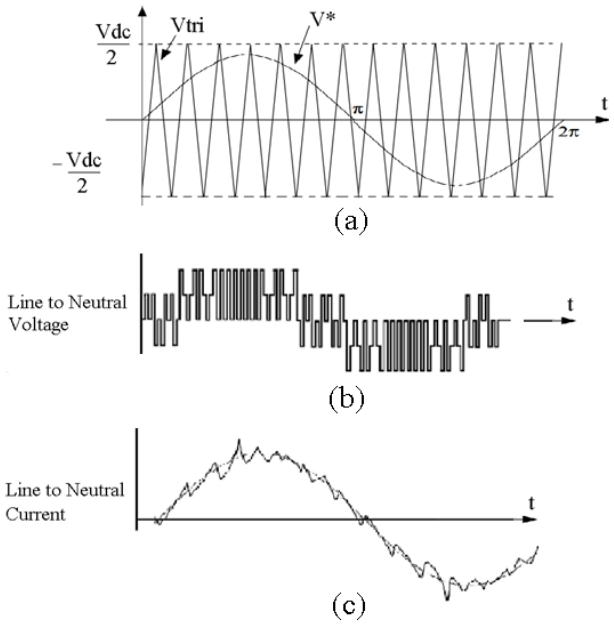

Figure 3-10 PWM drive voltage and current waveform adapted from[85]

In Figure 3-10 (a) Reference and Carrier Signal, (b) voltage, (c) Current

Where: V_{dc} Dc Link voltage, V*Reference Signal, V_{tri} Triangular Carrier Signal

The gate driver circuits are fired by the control board and by turning, alternating the waveform from positive to negative resulting in the creation of a three-phase output. How long the IGBT stays on defines the amplitude of the output voltage whilst how long the IGBT is off defines the output frequency as illustrated in Figure 3-11 [96].

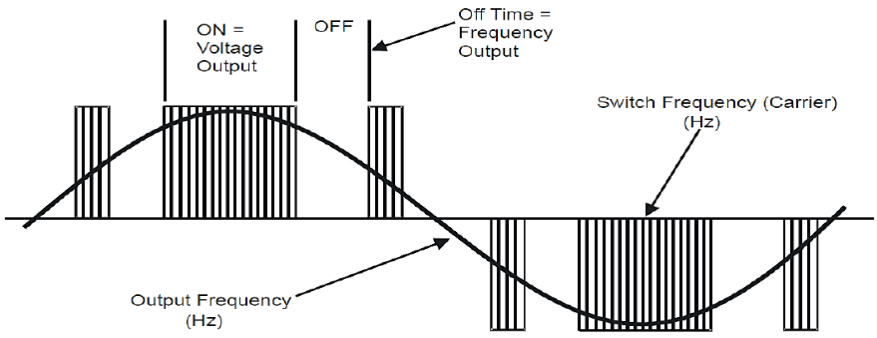

Figure 3-11 Frequency & voltage creation from PWM[96]

3.5 Flux Vector of (FOC)

Direct measurement of the flux from the stator of the motor facilitates the implementation of flux vector control or indirectly where the control variables are determined by the drive from the parameters of the motors (including the frequency and supply current) and the measurement of rotational position [101].

Indirect control of flux vector has two major classifications; closed loop and Sensorless (encoderless) flux vector control. Closed-loop vector control entails the determination of the rotor angle by means of a pulse encoder while sensorless control does not use any speed or position sensor.

3.6 Sensorless Field Oriented Control (FOC)

Sensorless FOC is used for controlling a standard AC induction motor without the use of encoder feedback. This technique calculates the ideal d and q-axis voltages using the model and the parameters of the motor to attain the needed level of currents for varying the loading conditions of the motor. The need for a voltage boost in a conventional inverter is replaced by information about the inductance and resistance of the stator. Sensorless drives provide the following [102]:

- A low starting current but a high motor torque at low output frequencies
- Is compact and require less maintenance
- Better dynamic response to variations in load and demand
- High power factor and automatically compensates for slip
- Is easier to apply as it does have required wires and has less electrical noise
- Associated with energy savings and does not need an encoder
- Applicable to different environmental conditions including high temperature

The same set of variables can be estimated using a Model Reference Adaptive System (MRAS). MRAS makes use of two independent machine models in its estimation [96, 102, 103], The first model is the voltage reference model in a stationary frame with no clear incorporation in terms of the speed. The second model is the adjustable mode with

estimated variables and makes use of the equations of stator current also in a stationary frame. For correction, the MRAS schematic and Speed loop in Sensorless was symbolised in Figure 3.12.

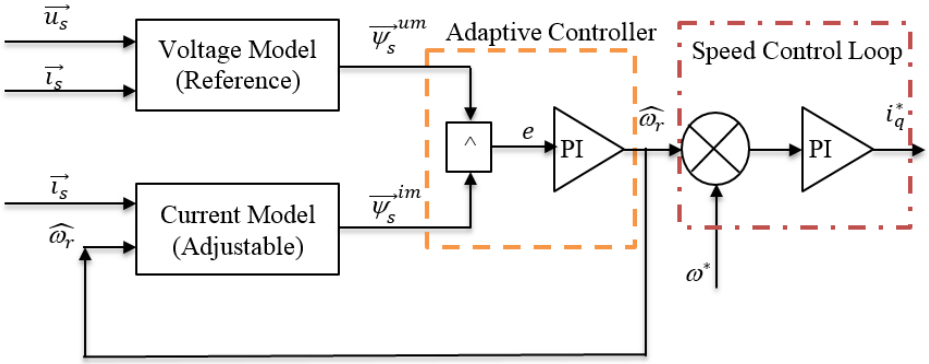

Figure 3-12 MRAS schematic and speed loop in sensorless, adapted from [28]

The motor equations and variables for both the reference and adaptive models are derived [2, 28, 104]:

$$\left[d\psi_{\beta r}^{u} / dt \right] = L_r / L_m \left[(u_{\beta s} - R_s i_{\beta s}) - \sigma L_s \left((di_{\beta s}) / (dt) \right) \right] \tag{3.9}$$

$$\left[(d\psi_{dr}^{u}) / (dt) \right] = L_r / L_m \left[(u_{\alpha s} - R_s i_{\alpha s}) - \sigma L_s \left((di_{\alpha s}) / (dt) \right) \right] \tag{3.10}$$

$$\sigma = 1 - \frac{L_m^2}{L_r L_s} \tag{3.11}$$

The changeable '(adaptive) model' is denoted as [28, 104, 105]

$$\left[d\psi_{\beta r}^{i} / dt \right] = 1/T_r \left[L_m i_{\beta s} - \psi_{\beta r}^{i} R_s i_{\beta s} + T_r \hat{\omega} \psi_{\alpha r}^{i} \right] \tag{3.12}$$

$$\left[d\psi_{\alpha r}^{i} / dt \right] = 1/T_r \left[L_m i_{\alpha s} - \psi_{\alpha r}^{i} R_s i_{\alpha s} + T_r \hat{\omega} \psi_{\beta r}^{i} \right] \tag{3.13}$$

existing error among any two models was computed as [28, 106]:

$$e = \left[\left(\psi_{\beta r}^{u} \psi_{\alpha r}^{i} \right) - \left(\psi_{\alpha r}^{u} \psi_{\beta r}^{i} \right) \right] \tag{3.14}$$

An adaptation mechanism generating an output for regulating the adaptive model can facilitate the evaluation and the correction of the error. In the adaptation mechanism, the PI controller is the most common technique, however other techniques such as neural network and fuzzy control systems can also apply. The estimated value produced by the adjustable model is replaced by the PI controller output. The quantity of the estimated variable is continually modified by MRAS and thus maintains the error between the two models [106, 107].

Rotor flux angle θe can then be calculated using the estimated speed as follows[28]:

$$\theta_e = \int \omega_e \, dt \tag{3.15}$$

The rotor circuit in a stationary frame form the source of the adjustable model equations [102, 103, 108, 109]:

$$\frac{d\psi_{dr}}{dt} = \frac{L_m}{T_r} i_{sd} - \omega_r \psi_{qr} - \frac{1}{T_r} \psi_{dr} \tag{3.16}$$

$$\frac{d\psi_{qr}}{dt} = \frac{L_m}{T_r} i_{sq} - \omega_r \psi_{dr} - \frac{1}{T_r} \psi_{qr} \tag{3.17}$$

$$T_r = \frac{L_r}{R_r} \tag{3.18}$$

T_r Is also monitored online by:

$$T_r = \frac{1}{slip} \times \frac{i_q}{i_d} \tag{3.19}$$

The ideal d and q-axis voltage components is determined by the motor model and is needed for the attainment of the magnetising current, key for varying load conditions [110, 111].

Torque regulation or full continuous torque at zero speed may not be achieved by a standard sensorless flux vector drive unless it is given a more complex circuitry. The estimation of flux leads to a current that generates a regulated motor torque [85]. For a sensorless control to provide stability and limit estimation error, good knowledge and

understanding of the machine to be controlled is needed; in such cases, an approach that is model-based is more reasonable [112, 113].

Figure 3-13 displays the FOC drive

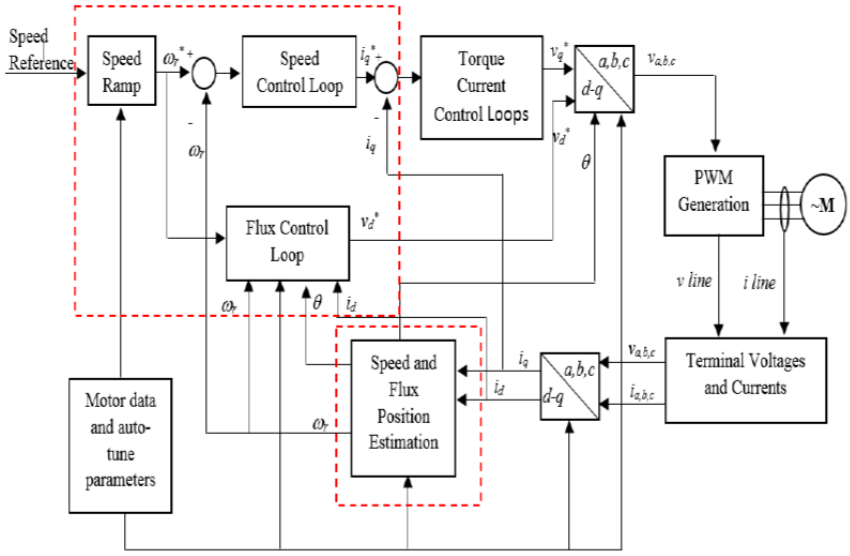

Figure 3-13 FOC drive[28]

3.7 Summary of Chapter 3

In this chapter, the paper discussed the principle of operation of ACIM and AC drives. By regulating the voltage and frequency of the power supply to the motor, an inverter is able to control the speed of rotation of an ACIM. From a perspective of condition monitoring, a fault occurring in the system will likely affect the power supply signals. With the drive in between the supply and the motor, the action of the drive can generate noise and thus make it difficult to detect a small change that may arise due to the fault. The FVC drive operates by the parameters of the three-phase supply into a certain reference frame implying that the signals are of a static type and are mainly used by the drive for control purposes. Hence, in fault detection and diagnostics, it makes sense to take into consideration these static parameters. Based on the fact they are readily available and their lack of need for extra measurements, provide further advantages. All the supply parameters are incorporated in the control strategy for control purposes.

Moreover, the voltage signals are more sensitive to both faults within stator and rotor than the current signals [41]. Fault detection can be facilitated by detecting these parameters based on the response of the control system. According to Kliman et al (1997) [114], fault detection based on the sensorless torque measurement is not sufficient, but it is useful in the detection of faults and can be applied in the status monitoring of the driven process.

Chapter 4 Signal Characteristics of Electrical Signals under Common Faults in a Motor System

This chapter presented induction motor faults and the presentation of several reviews on electrical parameters within a faulty and healthy situation in an induction motor. Furthermore, it focuses on the explanation of physical occurrences of defective induction motors having broken rotor bars, the air-gap eccentricity motor bearing defects, stator windings and shaft misalignment.

4.1 Three Phase Induction Motor Faults

This thesis concentrates on several kinds of ACIM faults identified, namely, a broken rotor bar, a fault that takes place inside the motor; gearbox oil deterioration and shaft misalignment as a mechanical fault that happens outside motor (external fault), and joint faults of shaft misalignment and broken rotor bars.

The faults are categorised as stator faults, motor bearing faults and rotor faults. These faults mostly take place within the motor.

4.1.1 Rotor Faults

Rotor faults account for approximately 10% of overall ACIM faults. These faults are caused by rotor winding. Faults are mostly BBRs owing to direct on-line starting and pulsating load. It leads to speed fluctuation, torque pulsation, vibration, arcing within the rotor, overheating and damaged rotor laminations [2, 115].

Rotor broken bars within ACIM are a widespread fault that frequently cause unanticipated failures and results in productivity loss. In recent years, this kind of fault has been progressively explored for creating sophisticated methods that allow on-line untimely diagnosis and detection of motor faults to evade any harmful effects of unanticipated failures.

Three key kinds of faults exist that may be linked with squirrel-cage rotor configurations. Firstly, inter-laminar voltages at times denoted as inter-bar voltages are attributable to shorts via the rotor core laminations. The second is the end-ring of rotor connector ruptures and thirdly the rotor-bar failures. These defects might stem from a broad diversity of pressures and manufacturing flaws, recurrent overcapacity, both electrical and thermal. Other than extreme vibrations owing to supply, electrical energy imbalances, variations in loads, and frequent early transients, might bring about accelerated defects of squirrel-cage rotor bars and other elements regarding structure [116]. Figure 4.1 (a) healthy rotor (b) two rotor broken bars. More details are shown in [61].

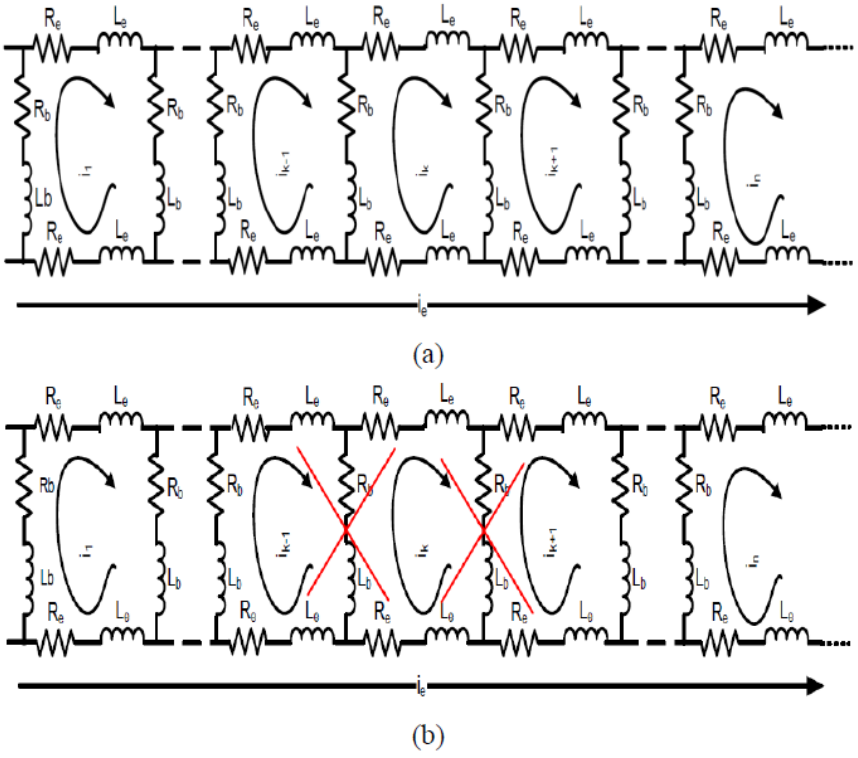

Figure 4-1 (a) healthy rotor (b) two rotor broken bars [61]

ACIM faults often generate additional frequency components in the voltage and current spectrum. The abnormal harmonics contain potential information of motor faults. Sidebands are usually the result of an amplitude or frequency modulation process. In the spectrum, they take the form of spectral components equally spaced on both sides of the carrier frequency, these sidebands will appear on both sides of the supply frequency, see Equation (4.2). There BRB fault(f_{brb}) can be calculated as below [117, 118]:

$$f_{brb} = (1-2ks) f_s \qquad (4.1)$$

Where *s is* the slip, and f_s is the supply frequency

This returning voltage disparity leads to a torque pulsation at the twice slip frequency$2f_s$ and a speed fluctuation [117, 119]. This prompts, in the stator winding, a right sideband voltage element at $(1+2ks)f_s$ upon which it relies on the mass inertia. As a result, the broken rotor bars bring about additional frequencies in the stator described by [120-122].

$$f_{brb} = (1 \pm 2ks) f_s \tag{4.2}$$

Wherein *k*=1, 2, 3….

The slip s will be as:

$$s = \frac{\left(f_s / p \right) - f_r}{f_s / p_s} \tag{4.3}$$

4.1.2 Motor Rotor Misalignment

Induction motors could be damaged due to air-gap eccentricity. The major reasons eccentricities occur are because of shaft deflection, the imprecise placing of the rotor with regard to the stator, bearing wear and stator core shift. Air-gap eccentricity leads to uneven radial forces and thus uneven magnetic pull that could result in the rotor-to-stator scrub, and eventually leads to breakage of the stator windings and the stator core. Also, eccentricity can result in harmonics and vibration within the current signal

Consequently, the disparity within the air gap may lead to the disparity of magnetic field circulation on the rotor so that the course of magnetic force is on the least air gap, this is known as an unbalanced magnetic pull. Eccentricity may be caused by faulty bearings, mechanised flaws and unstable rotor shaft[123, 124].

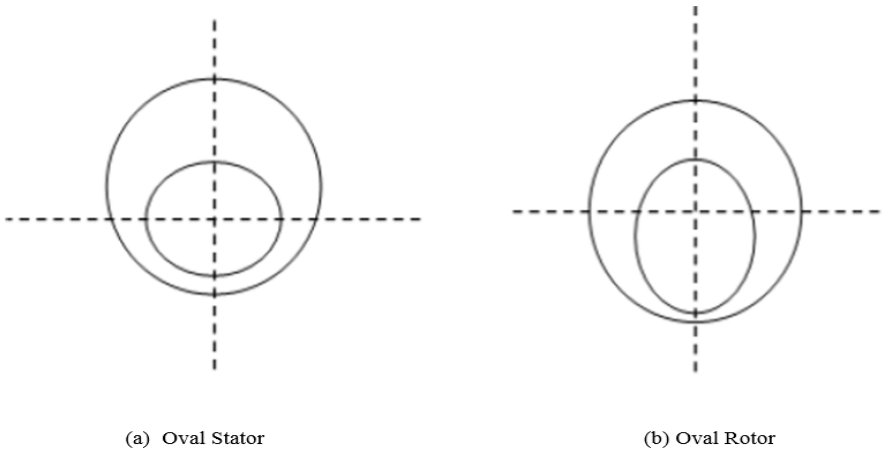

(a) Oval Stator (b) Oval Rotor

Figure 4-2 Eccentricity of air-gap[123]

Eccentricity could be categorised into two classes, dynamic & static eccentricity [123].

As demonstrated in Figure 4-2(a). The Oval stator is deemed to be a case of static eccentricity; this eccentricity can take place once the rotor rotation centre is taken out to up, elliptical rotator as within Figure 4-2(b).

Because of the occurrence disparity of eccentricity, sideband elements emerge around the slot harmonics consistent with voltage frequency continuum of the stator. The frequency elements within the stator voltages of an induction device having air-gap eccentricity are specified by [125, 126].

$$f_{ecc} = \left[\left(kN_b \pm n_d \right) \frac{1-s}{p} \pm m \right] f_s \qquad (4.4)$$

Where: f_s: supply frequency, s slip, n_d order number of eccentricity, (dynamic eccentricity is =1, static eccentricity is =0,), k an integer, N_b amount of rotor bars, p the number of pole-pairs, m: stator time harmonics that exist within the current supply that drives the machine, specified by positive and negative 1, 3, 5, …etc.

Once the dynamic and static eccentricities are occurring jointly, the spectral constituents may be presented around the basic frequency, these elements frequencies are specified by [124].

$$f_{mix} = \left(f_s \pm m f_r \right) \qquad (4.5)$$

Where, $f_r = (1-s) f_s / p$ (4.6)

f_r the mechanical rotational rate, p: the amount of pole pairs, m = +1,2, 3....

4.1.3 Motor Bearing Faults

Two bearings sets are located at both rotor ends of an induction motor to support the rotating shaft. These bearing will have the rotor in position and support it to revolve effortlessly by lessening frictions.

These bearing comprise of an outer race, an inner race, and a set of rolling components named (balls) within between both races. Generally, in situations of induction motor,

inner race is fastened to the shaft and the load is passed through the rotating balls, this activity will reduce the friction. Through the use of lubricant, the races friction will be reduced.

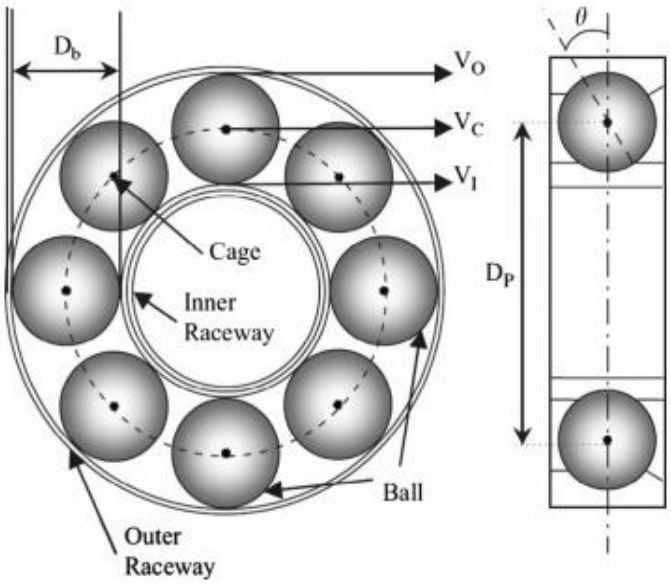

Figure 4-3 Construction of a ball bearing [127]

Figure 4-3 demonstrates a typical ball bearing. All physical harm of the inner race or within the outer race or on the balls' surface is referred to as bearing faults, a bearing is defined as the frailest constituent in an induction motor, it is the one biggest reason of a defect in ACIM. Shaeboub(2018)[41] have stated that, (about 40%–50% of the total) of motor fault flaws are as a result of bearing failure

Generally, this faults are due to lack of lubrication, installation errors, shaft misalignments, surface wear and tear, and even manufacturing faults. According to the elements affected, see Figure. 4.3, bearing faults can be categorised as inner race, outer race, ball element and cage faults.

In general these faults and consequences of bearing failure are due to causes such as [41, 128]:

- Lack of lubrication

- Installation errors including shaft misalignments
- Surface wear, tear and even manufacturing faults

Bearing faults are categorised into localised and distributed defects. Distributed defects are flaws that affect an entire region and is complex to characterise through distinct frequencies. Conversely, single-point flaws are localised and may be categorised in accordance with the subsequent affected components[128]:

- ✓ *Inner race fault*
- ✓ *Outer race fault*
- ✓ *Ball fault*
- ✓ *Cage* fault

Bearing defects may be detected through stator current analysis. Schoen et al.[128] asserted that this type of harm on an induction motor was a product of rotating eccentricities at bearing fault typical frequencies that result in periodical changes within the machine inductances. These have to produce extra frequencies within the stator current that may be estimated by [129]:

$$f_{Bf} = \left| f_s \pm k f_v \right| \tag{4.7}$$

4.1.4 Stator Faults

Stator of induction motor has several faults. These faults are categorised by faults within stator winding, also faults within laminations and frame of stator [3].

As demonstrated in Figure 4-4 Stator winding fault may be categorised into four major defects namely[3, 61, 130]:

a) winding short turn,
b) phase to phase,
c) open circuit,
d) short circuit.

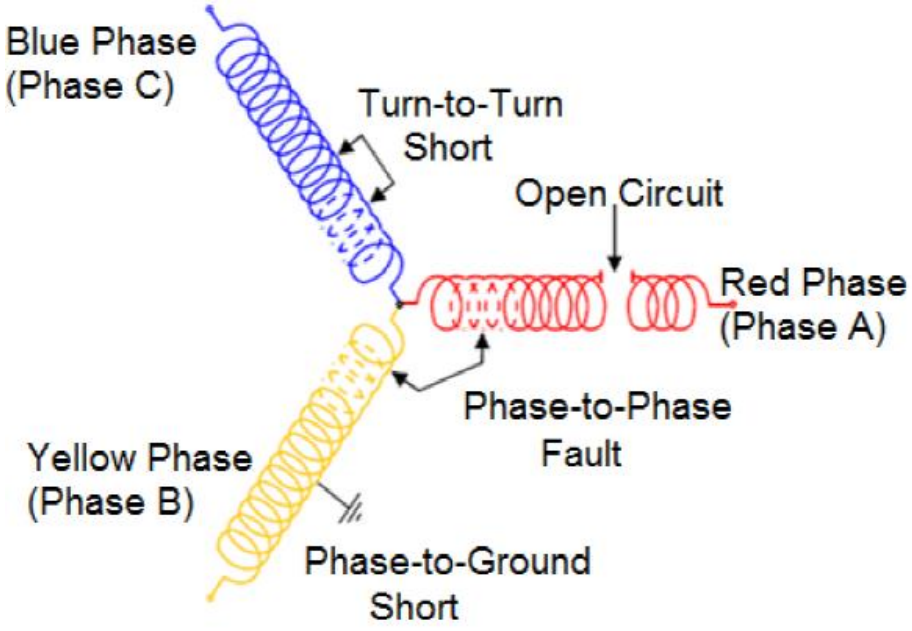

Figure 4-4 Star-connected stator illustrating diverse kinds of stator winding fault[61]

Normally, these unequal faults in the stator are connected to insulation failures that stem from diverse reasons like poor connection, overloading, etc. Therefore, the diverse kinds of winding flaws and their causes and consequences of stator winding may be summed up as below:

- *Mechanical Stresses*
- *Electrical Stresses*
- *Thermal stresses*
- *Environmental stresses*

Generally, stator faults lead to several problems like irregular allotment of the air-gap, fluctuation around the stator cross part that causes the stator voltages to be adjusted, the slots rate of the rotor and the characteristic frequencies in voltage indicators may be discovered at typical frequencies, stator defects frequency as [131, 132].

$$f_{SF} = f_S\left[\left(1 \pm m.N_b\left((1-s)/p\right)\right)\right] \qquad (4.8)$$

Equation (4.6) may be represented of rotor frequency as [61].

The rotor frequency f_r is calculated as ❖

$$f_r = \frac{1-s}{p} f_s \tag{4.9}$$

Equation (4.8) may be written as:

$$f_{SF} = f_S \pm m.N_b.f_r \tag{4.10}$$

The per unit slip *s* is determined as:

$$s = \frac{f_{slip}}{f_{sync}} = \frac{\left(f_s / p\right) - f_r}{f_s / p} \tag{4.11}$$

where *fr* rotor speed, *P* amount of pole-pairs, f_s supply frequency, *s* slip of motor, *Nb* amount of bars in the rotor, also m= 1, 2, 3…

4.1.5 Shaft Misalignment

Shaft misalignments within machines have a negative consequence on effectiveness, and in the long term could lead to disastrous failure owing to needless vibration [133], pressure on the motor, bearings and short-circuiting within rotor and stator windings. Moreover, shaft misalignments may boost the dynamic load that speeds up machine corrosion. Ideal placement of the driven shafts cannot be attained within the industry. Erroneous shafts aligning through couplings result in extra dynamic burdens and serious vibration issues in rotating machines that result in early damage and loss of energy. Within the industry around 30% of downtime of a machine is because of the incorrectly alignment of machines [134]. There has been a great deal of study in the experimental and investigative analysis of misalignments, taking into account dynamic and vibration forces that revealed that the vibration, determined at bearing houses owing to coupling misalignment, mostly happens at the even manifolds of the speed of the rotor [134, 135].

Tejas, Patel, et al. (2009)[136], have documented that several researches have been carried out using diverse detection and diagnosis methods for early and efficiently diagnosing shaft misalignments. These comprise vibration [136, 137], wireless sensors [134], model founded fault detection [138, 139], and motor current signature analysis(MCSA) [140, 141]. However, the majority of these researches were completed on motors fed either through V/Hz drives or direct mains.

As demonstrated in Figure 4-5, there are two basic kinds of shaft misalignments: initial kind is parallel misalignment that occurs once two shafts centre lines are not within the similar line, which may be separated to vertical and horizontal misalignment. The second type is angular misalignment that emerges where there are diverse angles linking the two shafts and there is a blend of the two earlier kinds [142].

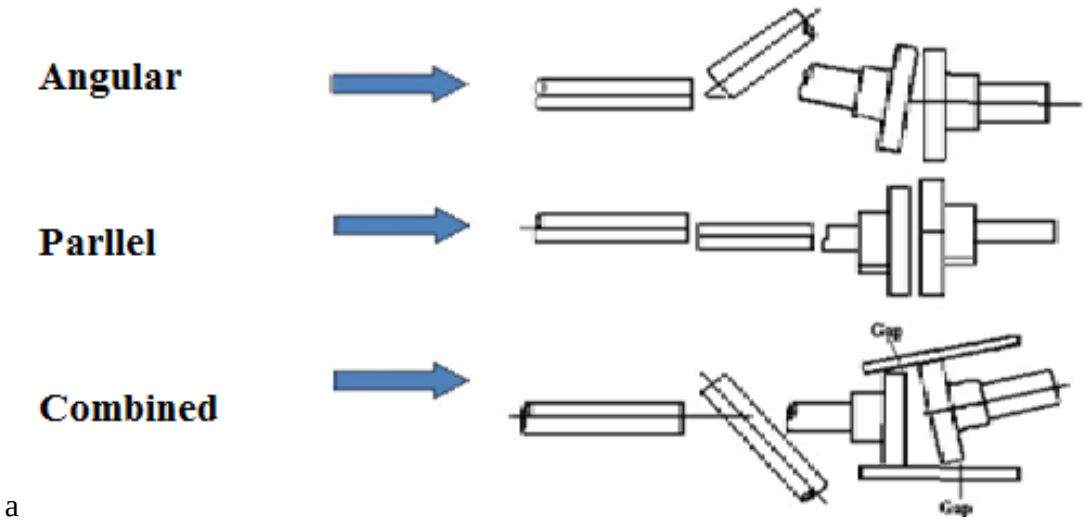

a

Figure 4-5 Types of shaft misalignment [143]

A reassessment of the literature shows that the research of shaft misalignments within mechanical systems driven through sensor-less VSD motors is insufficient [144, 145]. One of the main challenges in misalignment diagnosis with systems propelled through sensor-less regulation is that the drives recompense any dynamic consequences arising due to the fault and initiate additional noise to the determined data. Additionally, the harmonic substance at motor terminals from the output of the drive, in particular, stator

voltages and currents are elevated, which does not enable the recognition of small changes within supply parameters of the terminal [76, 112]. Misalignment flaws may be detected on the sensor-less drive, phantom amplitudes of shaft operating pace $f_s \pm f_r$, on which misalignment diagnosis may be extracted since these elements comprise both lateral and rotational vibrations.

4.1.6 Lubricating Oil Deterioration

As the most important specification of lubricants, viscosity is described as the internal opposition to flow by a fluid. Viscosity holds an inverse relationship with temperature and expresses connection with pressure. The key role of any lubricating oil is lessening the resistance between fixed and rotary machine parts, thus decreasing wear and temperature that result in elevated machine effectiveness. As researched within gear lubrication mechanisms, any rise in oil thickness will maintain extra oil on the meshing teeth surfaces and therefore is likely to create thicker hydrodynamic layers resulting in a lessening of frictional power [146, 147].

4.2 Electrical Parameters under Healthy Conditions

The sensor-less VSD controls the induction motor pace through decoupling the torque and field elements. These elements will be controlled independently using cascade regulation loops. The speed and torque will be regulated by obtaining the reference torque indication and reference pace, and subsequently sets the torque present element reference to the present loop. The voltage regulation loop institutes the reference torque electrical energy depending on the dissimilarity, involving the response torque voltage element and orientation from the torque loop. Once the speed is at, or more than the rated speed, the fluctuation is decreased via 1/ w_r. This regulation loop produces the reference field current element[33].

The controller instigates its output once the input shifts in the bandwidth of the controller. By altering the i_{qs} the electromagnetic torque will be regulated as:

$$i_{qs}^{*} = \frac{2}{3}\frac{1}{p}\frac{L_r}{L_m}\frac{T_e^{*}}{\psi_r} \tag{4.12}$$

whereas the motor flux is regulated as follows [148]:

$$i_{ds}^{*} = \frac{\psi_r^{*}}{L_m} \tag{4.13}$$

By employing the torque voltage reference, the slip frequency as [148]

$$\omega_{sl} = \frac{L_m}{T_r \psi_r} i_{qs}^{*} \tag{4.14}$$

Following this the electrical flux angle is measured as follows [148]

$$\theta = \int (\omega_{sl} + \omega_m)\, dt \tag{4.15}$$

Once a drive is functioning under healthy circumstances, perfect electromagnetic affiliation of the drive may be assessed in one of the three stages. Depending on the research in [60], the voltage and current signal in phase one for instance gives a simpler understanding of the consequence of an asymmetric fault like a BRB. By overlooking the superior order harmonics and intrinsic mistakes and denoting supply electrical signal, the voltage and current indication within phase for a healthy example of a motor may be defined as the subsequent connection [61].:

$$i(t) = \sqrt{2} I \cos(2\pi f_s t - \alpha_I) \tag{4.16}$$

$$u(t) = \sqrt{2} U \cos(2\pi f_s t) \tag{4.17}$$

Similarly, per phase power may be written as:

$$p(t) = IU[\cos(2\pi(2f_s)t - \alpha_I) + \cos(\alpha_I)] \tag{4.18}$$

The entire power of a three-phase IM may be obtained from 4.18 through the multiplication of one phase by three, or from the ensuing the total power within every phase.

The magnetic flux within the stator as:

$$\psi_s(t) = \sqrt{2}\psi \cos\left(2\pi f_s t - \alpha_\psi\right) \quad (4.19)$$

The electrical torque generated via the relations among the flux and current as:

$$T_e(t) = 3N_p \psi I \sin\left(\alpha_I - \alpha_\psi\right) \quad (4.20)$$

I , U, and ψ refer to the (RMS) of supply voltage, current and the connection flux in that order, α_I , α_ψ are the phases of the flux, current denoting supply current, and N_p is the amount of pole pairs

4.3 Effect of Fault on Electrical Parameters

Electrical or Mechanical anomalies lead to added load fluctuations that are normally modulated at frequencies, (f_r) linked to the rotating pace with supply frequency (f_s), then usually computed by [60, 149]:

$$f_F = \left[f\left(f_s, f_r\right)\right] \quad (4.21)$$

As a result, mechanical oscillations because of the fault are discovered to be sinusoidal and lead to:

(I_F) current amplitude of, (α_F) an angular dislocation of

Because of angular dislocation, the torque will be affected by oscillatory torque ΔT_e as:

$$\Delta T_e = 3N_p \psi \, \mathrm{I}_F \sin\left(2\pi f_F t - \left(\alpha_I - \alpha_\psi\right) - \alpha_\mathrm{F}\right) \quad (4.22)$$

The mechanical speed in induction motor is defined as:

$$d\omega_r t / dt = (1/j)\left[T_e - T_l\right] \quad (4.23)$$

Whilst the fault is occurring, the motor speed (ω) will oscillate by $\Delta\omega_r$ as shown in the subsequent Equations 4.24 and 4.25, and the motor speed (ω_r) will also oscillate because of the error. As a result, the fault will generate speed fluctuation $\Delta\omega_\mathrm{r}$ as follows:

$$\Delta\omega_{\mathrm{r}} = \frac{N_p}{J}\int \Delta T_e.\,dt = -\frac{3N_p{}^2\,\psi\ \mathrm{I}_F}{2\pi f_F J}\sin\left([2\pi f_F t] - (\alpha_I - \alpha_{\psi}) - (\alpha_{\mathrm{F}})\right)\,dt \tag{4.24}$$

Therefore in fluctuation, the angular location within the rotor will be [150]:

$$\Delta\theta = \Delta\alpha_{\mathrm{F}} = \frac{N_p}{J}\int \Delta\omega dt = \frac{3N_p{}^2\,\psi\ \mathrm{I}_F}{4\pi^2 f_F^2 J}\sin\left(2\pi f_F t - (\alpha_I - \alpha_{\psi}) - \alpha_{\mathrm{F}}\right)\,dt \tag{4.25}$$

The oscillation within the load is because of the mechanical fault effect in the torque element that modulates the speed of the motor, which leads to speed fluctuations which consecutively alter the rotor position.

Consequently, slip frequency will be influenced via fluctuations in rotor position and thus, the torque voltage component will also be influenced through the fault. The oscillation can be modulated by angular fluctuation as illustrated in the subsequent equation:

$$\psi_s^F(t) = \sqrt{2}\,\psi\ \cos[2\pi f_F t - \alpha_{\psi} - \Delta\psi\ \sin[2\pi f_F t - (\alpha_I - \alpha_{\psi}) - \alpha_{\mathrm{F}}] \tag{4.26}$$

Where $\Delta\psi = \dfrac{3N_p^2\psi I_F}{4\pi^2 f_F^2 J}$

$$\psi_s^F = \sqrt{2}\psi\cos(2\pi f_s t - \alpha_{\psi}) + \sqrt{2}\psi\Delta\alpha_F\sin(2\pi f_F t - \alpha_{\psi}) \tag{4.27}$$

Two sidebands at the basic supply frequency will also appear. The ensuing stator fluctuation variation is offered as [151]. The study within [150, 152], looks at the relationship between the stator fluctuation and the equal circuit hindrance which forms sideband elements around the main frequency of both voltage and current signals offered as [33, 60, 153]

$$i_A^F(t) = \sqrt{2}I\cos(2\pi f_s t - \alpha_I)$$
$$+\sqrt{2}I_l\cos[2\pi(f_s - f_F)t - \alpha_I - \alpha_F - \phi]$$
$$+\sqrt{2}I_r\cos[2\pi(f_s + f_F)t - 2\alpha_\psi + \alpha_I - \alpha_F - \phi]$$

(4.28)

$$u^F(t) = \sqrt{2}U\cos(2\pi f_s t)$$
$$+U_l\cos[2\pi(f_s - f_F)t - \alpha_F - \phi)$$
$$+U_r\cos[2\pi(f_s + f_F)t - 2\alpha_\psi + \phi_F - \phi]$$

(4.29)

Where I_l, I_r, U_l, U_r : root mean square values of the lesser and the higher sideband elements of the electrical energy and current in that order.

α_ψ : phase angle linking the stator fluctuation and current, α_I : phase angle between voltage and current, both at $(f_S - f_F)$

φ : angular displacement of motor equivalent circuit impedance at supply frequency, &

f_F : fault frequency:

Equations (4.25) and (4.26) demonstrate that the faulty case of voltage and current signal, show extra elements contrasted to that of a healthy situation. The ensuing power within the case of the fault is defined by subsequent simplified method [33]. An efficient analysis may be applied by barring the phase angles from trigonometric equations where in the offered characteristics are near to an authentic power signal.

$$
\begin{aligned}
p^F(t) = IU[&\cos\left(2\pi(2f_s)t - \alpha_I\right) + \cos(\alpha_I)] \\
&+ (IU)_l \cos(2\pi(2f_s - 2f_F)t - 2\alpha_F - 2\varphi) \\
&- (IU)_r \cos\left(2\pi(2f_s - 2f_F)t - 2\alpha_\psi + 2\varphi_F - \varphi\right) \\
&+ (IU)_l \cos(2\pi(2f_s - f_F)t - \alpha_F - \varphi) \\
&-(IU)_r \cos\left(2\pi(2f_s - f_F)t - \alpha_\psi + \varphi_F - \varphi\right)
\end{aligned}
\tag{4.30}
$$

Where, $\omega_s = 2.\pi.f_s$, $\omega_f = 2.\pi.f_F$,

ω_s: angular of the supply frequency & ω_f: angular fault frequency.

From equation (4.30), it may be demonstrated the power continuum have extra features of frequency elements compared to the electrical energy and current. In particular, there will be two sidebands at $2f_s \pm 2f_F$, these sidebands can be located at $2f_s \pm f_F$.

Both sidebands amplitude will have the ability to alter with the load variations, therefore will alter based on motor cases [33].

Because of the drive's controller, these characteristic elements in every electrical parameter will incite to maintain the system pace. Nevertheless, because of the drive structure, such frequency elements might or might not be felt by the entire drive controllers based on the drive's design and tuning parameters.

Depending on the drive's structure and function, the small shifts, because of incipient faults, could be covered through the drive's noise owing to faults, the drive will control the pace and current by tuning the parameters. These activities make the detection very difficult and more sophisticated signal processing methods have to be employed [33, 60].

4.4 Summary of Chapter 4

This section has in brief reviewed major faults for the AC induction motor as a vital key in fault recognition. Electrical faults like stator and rotor faults, and mechanical faults

that are motor bearing defects, shaft misalignment, and air gap eccentricity. Electrical parameters of both faulty and healthy cases are intensely explored.

Depending on function and structure of the AC drive, the entire power supply signals are very likely to be impacted throughout the fault. Therefore, the drive will control voltage and speed to achieve the required speed. Following this, the sidebands will emerge depending on the motor faults and the activity of the drive may raise the noise level generating further challenges in detecting little changes within the explored signals as a result of the fault.

Chapter 5 Simulation Studies of an Induction Motor with Field Oriented Control for Fault Diagnostics

In this chapter, the accomplishment of a variable speed drive field adjusted with the use of Simulink/ is presented Matlab for gaining a quantitative understanding of the outcomes of diverse faults. The model used is chosen from the equipped modules that the Simulink library presented and was adjusted to ensemble the test rig induction motor. The first section illustrates an induction motor model that is three-phase. In addition, it brings in the equations needed in field-oriented control modelling. Included is the study of how the responses of the sensorless VSDs are affected by the BRB and MA under different loads. Finally, these predicted outcomes are evaluated by experimental ones

5.1 Introduction

It is very important to use a model that is accurate so that valuable information is extracted for the monitoring of induction motor condition, this is because it gives room for precise fault signatures to be accurately quantified and extracted. Computer simulation in conjunction with mathematical modelling can be employed so that it can efficiently examine, get enhanced insight and advance the comprehension of sensorless variable speed drive performance. It entails analysing the system response in diverse load conditions and speed. The Matlab/Simulink environment mathematically represent and implements the dynamic state of the motor together with the drive.

Matlab/Simulink is a potent package environment and is the most excellent choice because of its efficiency and readiness to employ sets of embedded constituents that are suitable for diverse applications. This model was formed as blocks joined through lines. Every block employs diverse purposes on its outputs to inputs and illustrates the consequences correspondingly. The block's outputs form inputs to other blocks, represented through lines that join the suitable out/in ports.

Furthermore, Matlab/Simulink can integrate modules in relation as to what is appropriate to simulate electrical systems and power, for instance, power electronics machines and converters. Modules are generally used and can be adjusted to fit any specific application in a number of cases [154].

To conclude, the aim of this chapter is to portray the ACIM (induction motor's) mathematical models with the FOC and executing a computer simulation. The Simulink model is applied to study the outcomes of broken rotor bars, combined faults on electrical supply parameters, misalignment in addition to the impact of load oscillations due to mechanical blunders on the system response, i.e. electrical supply strictures. The model structures had the same features as those of the test rig.

The outcomes confirm the control system's behaviour in the existence of mechanical and electrical faults. Therefore, it is possible to apply a foundation of fault detection and diagnosis.

5.2 Model of AC Induction Motor with Field Oriented control (FOC)

5.2.1 Modelling the AC Induction Motor

In order to facilitate the investigation of the outcomes of changing system parameters under diverse operating conditions and faults, the mathematical model of AC three-phase induction motors in [155] was researched. It claimed that description of the three phases as coupled rotor and stator poly-phase circuits when it comes to generally assumed phase variables in rotor and stator currents known as, $i_{ra}, i_{rb}, i_{rc}, i_{sa}, i_{sb}, i_{sc}$, θ_r refers to the angular displacement between rotor and stator windings and the rotor speed ω_r .

By describing the stator and rotor electrical circuits' the squirrel cage IM model can be obtained, the equation of stator voltage vectors and stator and rotor current vectors, are represented in the following [28, 156-158].

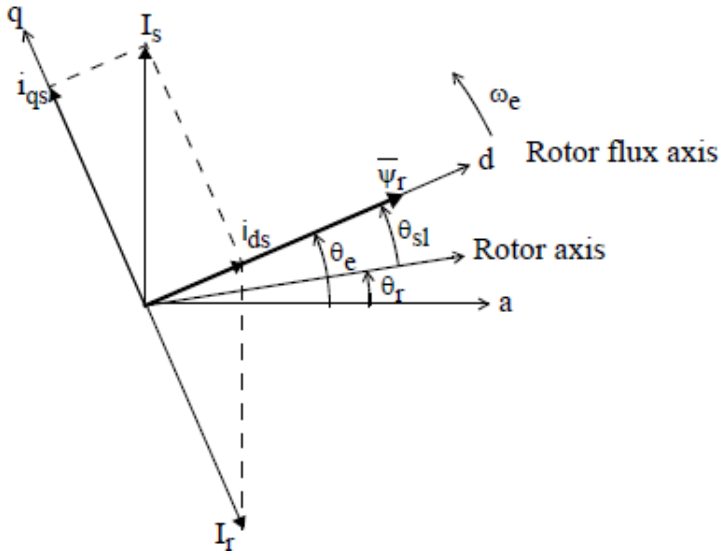

Figure 5-1 Field-oriented control principle[159]

$$\frac{\mathrm{d}\psi_\mathrm{r}}{\mathrm{dt}} = -\mathrm{R}_\mathrm{r} i_r \tag{5.1}$$

$$\frac{d\psi_s}{dt} = u_s - R_s i_s \tag{5.2}$$

$$\psi_\mathrm{r} = \mathrm{L}_r i_r + \mathrm{L}_m i_s \tag{5.3}$$

$$\psi_s = L_s i_s + L_m i_r = \frac{L_m}{L_r}\psi_r + \sigma L_s i_s \quad (5.4)$$

$$L_r = L_{lr} + L_m \quad (5.5)$$

$$L_s = L_{ls} + L_m \quad (5.6)$$

the motor electromagnetic torque (T_e) can be represented as:

$$T_e = ([J\frac{(d\omega_r)}{(dt)}] + [B_m\omega_r] + T_l) \quad (5.7)$$

Where T_e represents electromagnetic torque, T_l refers to load torque, J is motor and load total inertia, B_m system viscous friction coefficient.

The above model is challenging and complex to use for applications alike FOC , of which every electrical variable, (for instance magnetic flux, voltages, currents etc.) is in a vector form and denotes the values (matrix) of three-phase [160]. Complex space vectors can be illustrated with the use of two orthogonal axes only. The motor is looked at as a 2-phase machine. When the 2-phase motor model is used, it makes the control design simpler and lessens the number of equations. However, the effects of saturation or the higher order harmonics of the supply fundamental are ignored, temperature effects are not included, and no asymmetric impacts are considered from either rotor or stator. It is possible to simplify the ACIM model by carrying out the Park and Clark vector transforms. Firstly, the transfer of the sinusoidal three-phase system into a corresponding 2 orthogonal stationary reference frame by Clark as [161, 162]:

$$\begin{bmatrix} u\alpha \\ u\beta \end{bmatrix} = \frac{2}{3}\begin{bmatrix} 1 & 1/2 & -1/2 \\ 0 & \sqrt{3}/2 & -\sqrt{3}/2 \end{bmatrix}\begin{bmatrix} u_a \\ u_b \\ u_c \end{bmatrix} \quad (5.8)$$

The following formula shows how the reverse Clark transformation reference frame can be written:

$$\begin{bmatrix} i_a \\ i_b \\ i_c \end{bmatrix} = \frac{2}{3}\begin{bmatrix} 1 & 0 \\ -1/2 & -\sqrt{3}/2 \\ -1/2 & \sqrt{3}/2 \end{bmatrix}\begin{bmatrix} i_\alpha \\ i_\beta \end{bmatrix} \quad (5.9)$$

Below, is Transforms 2 orthogonal vectors on a fixed reference into orthogonal vectors on a rotating reference frame that rotates through a particular angle with the use of the Park transform (d-q) exemplified as [163]:

$$\begin{bmatrix} i_\alpha \\ i_\beta \end{bmatrix} = \begin{bmatrix} \cos\theta & -\sin\theta \\ \sin\theta & \cos\theta \end{bmatrix}\begin{bmatrix} i_d \\ i_q \end{bmatrix} \quad (5.10)$$

By using the inverse Park transformation, the system returns to 2 phase stationary system as:

$$\begin{bmatrix} u_d \\ u_q \end{bmatrix} = \begin{bmatrix} \cos\theta & \sin\theta \\ -\sin\theta & \cos\theta \end{bmatrix}\begin{bmatrix} u_\alpha \\ u_\beta \end{bmatrix} \quad (5.11)$$

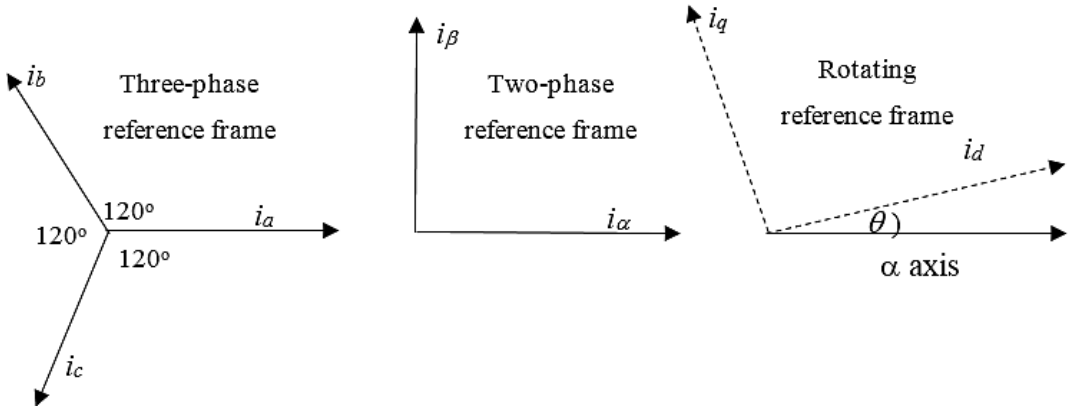

Figure 5-2 Reference frames[28]

The stationary reference frame constituents are therefore projected to a reference's frame, rotating in a particular rotating angle (θ), as shown in Figure 5-2. The frame of reference's selection will define the angle (θ). A point in case is the synchronised reference frame the $\theta = \theta_s$, whereby θ_s is the electrical angle of the stator flux; whereas the rotor reference frame is an indication that $\theta = \theta_r$, whereby θ_r is the electrical angle of the rotor flux; and the stationary reference frame is achieved in $\theta = 0$[161],

As illustrated in Figure 5-3 it is possible to derive the IM model from the d-q motor equivalent circuit through stating the voltage equations of rotor and stator [155, 159, 164, 165]:

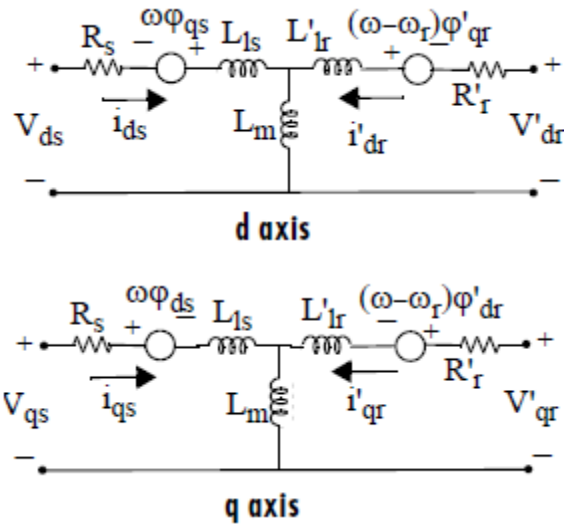

Figure 5-3 d-q Induction motor equivalent circuit [159]

$$V_{ds} = R_s i_{ds} + \frac{d\psi_{ds}}{dt} - \omega\psi_{qs} \quad (5.12)$$

$$V_{qs} = R_s i_{qs} + \frac{d\psi_{qs}}{dt} + \omega\psi_{ds} \quad (5.13)$$

$$0 = R_r i_{dr} + \frac{d\psi_{dr}}{dt} - (\omega - \omega_r)\psi_{qr} \quad (5.14)$$

$$0 = R_r i_{qr} + \frac{d\psi_{qr}}{dt} + (\omega - \omega_r)\psi_{dr} \quad (5.15)$$

Whereby the rotor and stator fluxes are derived from:

$$\psi_{ds} = L_{ls} i_{ds} + L_m i_{dr} \quad (5.16)$$

$$\psi_{qs} = L_{ls} i_{qs} + L_m i_{qr} \quad (5.17)$$

$$\psi_{dr} = L_{lr} i_{dr} + L_m i_{ds} \quad (5.18)$$

$$\psi_{qr} = L_{lr} i_{qr} + L_m i_{qs} \quad (5.19)$$

It is possible to write rotor and stator currents as:

$$i_{ds} = \frac{1}{x_{ls}}(\psi_{ds} - \psi_{dm}) \quad (5.20)$$

$$i_{qs} = \frac{1}{x_{ls}}(\psi_{qs} - \psi_{qm}) \quad (5.21)$$

$$i_{dr} = \frac{1}{x_{lr}}(\psi_{dr} - \psi_{dm}) \quad (5.22)$$

$$i_{qr} = \frac{1}{x_{lr}}(\psi_{qr} - \psi_{qm}) \quad (5.23)$$

This is despite the fact that rotor and stator inductances are computed from:

$$\mathrm{L}_r = \mathrm{L}_{lr} + \mathrm{L}_m \quad (5.24)$$

$$\mathrm{L}_s = \mathrm{L}_{ls} + \mathrm{L}_m \quad (5.25)$$

The following is how the mechanical model is given [155, 164, 165]:

$$T_e = 1.5N_p\ (\psi_{ds} i_{qs} - \psi_{qs} i_{ds}) \quad (5.26)$$

Where: $\psi' = d\,\psi\,/dt$

Below is how the motor speed can be achieved from the moment of inertia, the machine torque and load torque [155, 164, 165]:

$$\frac{d\omega_{\mathrm{m}}}{dt} = \frac{1}{J}(T_e - B_m\omega_{\mathrm{m}} - T_l) \quad (5.27)$$

Given that T_e stands for electromagnetic torque, T_l is load torque, J is load and motor total inertia, B_m system viscose friction coefficient

5.2.2 Modelling the Field Orient Control Drives

When applying the FOC scheme, the torque current component iqs are perpendicular to the ids, while the rotor field is lined up with the field current component ids. For this to be accomplished, the reference frame is lined up to the rotor flux vector and this is carried out by selecting the equivalent to the rotor flux's speed. Therefore details of the rotor flux space vector's position is needed as illustrated in Figure 5.4[148, 159].

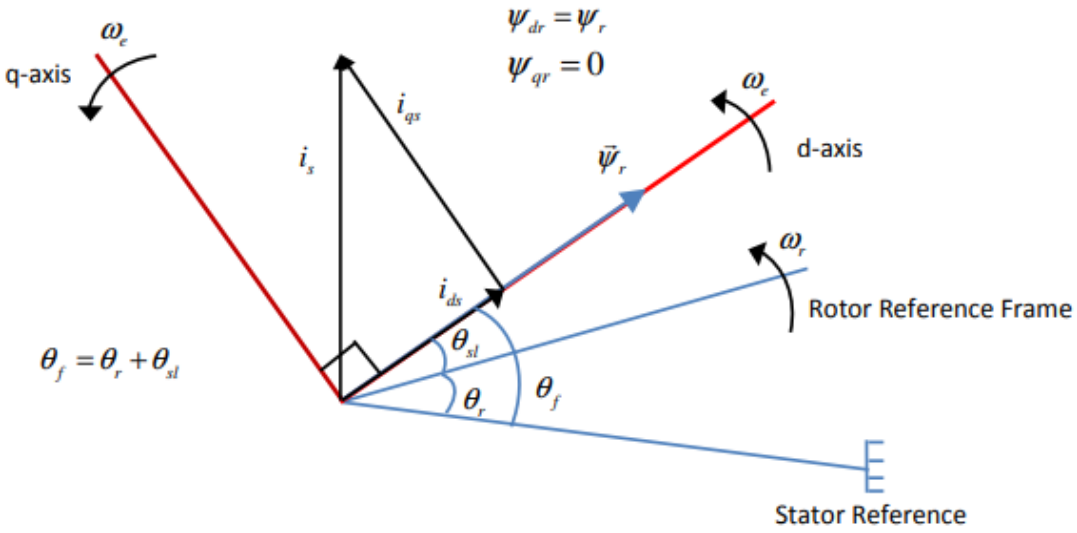

Figure 5-4 Phasor diagram describing the FOC scheme[166]

As previously discussed in Chapter three, FOC adjusts the value of slip to ensure that the rotor flux vector is lined up using a co-ordinator which is a synchronised reference. The simplified system of a control which is FOC is clearly illustrated in Figure 5.5 [167].

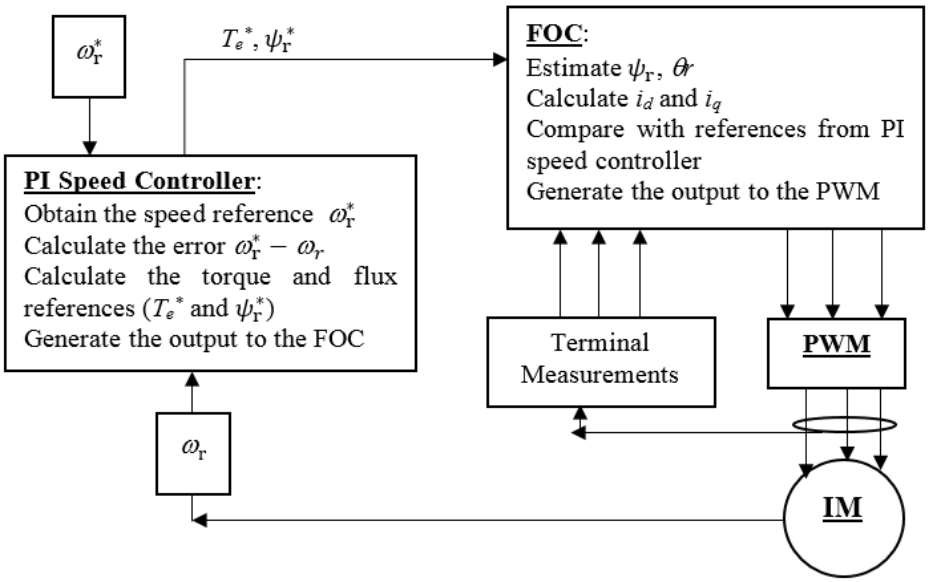

Figure 5-5 A FOC straightforward system

As a result, the rotor flux is lined up with the d axis, as illustrated in Figure 5-4, so as to $\psi_r = \psi_{rd}$ & $\psi_{rq} = 0$; consequently from previous equations the rotor flux is approximated with the use of the equation below [167, 168]:

$$\psi_r = \left[\frac{(\_ L_m)}{(1 + T_s)} \right] (i_{ds}) \tag{5.28}$$

$$i_{ds}^* = \left[\frac{(\_ \psi_r^*)}{(L_m)} \right] \tag{5.29}$$

whereas the slip frequency is determined with the use of the i_{qs}^* as follows [167, 168]:

$$\omega_{sl} = \left[\frac{L_m}{T_r \psi_r} \right] (i_{qs}^*) \tag{5.30}$$

This is how the electrical flux angle is defined [167, 168]:

$$\theta = \int [\omega_m + \omega_{sl}] dt \tag{5.31}$$

The i_{qs}^* is determined deriving from the torque reference as pointed out [167, 168]:

$$i_{qs}^* = 1.5 \left(\frac{1}{p} \right) \left[\frac{L_r}{L_m} \right] \left(\frac{T_e^*}{\psi_r} \right) \tag{5.32}$$

Consequently, the current reference values of the stator current components are changed into three-phase current references, i_a^*, i_b^*, i_c^* with the aim of comparing them with the measured values in the present regulators. Following this, the current regulators create the inverter gating signals' reference voltage [167].

Equations 5.28, 5.32 exhibit that it is possible to adjust the electromagnetic torque separately as the flux constant is maintained. The electromagnetic torque is also compared to the i_{qs}, and the flux is correlated to the field current component i_{ds} through a linear first order function by means of T_r (the rotor time constant).

5.3 Model of ACIM with Broken Rotor Bars

The modified rotor resistance matrix, in this case, can be written as[169]:

$$r_r^* = \begin{bmatrix} (r_r + \Delta r_{ra}) & 0 & 0 \\ 0 & (r_r + \Delta r_{rb}) & 0 \\ 0 & 0 & (r_r + \Delta r_{rc}) \end{bmatrix} \tag{5.33}$$

whereby Δr_{ra} , Δr_{rb} , Δr_{rc} stand for rotor resistance changes in phase a, b and c, as a result of BRB.

A healthy induction motor's phase rotor equivalent resistance is given as:

$$r_r \approx \left[(2N_s)^2 \Big/ (N_b/3) \right] r_b \tag{5.34}$$

whereby r_b stands for the rotor bar resistances, N_s & N_b are the equivalent stator winding turns and the number of total rotor bars. When there are n_{bb} BRBs, the increment $\Delta r_{ra,b,c}$ in every phase is achieved by[169]:

$$r_r^* \approx \left[(2N_s)^2 \Big/ [(N_b/3) n_{bb}] \right] r_b \tag{5.35}$$

$$\Delta r_{ra,b,c} = r_r^* - r_r = \frac{(2N_s)^2}{N_b/3 - n_{bb}} r_b - \frac{(2N_s)^2}{N_b/3} r_b = \frac{3n_{bb}}{N_b - 3n_{bb}} r_r \tag{5.36}$$

For BRB to be simulated, the rotor resistance matrix in Equation (5.37) should be substituted using the modified rotor resistance equation (5.41) to *dq0*

$$\Delta r_r^{*qd0} = \begin{bmatrix} r_{r11} & r_{r12} & r_{r13} \\ r_{r21} & r_{r22} & r_{r23} \\ r_{r31} & r_{r32} & r_{r33} \end{bmatrix} \tag{5.37}$$

The matrix elements are given as:

$$\Delta r = r^*_r - r_r \approx \frac{3n_{bb}}{N_b - 3n_{bb}} r_r \tag{5.38}$$

The illustration below shows how the change in resistance has been computed by Equation 5.38 starting: calculate r_r by the Equation 5.34 as shown in Table 5-1:

n_{bb} = Number of rotor bar faults (healthy=0, 0.5 BRB=0.5, 1 BRB=1, 2BRB=2)

N_b = Number of rotor bar=28, r_r = Rotor resistance (1.395 π)

$\Delta r_{healthy}$ = 0.000000000001 π, $\Delta r_{0.5BRB}$ = 0.07896226 π

Δr_{1BRB} =0.1674 π, Δr_{2BRB} =0.38045455 π

Δr_{3BRB} =0.66078947π, Δr_{4BRB} =1.04625 π

Table 5-1 Change in resistance of rotor in (Ω)

Cases	***BRB Severity*** n_{bb}	***Change in resistance*** Δr ***(Ω)***
Base line	0	≈ 0
Half BRB	0.5	0.07896226
One BRB	1	0.1674
Two BRB	2	0.38045455
Three BRB	3	0.66078947
Four BRB	4	1.04625
Five BRB	5	1.60961538

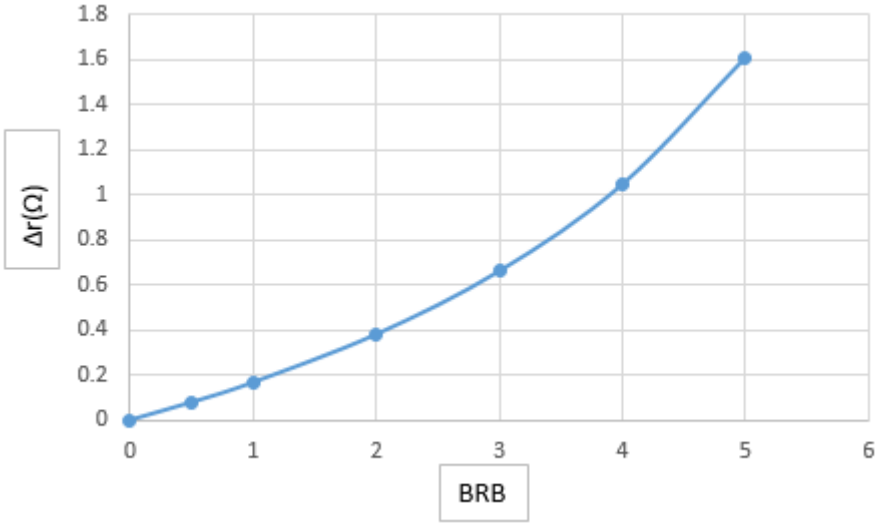

Figure 5-6 Change in resistance of rotor in (Ω)vs BRB severity

5.4 Model of Induction Motor with Shaft Misalignment

More loads will be added to the mechanical system by misalignment, this load, therefore, this will be described as load oscillation

In the load reference, oscillatory signals around the system angular speed were included with the aim of examining the system's response under load oscillation conditions.

The angular speed is incorporated and delivered via a cosine function and multiplied by a gain before adding to the load reference[28].

The fluctuation with an amplitude of ΔT is therefore going to be modulated with the use of the system speed, since ΔT sets the size of oscillations that represents the fault sternness. Below is how the oscillation is added to the load torque reference value as follows:

$$T_{OSC} = \Delta T.\cos\theta \tag{5.39}$$

$$\theta = \int (\omega_r).dt \tag{5.40}$$

5.5 Model Validation

This procedure was carried out to provide a comparison of the response of the model to load variable and the response of the rig. Prior to attempting this, the following is a short explanation of the trial rig applied in this project. The trial rig has a number of parts; both system electronics (control) and electromechanical. The induction motor simulation estimation parameters of the rotor that were used for the procedure have been taken from the drive of variable speed. A few of these factors were acquired from the nameplate of the motor. However, some were approximated in the process of auto-tune accomplished using the drive. The motor conditions are enumerated in the data sheet. The representation diagram displays the vital structural components of the rig test. It made up of a three-phase including; Induction motor, flexible connectors and DC motor used as a load device, the representation chart in Figure 5-7 displays the vital important structural components of the test rig

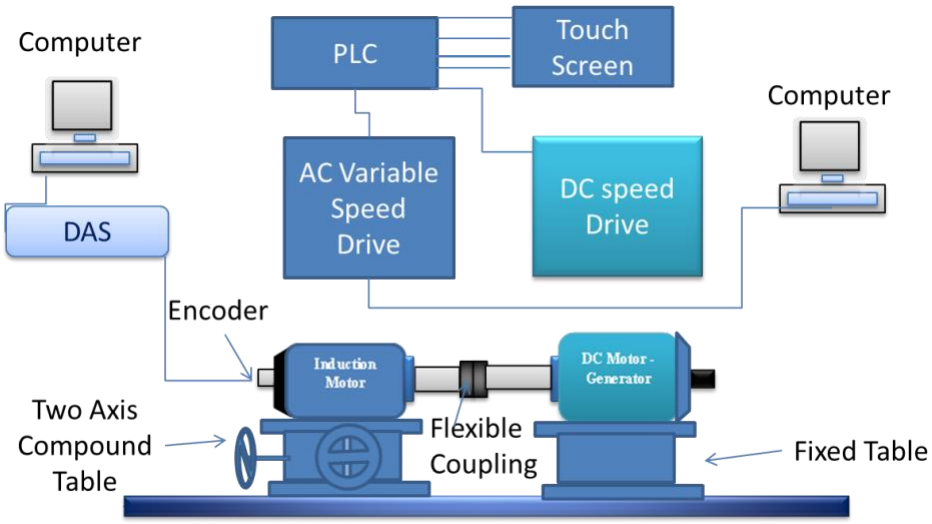

Figure 5-7 Representational diagram of the test rig

To validate the model and simulation method, the current line signals and voltage sourced of both rig and model are presented in Figure 5-8. It demonstrates current line and signals of voltage from both the model and rig are related. The relationship has been achieved at a constant state and full speed in between load 0% and 100%. Figure 5-8 (a) and (b)

explain signals of the current in the domain of time, whereas Figure 5-8. (c) and (d) demonstrate the voltage in the domain of time.

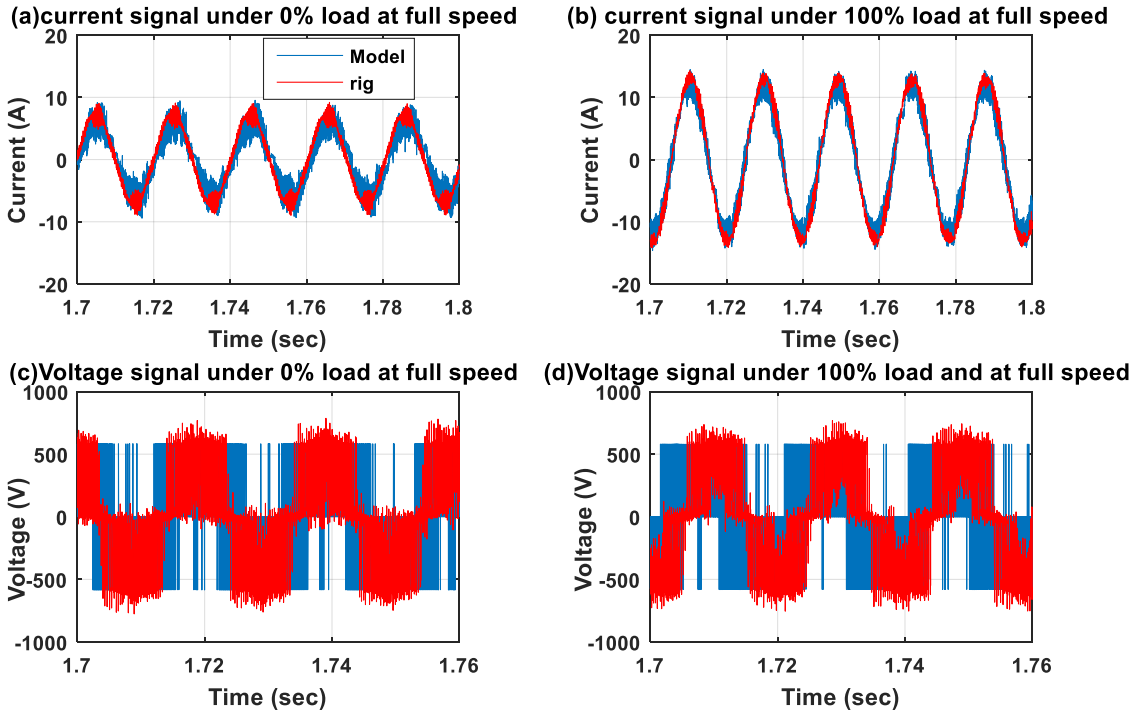

Figure 5-8 Waveform comparison between predicted and measured voltage and current signals compared at full speed under load (0% and 100%)

Figure 5-9 are spectra of current and voltage signals, which is obtained by applying Fourier transform to the time domain signals. Signals of voltage and current of model prediction showed the same variations as those sourced from the rig in the voltage and current under load 0% and 100% circumstance.

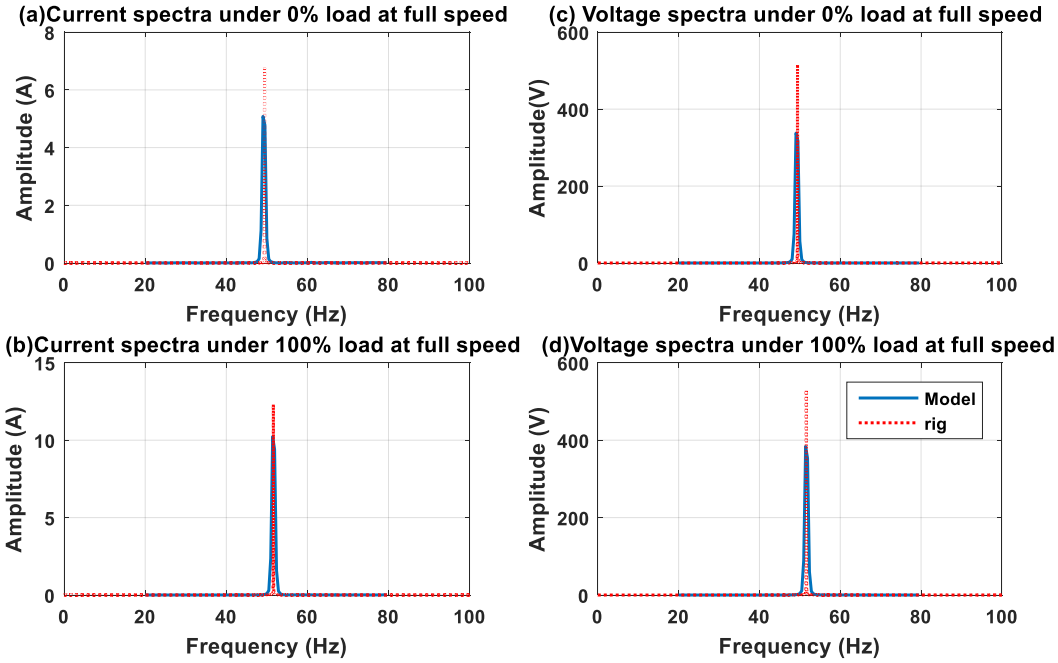

Figure 5-9 Spectrum comparison between predicted and measured voltage and current at 100% speed under load (0% and 100)

5.6 Effect of BRB Conditions

Figure 5-10 shows the characteristic of spectral amplitude with healthy and BRB in ACIM scale of signals of stator current below baseline (BL health) and varied circumstances of BRB (broken rotor bar) at a top speed below 100% load having sensorless mode illustrating the large appearance of sidebands if the BRB is used.

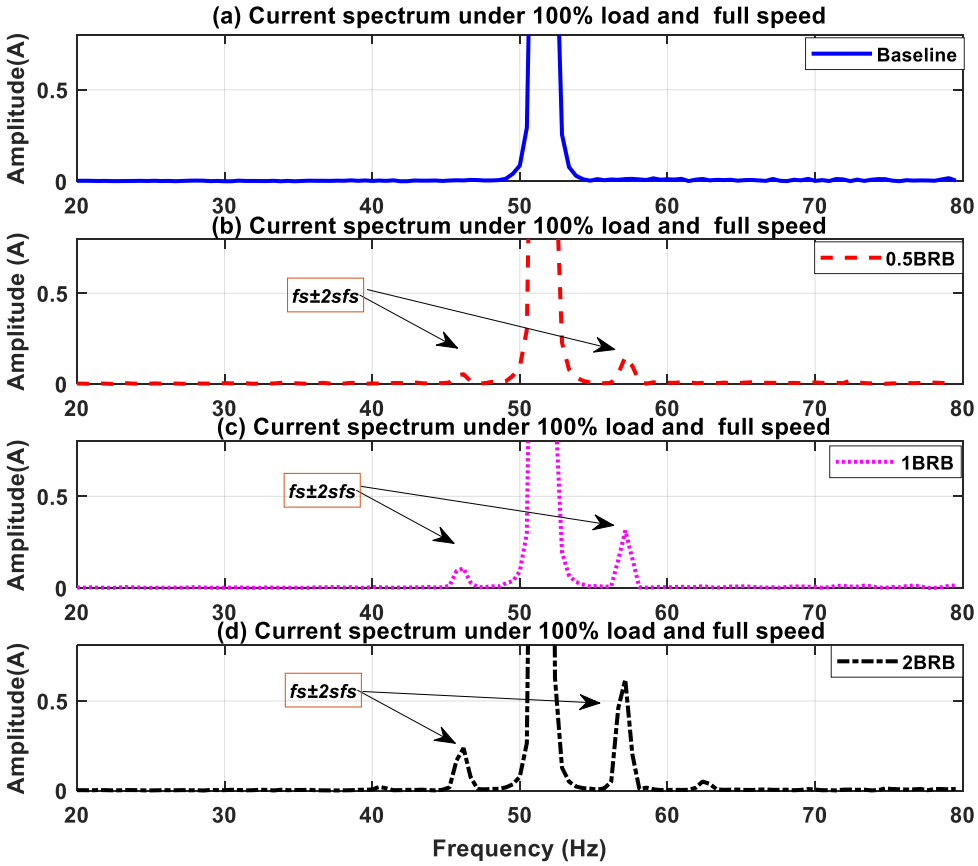

Figure 5-10 General characteristic of BL and BRB cases

5.6.1 Diagnosis of BRB based on Current Signal

As illustrated in Figure 5-11, the signals of spectrum current below BL (health) (baseline) and various circumstances of BRB (0.5, 1, 2) at a top speed below 100% weight having a mode of VSD, the sidebands could have indicated in diverse BRB, the sidebands rise with the increase in BRB, the spectrum of current offers fine indications.

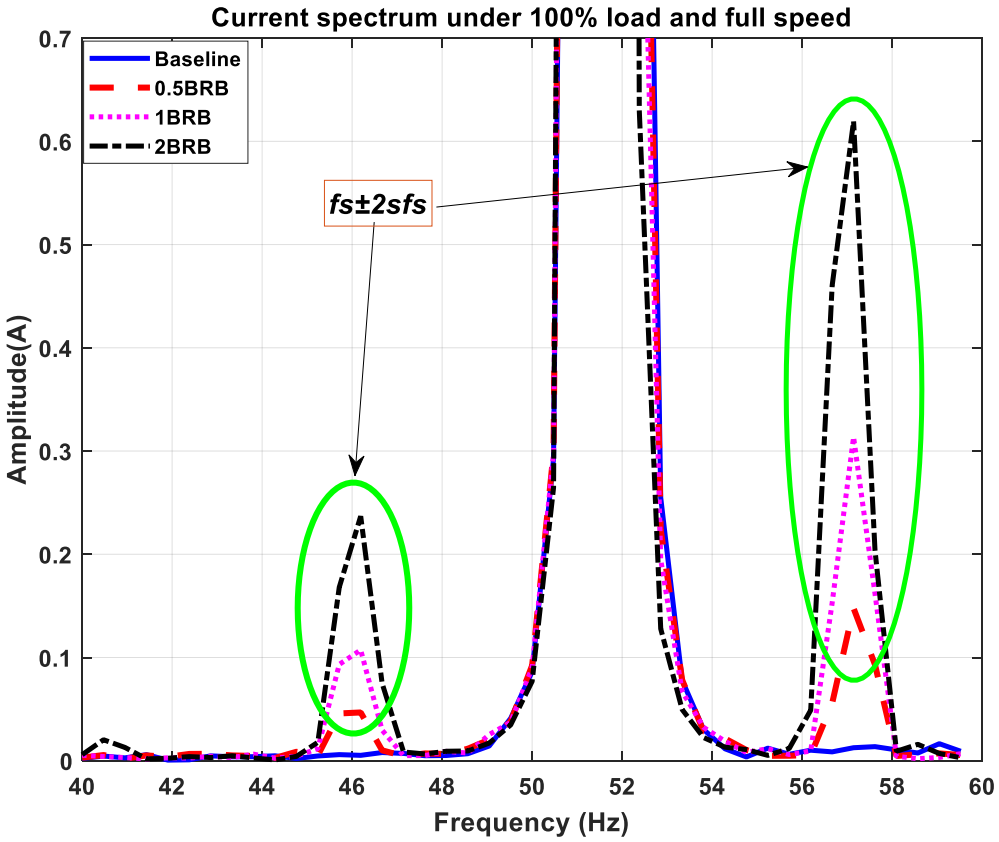

Figure 5-11 Spectrum of current under 100% load with top (100%) speed

Figure 5-11 highlights the electric current spectrum from which it can be observed that rotor faults of an induction motor cause additional components appearing as the sidebands around the supply frequency. It also means the fundamental supply component is modulated by the addition components, making the current signal become nonlinear. In current and voltage spectra, these additional components show as asymmetric sidebands around the supply frequency. The amplitudes of these sidebands are influenced by rotor inertia, load variation, power factor and machine impedance. In Figure 5-11, the amplitude of upper sideband fs+2sfs is noticeably larger than lower sideband fs-2sfs. As a result of the unexpected vibrational behaviour of broken bars, the characteristics feature value of torque are changed and cause the speed of motor and variation in torque level curve to change, as shown in the upper sideband, respectively, the change in the lower sideband is because of real BRB faults[61].

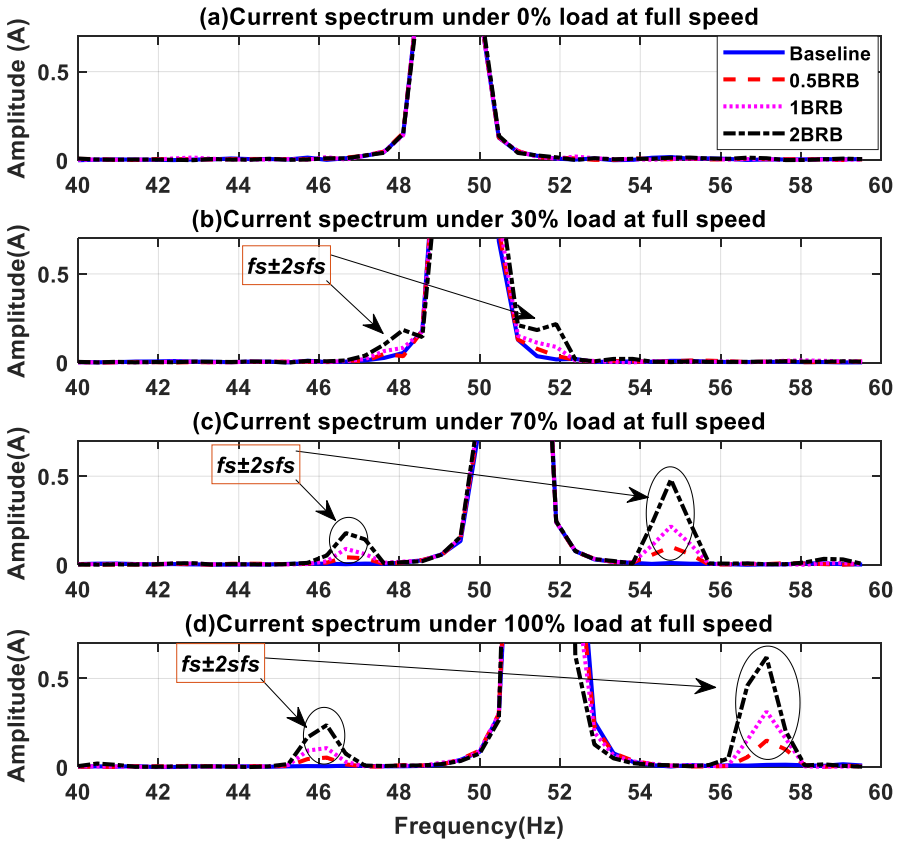

Figure 5-12 Current spectrum under different loads at 100% speed

Figure 5-12 presents the current spectrum signals below Baseline BL (health) and varied instances of BRB, denoted as 0.5BRB, 1BRB and 2BRB at full speed when the motor is applied with 0%, 30%, 70%, and 100% loads and supplied with sensorless mode of VSD. It cannot show the sidebands underload 0% load as the rotor slip is very small. Moreover, the sideband could have indicated under a greater load as the sideband rises with BRB and loads upsurge, showing that the spectrum of the current signals offers good designate of BRB problems.

5.6.2 Diagnosis of BRB based on Voltage Signal

Figure 5-13 presents the spectrum of voltage under load 100% at full (100%) speed, the *fs±2sfs* sidebands correlated with a damaged bar of the rotor. The sideband adjustment in the intensity of components rates as a result of BRB in machinery, in comparison with the healthy motor, it provides good BRBs diagnosis.

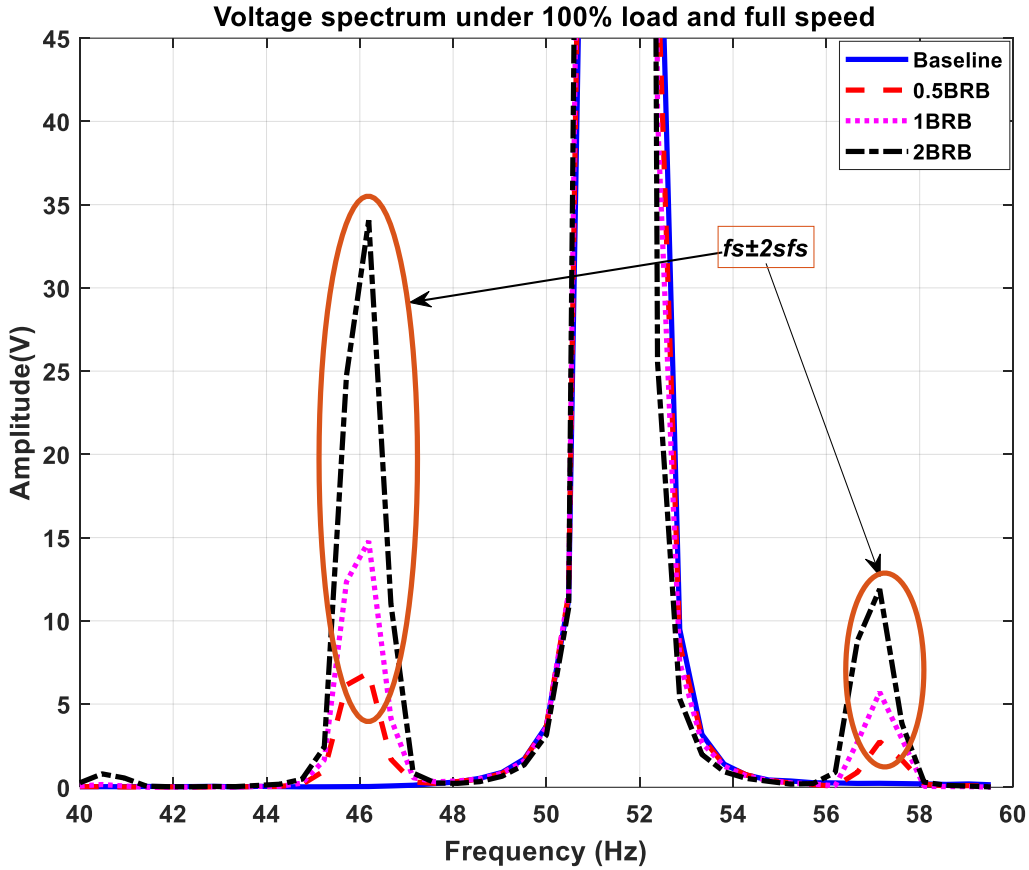

Figure 5-13 Spectra of voltage signals under load 100% at highest (100%) speed

The voltage spectra for various BRB scenarios along with the healthy Baseline (BL) condition are presented in Figure 5-14, which is obtained when the system operates with 100% speed under 0%, 30%, 70%, and 100% loads on VSD mode. It cannot perceive the sideband under load 0% due to very small slip. Moreover, the sidebands exhibit a gradual increase of amplitudes with the BRB severity and operational loads. Especially the range of voltage provide enhanced indication compared to current spectrum in Figure 5-12. It shows that the voltage signal can have more accurate information for diagnosing the fault

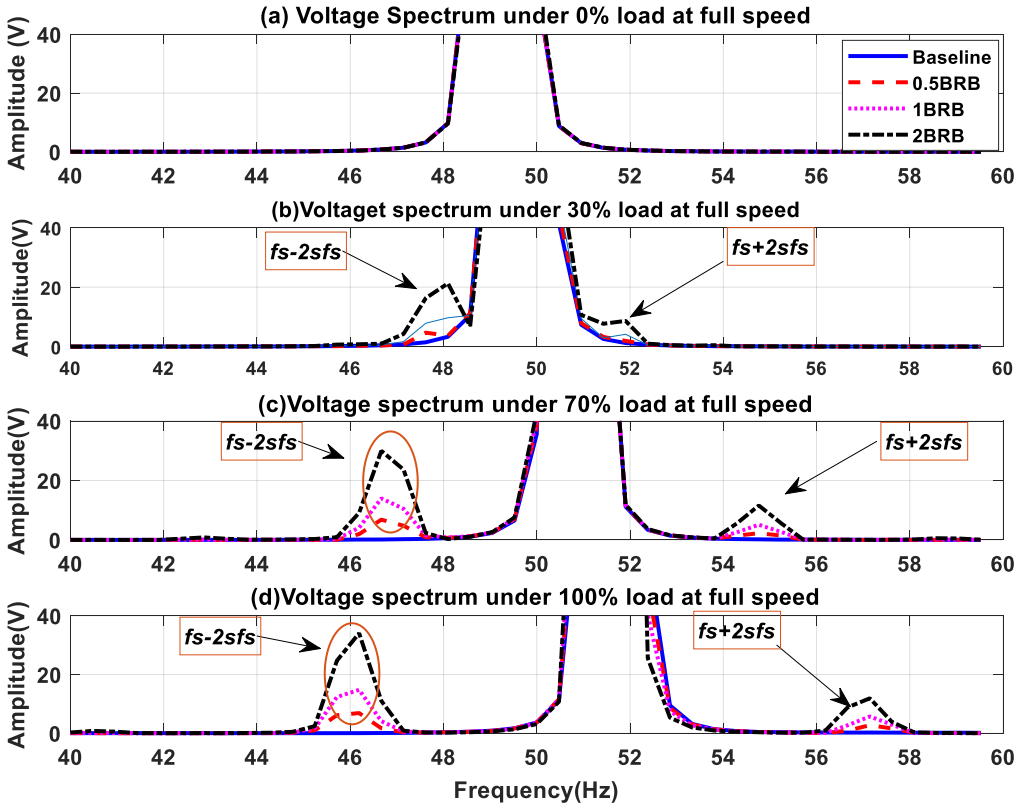

Figure 5-14 Spectrum of voltage in varied load at 100% (top) speed

5.7 Effect of Shaft Misalignment Conditions

Figure 5-15 shows how the range of replicated stator signals of current under BL (health baseline) and various situation of the misaligned shaft (MA) at top-most speed under 100% load having sensorless mode depicts the intensity of sidebands at $f_s \pm f_r$ when the (MA) is used.

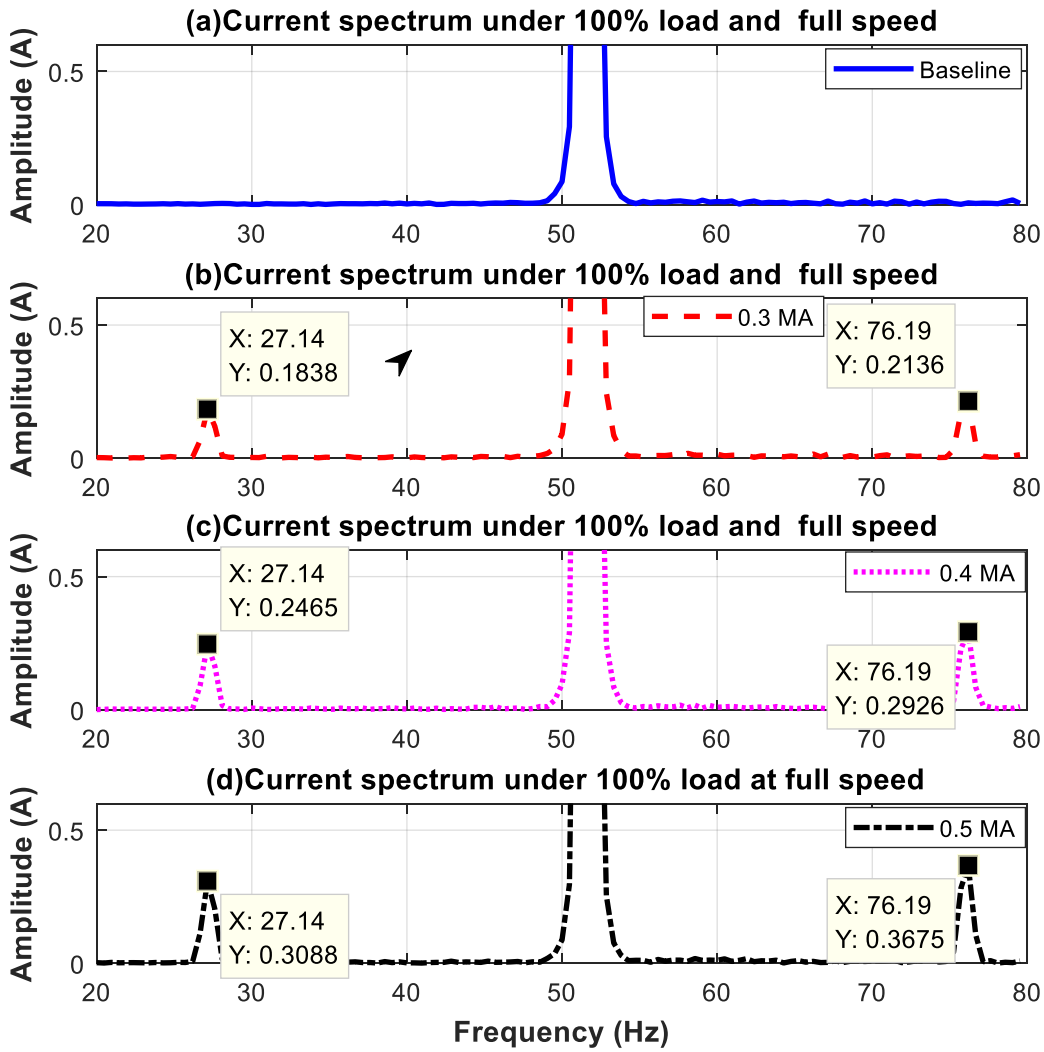

Figure 5-15 General features of misalignment and healthy situations

5.7.1 Diagnosis of Misalignment based on Current Signal

Figure 5-16 clearly illustrates that the spectrum of current signals under diverse misalignment (MA) cases and BL (health) at full speed, under load 100% under sensorless mode. It can see the amplitude $f_s \pm f_r$ under diverse (MA). When the MA raises the amplitude increases by a similar amount in current and voltage, this is due to the impact of MA in vibration above the voltage and current.

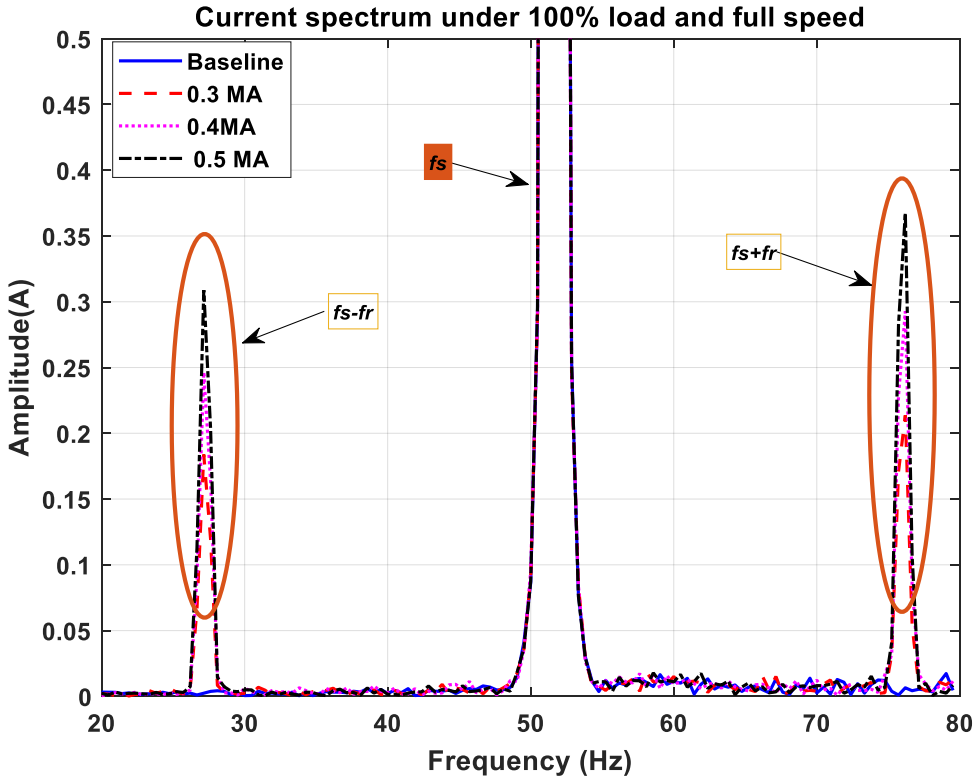

Figure 5-16 Current spectra under full load at full speed

Figure 5-17 clearly illustrated that, the spectrum of voltage and current signals under diverse misalignment (MA)cases and BL (health) at full speed under load 0%, 30%, 70%, and 100% under sensorless mode. Under diverse load, it can be seen the amplitude $f_s \pm f_r$ in a situation where the MA raises the amplitude increase in each and every load.

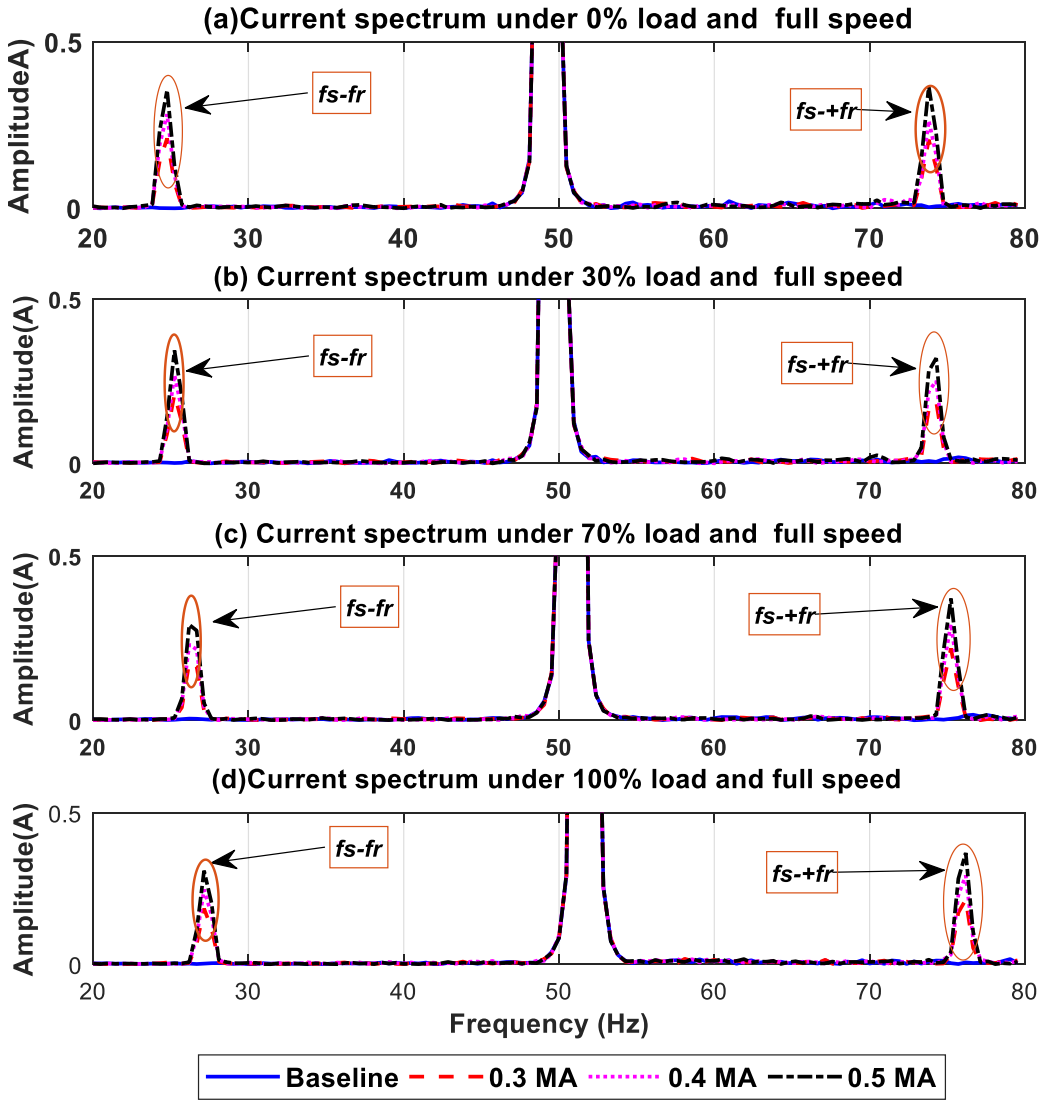

Figure 5-17 Current spectra under different load at full speed

5.7.2 Diagnosis of Misalignment based on Voltage Signal

Figure 5-18 shows that, the spectrum of voltage signals under BL (health) and different cases of misalignment MA at full speed under load 100% under sensorless mode. It is capable of seeing the amplitude $f_s \pm f_r$ under diverse (MA) cases. In a situation where the MA raises the amplitude there is an increase in each and every case whereas in Figure 5-19, the spectrum of voltage signals under BL (health) as well as diverse misalignment cases of MA at full speed under load 0%, 30%, 70% and 100% under sensorless mode. It

is capable of seeing the amplitude $f_s \pm f_r$ under diverse load. This is in a situation where the MA increases, the amplitude increase in all loads has similar outcomes in current and voltage as a result of the impact of MA in vibration above voltage and current.

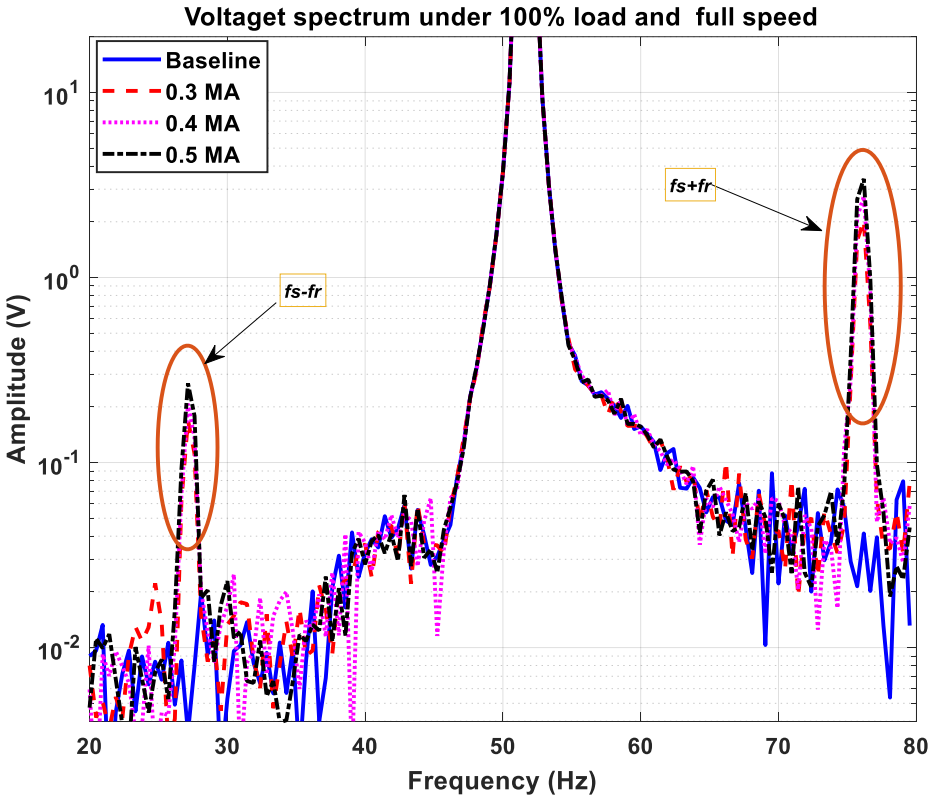

Figure 5-18 Spectra of Voltage under complete load at 100% speed

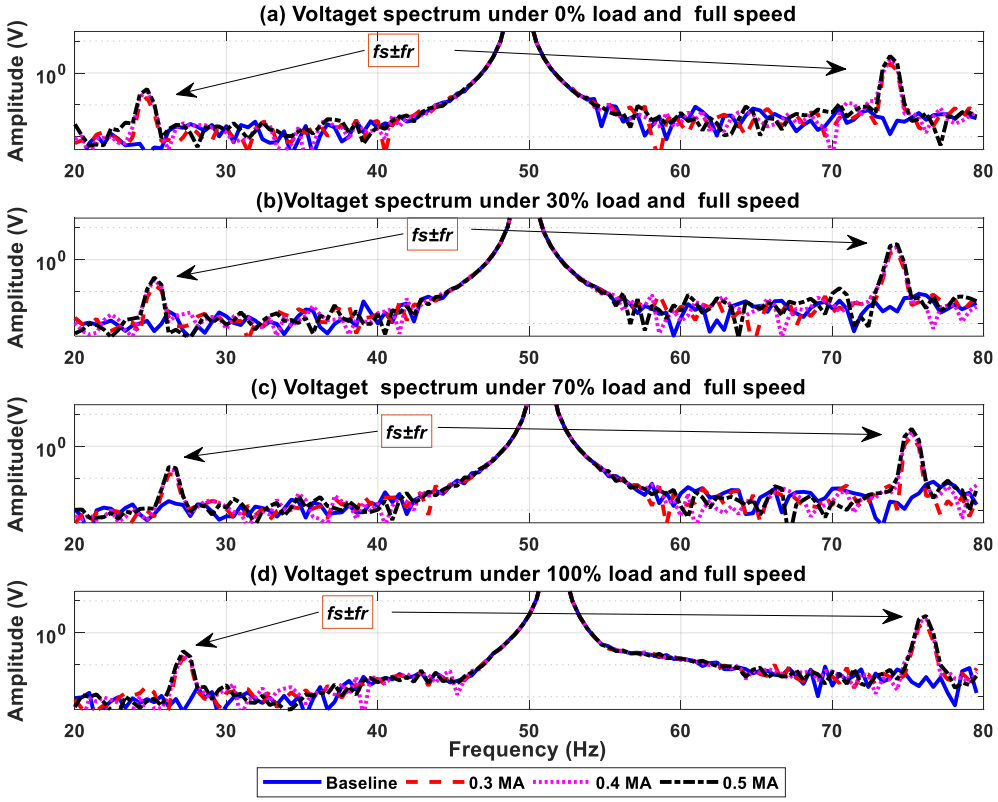

Figure 5-19 Spectra of voltage signals under various loads at 100% speed

5.8 Effect of Combination of BRB and Shaft Misalignment Conditions

As presented in Figure 5-20, the range of imitation stator signals of current under BL (baseline, healthy) and various cases of the damaged bar of the rotor (1BRB& 2BRB) at 100% speed under 100% load in sensorless model displays large readings of sidebands during application of the BRB. Also it shows two instances of MA (0.3 & 0.5), both can perceive the conduct of an organisation under varied conditions and the voltage in Figure 5-21.

h

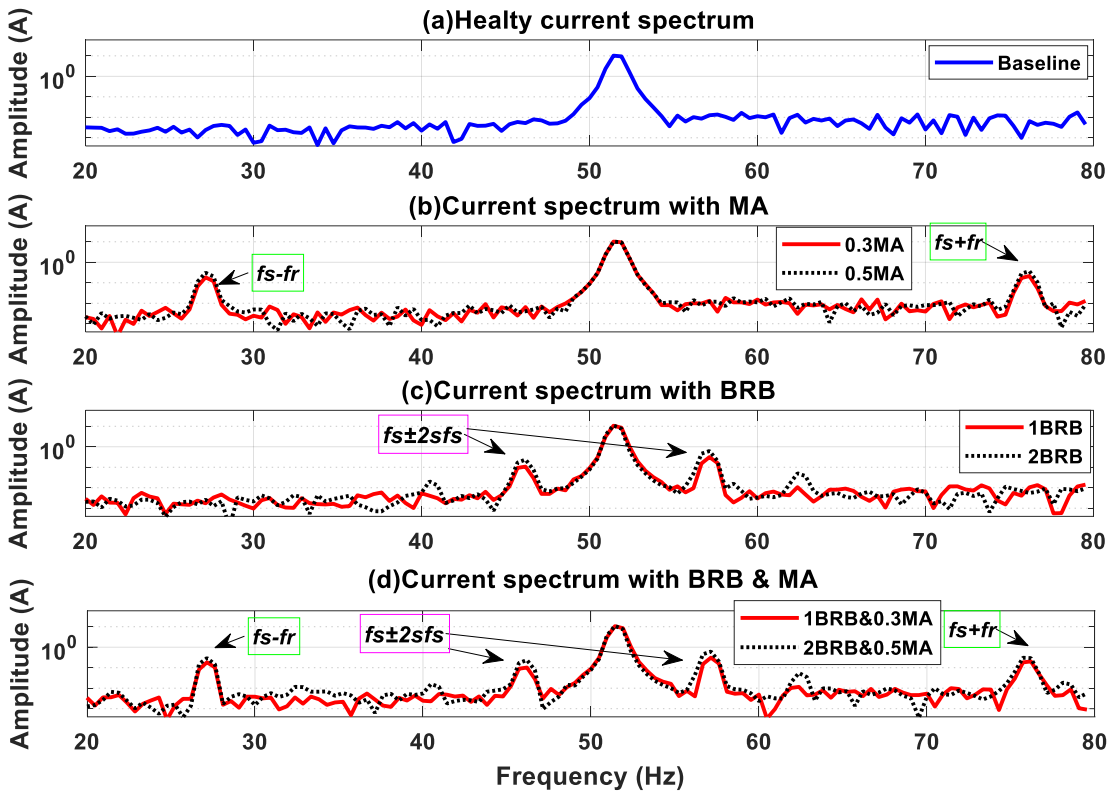

Figure 5-20 General features of current signals for faulty and healthy cases

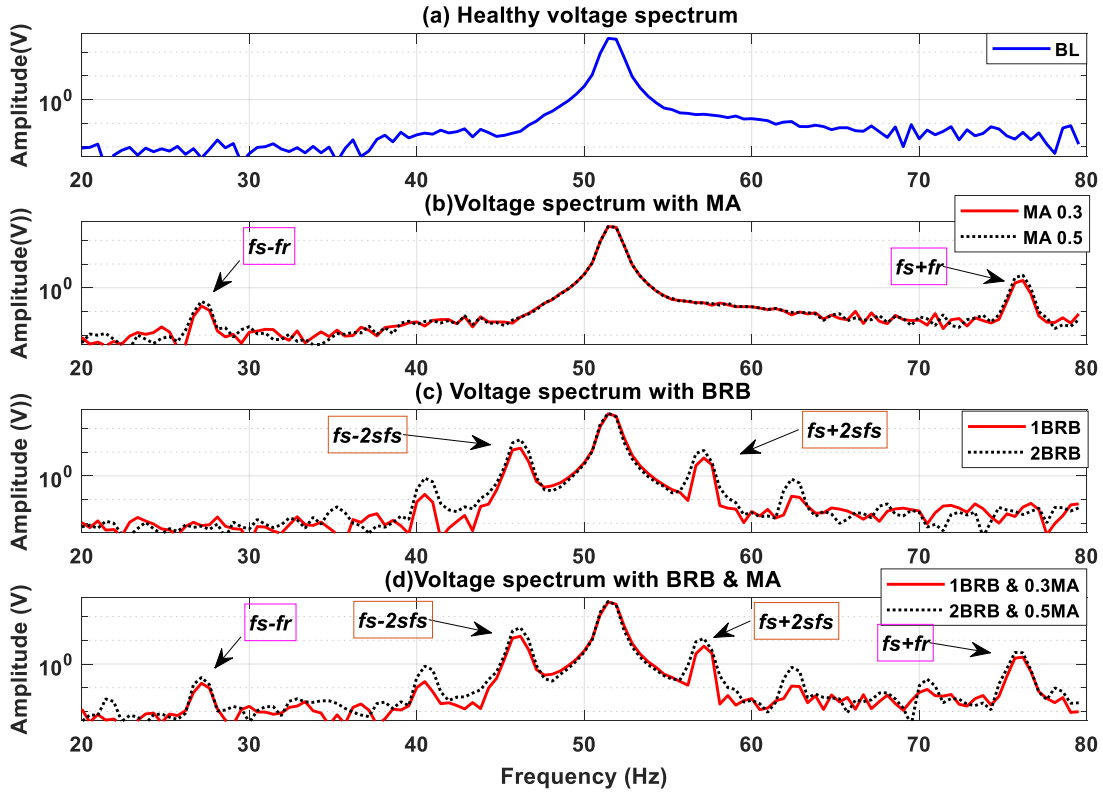

Figure 5-21 General features of voltage signals for faulty and healthy operations

5.8.1 Influence of Prompted Misalignment on The Characteristics of BRB Cases.

As shown in Figure.5-22 and 5-23, the spectrum of currents vary in the sideband frequency amplitudes of 2BRBconstituents as a result of varied misalignment in the machine are reduced if the misalignment improves under similar factors. Conversely, in the spectrum of voltage, the sideband frequency amplitudes in 2BRB under similar factors escalate if misalignment upsurges.

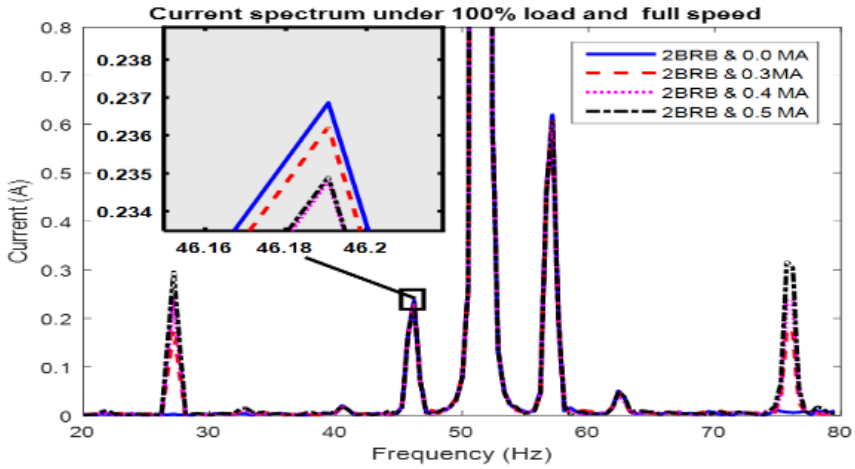

Figure 5-22 Results of misalignment on the characteristics of BRB; current

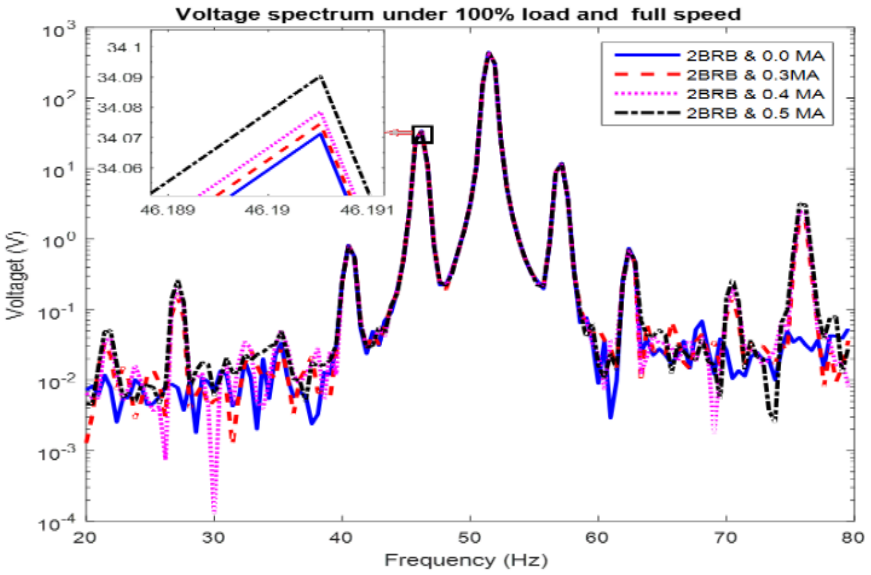

Figure 5-23 Results of misalignment on the characteristics of BRB; voltage

5.8.2 Effects of Induced BRBs on The Features of Misalignment Cases

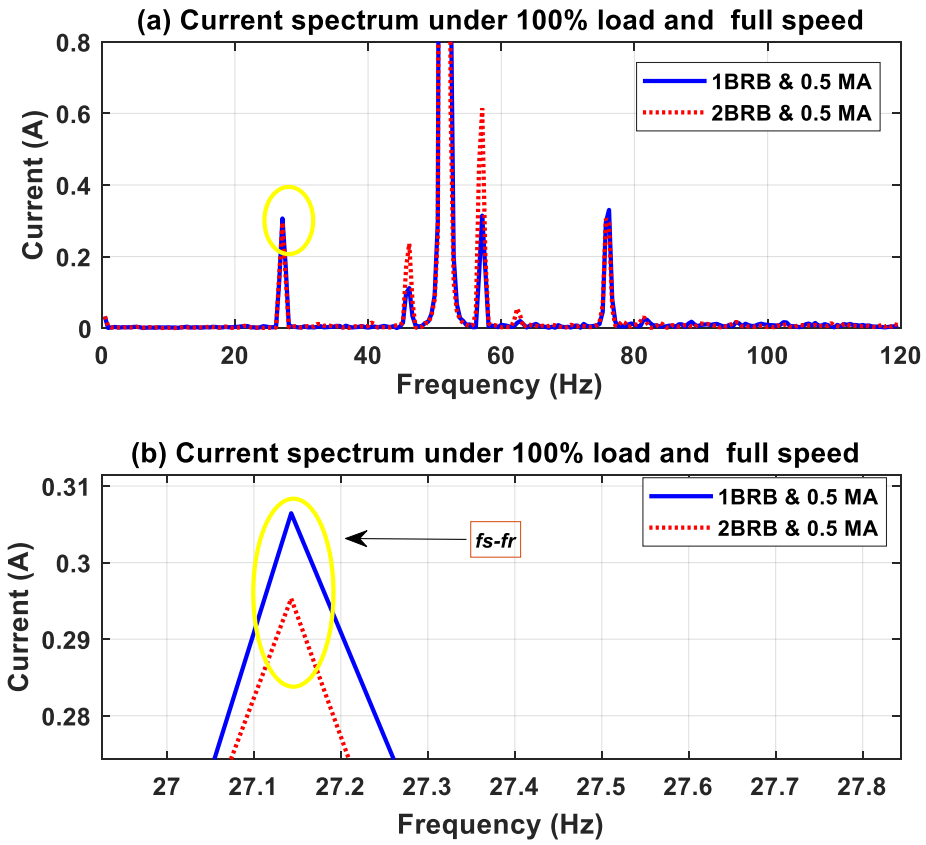

Figure 5-24 Results of BRB on the characteristics of misalignment on current

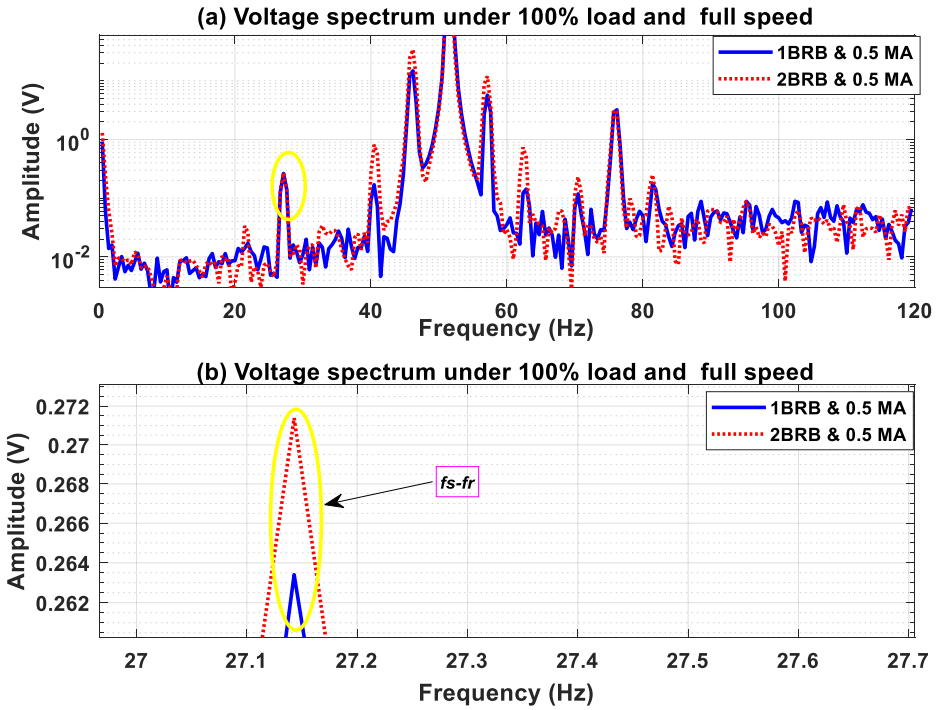

Figure 5-25 Results of BRB on the characteristics of misalignment on voltage

Figure 5-23 demonstrates that the sideband spectrum amplitudes of (*fs-fr*) current are varied under similar MA, unlike BRB. It can be seen from the top of MA under 2BRB less than 1 BRB were lowered under similar factors. Yet, in Figure 5-22, the spectrum of voltage and the side band amplitudes frequency (*fs-fr*) of 2BRB under similar factors seem larger than 1BRB when identical misalignment is used. This is because of the difference in VSD voltage required to achieve preferred vibration speed compared to voltage and current.

5.9 Summary of Chapter 5

This chapter presents the study of the diagnostic features through numerical simulations using ACIM mathematical models consists of voltage, current, and flux linkage equations, Especially, the BRB is modelled by increasing the rotor resistance values and misalignments is by.an oscillatory load applied to the rotor.

The purposes of mathematical modelling include monitoring the states of a modelled system, and fault detection. The Simulink model was used to study the outcomes of

broken rotor bars, misalignment, and combined faults on electrical supply parameters, in addition to the healthy ACIM model. The simulation is based on the same features as the test rig. It was carried out using both healthy and fault model under zero, 30%, 70% and 100% of full load. The outcomes clearly confirm, the system's behaviour in the existence of mechanical and electrical faults. Therefore, it is possible for a foundation of fault detection and diagnosis to be applied.

Finally, the results for both healthy and fault cases predicted by the model are compared with the equivalent measurements taken during the experimental tests. The achieved results conclude that the predicted outcomes based on the model are very alike to the experimental consequences and so the electrical signals can be relied on for the detection of motor faults.

Chapter 6 Test Facilities and Test Procedure

In this chapter, a detailed examination of the general specifications of the test rig facility employed in this study is conducted. Wider spectra of systems are also examined such as mechanical control systems as well as the electrical and mechanical faults arising from the induction motor electrical signals. In addition, there is also an explanation of the instrumentation employed such as sensors, equipment and acquisition systems. Lastly, the assessment of the repeatability checks for the different signals is conducted.

6.1 Introduction

In this research, the test rig utilised is very critical since it allows the operator to execute a series of tests that are repeatable and deterministic in nature thus enabling the obtaining of data even in different fault, speed and load conditions. In addition, identically repeatable tests can be performed for both fault and health instances. It is also possible to institute changes for severe faults while accurately applying the same parameters and tests. The building and designing of the test rig is done in a way that it allows simulation of real industrial applications. Moreover, the equipment used is designed in a manner that suits the industrial use and applications in a typically used environment. This chapter also explores the test rig's construction as well as the data acquisition, software used and the test rig's operation.

6.2 Test Rig Construction

In the examination of the test rig, the understanding of its two main parts is crucial. These parts include the control system/electrical part and the electro-mechanical/mechanical part.

6.2.1 Mechanical and Electromechanical System of Test Rig

The electro-mechanical and the mechanical part is made up of flexible coupling, DC motor, 4kW 3 phase AC induction motor with speed 1420 RPM, flexible spider coupling which connects each element to another next to it, a tachometer is attached to the DC motor as well as the encoder which is coupled to the AC motor shaft as demonstrated by Figure 6-1 below.

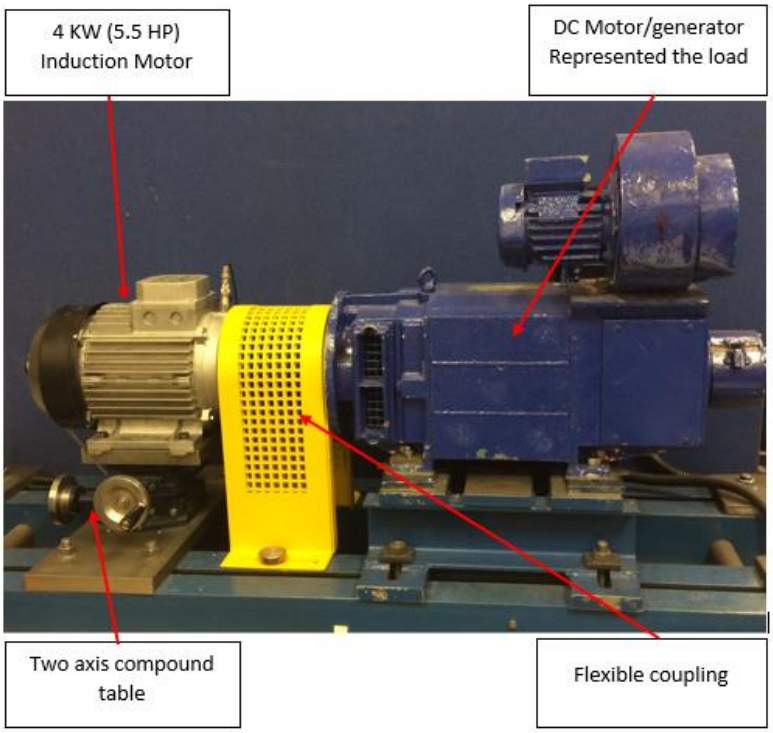

Figure 6-1 Electromechanical and mechanical Parts of the test rig

6.2.1.1 AC induction motor:

The Table 6-1 clearly shows the ACIM technical specification employed in the test rig.

Table 6-1 Specifications of ACIM

parameters	value
Number of phases	3
Motor power	4 (kW)
Rated voltage (Δ/Y)	230/400 (V)
Motor speed	1420 (rpm)
Number of poles	4 poles/phase
Supply frequency	50 (Hz)
Number of stator slots	36
Number of rotor slots	28
Rated current (Δ/Y)	15.9/9.2 (A)

6.2.1.2 DC Motor

The test rig uses a Siemens DC generator, or DC motor, working as a force load which can be used through the Siemens micro master controller. The max power is approximately ten kilowatts when the speed is 1720 RPM, the current and Armature voltage is 35 A and 350 V. Also the DC motor can be used deliver the torque loads, which make the control of load easier.

6.2.1.3 Spider Flexible Coupling

As shown in Figure 6-2 the spider flexible coupling provided a flexible joining between the drive shaft of the AC motor and DC generator. This coupling has a three parts close fitting connection to ensure perfect alignment. The specifications and type of Flexible Coupling are shown in Table 6-2.

Figure 6-2 Flexible coupling

Table 6-2 Specifications of flexible coupling

Manufacture	Sinocera
Type	Fenner
Size	130
Outer diameter	130 mm
Border diameter	14-42 mm
Hub diameter	105 mm
Hub length	18 mm
Rubber width	36 mm
Taper lock bush size code	1610

6.2.2 Electronic Part of Test Rig

Figure 6-3 demonstrates the electronics or control system, which is made up of the DC drive, power supplies, AC variable speed drive, circuit breakers intended to protect both DC and AC motors, circuit breakers for protecting the drivers and a programmable logic controller (PLC).

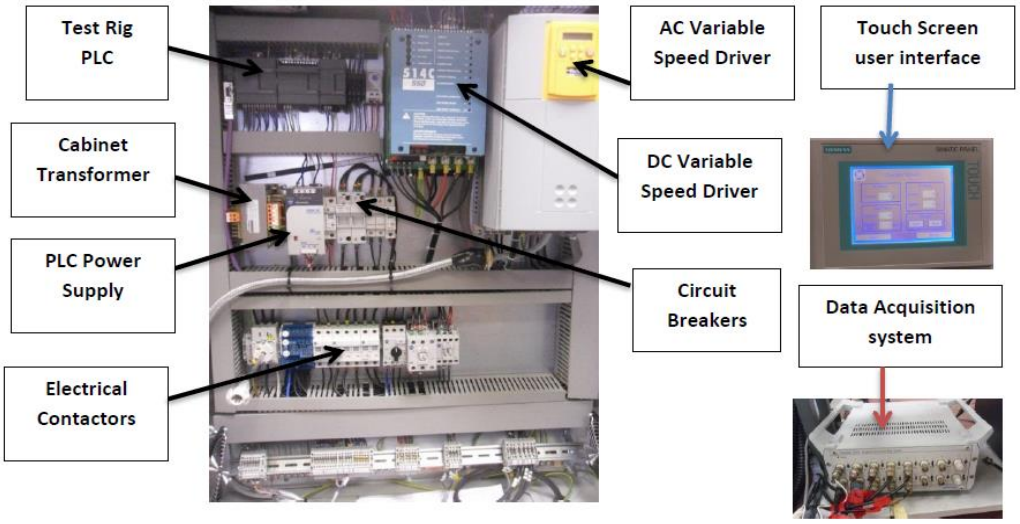

Figure 6-3 Photograph of Electronic side (control system) in the test rig

6.2.2.1 The Variable Speed Drive (AC)

The Parker 650V is the variable speed drive (VSD). This VSD has 2 inputs which are analogue, 6 digital inputs, 1 analogue output and 2 digital outputs. Moreover, it also has slip compensation, a sensorless vector having automatic fluxing, frequency/volt control having linear/fan low profile and two-speed control modes. Table 6-3 presents the drive's specification.

Table 6-3 The parker 650 V drive technical specifications

Product Description	AC variable speed drive
Model	650 V
Frequency Output	0-240 Hz
Current Output	0-33 A
Voltage Output	0-460 v ±10%
Rated motor power	15 kW
Frequency Switching	3 kHz nominal
Voltage Boost	0-25%
Flux Control	1. V/F control with linear or fan law profile 2. Sensorless flux vector
V/Hz Profile	-Constant torque - Fan Law
Inputs Analogue	2 inputs – one is configurable; voltage or current
Outputs Analogue	1 configurable voltage or current
Digital Inputs	6 configurable 24V DC inputs (2 suitable for encoder)
Basic error	± 0.5% of full range

6.2.2.2 DC Variable Speed Drive

The test rig DC motor/generator plays a critical role in providing a controlled variable load, specifically on the AC motor. The Parker 514C series is the DC drive utilised in this study because this drive is intended to be used in an industrial application. The DC Shunt wound motor's speed is regulated by this drive. Therefore, in all the four Quadrants of the operation, the motor speed is also controlled by this drive, through controlling the DC motor's speed by use of a linear system that is closed looped as well as providing armature voltage's feedback signal. table 6-4 shows the specification of the DC drive.

Table 6-4 The 650 V DC drive technical specifications

Product Description	DC speed drive
Model	514C
Control Action	Closed Loop with Proportional Integral Control
Speed Feedback	Selectable: Armature Voltage or Tacho-generator
100% Load Regulation	2% when Armature Voltage mode used; 0.1% when Tacho-generator mode selected
Maximum Torque/Speed Range	20:1 when Armature Voltage mode used; 100:1 when Tacho-generator mode selected
inputs Analogue	7 non-configurable inputs
outputs Analogue	7 outputs: Setpoint Ramp, Total Setpoint, Speed, Current Demand, Current Meter (Bipolar or Modulus), +10V reference and -10Vreference.
S Ramp and Linear Ramp	Symmetric or asymmetric ramp up and down rates
Current Limit	Adjustable 110% or150%
Supply Voltage	110 – 480 Vac ± 10%
Nominal Armature Voltage	90 Vdc at 110/120 Vac 180 Vdc at 220/240 Vac 320 Vdc at 380/415 Vac
Overload	150% for 60 seconds
Field Current	3 A DC

6.2.2.3 Software for Data Acquisition

The information gathered by the data acquisition system following the test rig being carried out is relayed to the PC in order to be processed and analysed. In order to enhance speed indication, the data acquisition system has the encoder directly connected to it. For signals to be analysed, all of them are transferred into Matlab format, which will also be studied and investigated by the help of Matlab code specifically designed for these kind of scenarios. Figure 6-4 is a photograph of the data acquisition system; Table 6-5 shows the data acquisition system's main specifications.

Figure 6-4 Photograph Global Sensor Technology YE6232B DAQ system

In the process of conducting the experiment by the help of YE6232B DAQ system comprising of 16 channels having a 24-bit converter, which operates digitally and also in an analogue manner with a maximum of 96 kHz frequency of sampling, all the data was collected. Moreover, in a set of 30 seconds, each set of the dynamic data has been collected, and the length of each set's collected data is 30*96000= 2880000 data points. To guarantee that there are no captured aliased frequencies, the data acquisition system is fitted with the antialiasing filter which is used to perform automatic regulations and a cut-off frequency in a low pass filter which is determined by the pre-selected sampling.

Table 6-5 Technical specifications of the DAQ system

Parameter	Performance
Manufacturer	Sinocera YE6232B
Number of Channels	16 channels
A/D resolution	24 bit
IEPE power supply	4 mA/+24 VDC
Input range	±10V
Gain	Selectable either 1, 10 or 100
Filter	Anti-aliasing
Sampling rate (maximum)	96kHz per channel, Parallel sampling
Interface	USB 2.0

6.2.3 Measuring Devices and Equipment

6.2.3.1 Current and Voltage Transducers

The power supply measurement box, which is shown in Figure 6-5, was designed to measure both currents and voltage by utilising the current and voltage transducers that are demonstrated in Figure 6-5. Every transducer produces a voltage output, which is corresponding to the measured parameter's amplitude. The data acquisition system has been connected to this device. The three line currents and voltages represent the measured box's inputs whereas the three line currents and voltages represent the outputs. The LEM LV 25-P is the voltage transducer while the ABB EL55P2 is the current transducer. Table 6-6 and 6-7 respectively show the voltage and current transducers' specifications.

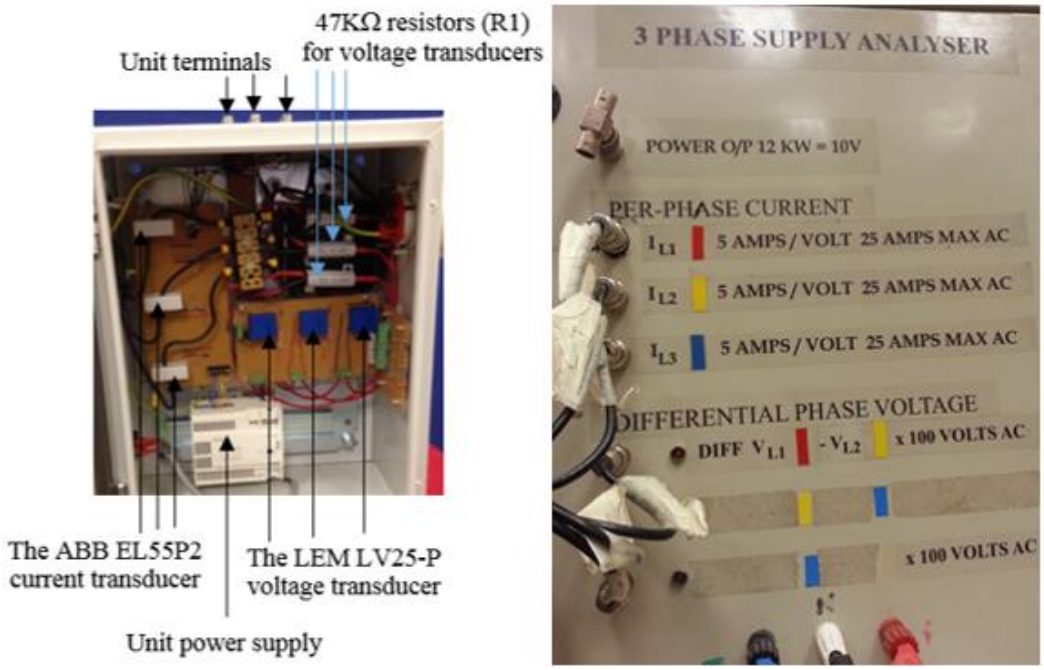

Figure 6-5 Electrical supply parameters measuring device

Table 6-6 Specifications and type of voltage transducer

Brand and Type	*LEM* Voltage Transducer LV 25-Pt
Primary nominal voltage (V_{pn})rms	10:500 V
Primary nominal current (I_{pn})rms	10 mA
Primary current, measuring range	0 : ±14 mA
Secondary nominal current (I_{sn})rms	25 mA
Supply voltage (±5%)	± (12:15) V
Current consumption	10(@±15V) + I_s mA
Overall accuracy	±0.9% @ (I_{pn} , 25°C and ±15V)
Linearity error	<0.2%
Response time to 90% of I_{pn} step	40µs

Table 6-7 Specifications and type of current transducer

Technology	Hall Effect
Primary nominal current (I_{pn}) rms	50 A
Supply voltage (Va)	±(11:15.7) V
Measuring range @ Va	0:±80 A
Secondary nominal current (I_{sn}) rms	25 mA
Thermal drift/ I_{sn}	$2*10^{-4}$ /°C
Bandwidth (-1 dB)	0:200 kHz
Accuracy	±0.5% @ (I_{pn} , 0:70°C and ±15V)
Linearity	Better than 10^{-3}
Response time	<0.1 µs

6.2.3.2 Accelerometers and Thermocouples

Accelerometers: these are devices fixed on the end-caps of bearing and are used to quantify the motor casing's vibration. Additionally, these devices were placed vertically as well as horizontally on the drive, so that each one was connected to the DAS.

Thermocouples: the induction motor's temperature is taken using K type thermocouples. When the signal from the thermocouple is received, it is then sent to the temperature-processing unit in order to be filtered and magnified.

6.2.3.3 Shaft Encoder

Shaft Encoder is a device that is used to quantify the IAS (the instantaneous angular speed), and through the analysis of its data, the IAS is usually achieved. In every angular degree, there was a squared pulse output produced and measured. Additionally, in every complete revolution, the square pulse produced was 100. The Hengstler shaft encoder that the torsional rigid rubber coupling connects it to shaft motor is shown in Figure 6-6. The encoder's outputs, which are connected to the DAS both channel through 1 and 2. The IAS calculation is based on the square waves periodic spacing rather than their strength. The description of the encoder is presented in Table 6-8.

Figure 6-6 Hengstler Shaft Encoder

Table 6-8 Specification of encoder

Manufacturer	HENGSLER
Type	RI 32
Mounting	Round flange
Number of pulses	100
Shaft diameter	5 mm
Maximum speed	6000 rpm
Operating temperature	-10 – 60 C
Supply voltage	DC 5V 10%

6.2.3.4 Dial Indicator

The Dial indicator is important because it uses d in order to align the rig. Furthermore, this indicator is referred to as EDI-125, having the accuracy of ±0.005mm, as well as a measurement range of 12.7 mm and a resolution of 0.001 mm. For the Dial Indicator to be fitted on the shaft and easily adjusted for alignment, the indicator is fitted to a magnetic base as shown in Figure 6-7 below, which demonstrates how the indicator works during the process of alignment.

Figure 6-7 Digital dial indicator for shaft alignment (test rig)

6.3 Test Rig Operation

When operating the test rig, the operator enters the required setting into the test rig in order to program it through a touchscreen interface on the PLC. These settings encompass the time duration for every cycle as well as the load setpoint and the speed setpoint. The number of program cycles that can be programmed can go up to 15. Moreover, whenever the operator begins that test, the PLC plays the role of sending the required values to the DC speed drive and the AC VSD.

The PLC facilitates the AC VSD by supplying it with the required speed to accurately run the AC motor through that speed. Additionally, it is enhanced by the built-in (MRAS) and PID controller, allowing the AC VSD to adjust accurately and control the motor speed at the high starting torque, this is continually executed by the help of motor simulation and supports the motor instead of waiting for the speed supply from the tachometer or encoder.

The DC drive is critical in receiving of the load setpoint supplied by the PLC. Moreover, the DC drive will provide the control signal to the DC motor thus helping in varying the load on the AC motor based on pregame. The field and armature currents of the DC motor are effectively and continually regulated by the DC drive by the use of three-phase supplying two phases. There is a proportional variation between DC motor variation and the load onto the AC motor variation. This scenario is very significant since it allows an effective study of the control system behaviour at different load and speed conditions.

In the process of AC motor rotating, it rotates the DC motor at the same speed in which it is rotating. The feedback signals are obtained by the PLC from both the DC speed driver and the AC VSD, which include the speed feedback, the DC armature current (load feedback) and the AC current. The set points and all the feedback signals are channelled to the computer through a data acquisition system for them to be analysed. However, after the changes/amendment, nearly all the signals within the AC drive are controlled and observed by the help of the drive's P3 port and the DSEL's software run on a separate PC.

6.4 Faults Seeded

Two defects were considered. These include breakage of the rotor, misaligned shaft, and joint fault (damaged rotor bar having shaft misalignment). The studied errors mean numerous similar errors occurred in the mechanical and electrical structures. Moreover, these faults recognise the supply of power constraints inside a less censored system of controlled transmission is not yet understood. Assessments were executed to note the fault recognition performance system and to study the analysis capabilities of the supply of power limitations, majorly in the mechanical system instance motivated by a sensorless (VSD).

6.4.1 Broken Rotor Bar

The usual instrument of failure due to damages or cracks of bars of the rotor joining the terminal-rings could be as a result of thermal or physical rotation of the rotor throughout the process. This type of fault is often experienced by a number of industrial appliances. The broken bar occurs due to vigorous vibrations and drop in speed rotation. After cracking of the rotor bar, overheating close to the crack occur happens. The cracked bar might disturb the neighbouring bars as this can occur at the beginning of operation, so that the neighbouring bars convey more current leading to more thermal tensions. The high thermal tension may result in the destruction of the laminated rotor. The rotor faults equate to approximately 10% of all failures of electrical machines.

Cases of three BRB having varied BRB difficulties and single baseline instance were investigated using four motors of similar features and in similar working environments. Figure 6-8 illustrates how the case of first BRB consists of a motor having partial BRB that is made by piercing a hole in any part of the twenty-eight bars until the bar is penetrated halfway. The next is made up of one full bar where damaged is formed by boring the hole through the bar's depth. While the third, coupled by the incessant bar damage was made by boring double bars sidewise to through the depth. These three faults situations were made in three individual motors with similar features, and were examined.

Figure 6-8 Pictures describing BRB Faults

6.4.2 Fault involving Misalignment of Shaft

The faultless position of the shafts driving and driven is not attainable in industry. Inappropriate alignments of shafts by doubling results to add vigorous loads and serious problem of vibration in machines rotating results to primary faults and loss of energy.

Disarrangement of shafts have an undesirable effect on productivity and in the long-term disastrous faults due to unrequired vibration, bearings, motor strain and stator short-circuit and rotor windings. In motors of physical induction failures like shaft disorder and unbalance load, faults could be identified through frequencies of sidebands at $f_s \pm f_r$ in the frequency of stator current bands.

Three cases of misalignments and a single case of baseline were examined using four motors of similar features within the same working settings. Adjustments were made in these misalignments through the compound table to repair the motor in the preferred case as shown in Figure 6-9. These three failure scenario's were prompted in three distinct motors having the similar features as presented in Table 6.1 and were noted to have adjacent baseline marks prior to the failure being generated.

As presented in Figure 6- 10, to produce misalignment cases in test rig will require the use of adjusting the compound table, the misalignment was introduced to the rig by adjusting the two-axis compound table.

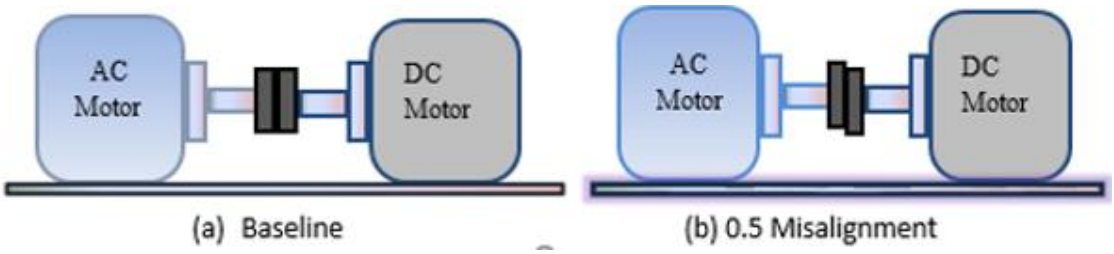

Figure 6-9 Diagram of BL & MA (misalignment)

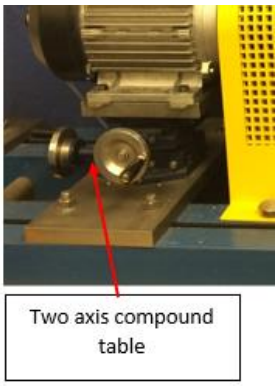

Figure 6-10 Adjusting compound table

6.4.3 Combination Faults (Misalignment and Broken Rotor Bar)

Several studies have been conducted in this area looking at the detection of the induction machines' faults. However, most of these studies have largely focused on only one fault. On the other hand, a number of mixed or combination faults occur in the real industry. Moreover, many research papers have explored the combination of broken rotor bars as well as the associated electricity. In an induction machine, several broken rotor bars and the intrinsic electricity or coupling misalignment is a common occurrence. The previous paragraph has examined this scenario and indicates that the combination or mixed faults are of broken rotor bars' synchronised presence as well as intrinsic eccentricity. As a consequence, this study is aimed at analysing the effects of combination faults experimentally and theoretically as well as the misalignment and broken rotor bars information that the AC drive system (sensorless) provides. In addition, this study seeks to examine the impacts of the various combination fault of both BRB and MA damages

under the control operation (sensorless), which is necessary to diagnose faults by utilising the information obtained from the sensorless (VSD).

6.5 Test Procedures Repeatability Check

- Data has been collection under a controlled environment.
- Through performing a number of tests, the baseline data is collected.
- The number of utilised AC induction motors is four namely; one, two, half and healthy BRB.
- There are a number of misalignments' severities induced including the baseline 0.3mm, 0.4mm and 0.5 mm.
- Different speeds were considered which are 70% and 100% as well as load conditions such as 0%, 30%, 70%, and 100%.
- Lastly, the data is analysed in order to investigate the system's response to the changes. The various signals are also investigated such as the power, voltage and current. In addition, the temperature is also checked to fulfil the comparison and benchmarking intents. The speed is also checked to see whether it influences the misalignment, the system behaviour and the BRB. The system speed is very critical in enabling the control system to maintain the rig's speed at the setpoint. Figure 6-11 presented the typical cycle of the test.

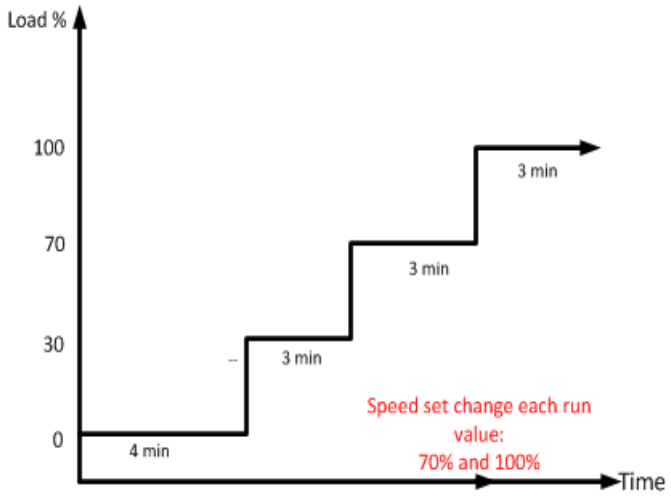

Figure 6-11Typical Cycle

6.6 Summary of Chapter 6

This chapter is very important since it examines in detail the test rig facility's general specifications employed in this study. The test rig's construction begins by the building of the mechanical systems, the control systems as well as the electrical and mechanical faults seeding for the induction motor electrical signals' experimental study. Moreover, this chapter examines the instrumentation used in this study such as data acquisition systems, sensors and measuring equipment. Lastly, this chapter explores the repeatability check assessment for the different signals.

In this chapter, two different faults were examined, which include the internal and external faults that encompass the broken rotor bar as well as the shaft misalignment. The faults focused on in this study are those most occurring in the mechanical transmission systems. However, the existing researchers have not adequately examined the detection of these faults using the power supply parameters in sensorless and controlled transmission systems. The test performed is aimed at examining the performance of the fault diagnosis planner, as well as examining the power supply's diagnosis capabilities in specific temperature, load and speed, especially in a case in which the mechanical transmission system is driven via the VSD.

Chapter 7 Experimental Results and Evaluation of Diagnostic Approaches

This Chapter examines the results of the experimental work obtained from seeded mechanical faults' identification through the analysis of these faults' effects on the parameters of the electric power supply. This chapter begins by providing a preview of the effect of a broken rotor bar having a three-degree severity in an otherwise healthy motor, under sensorless Variable Speed Drive, on the parameters of the electric supply. Next the effects on the power supply parameter of shaft misalignment with three degrees of severities, under the same conditions, was investigated. Finally, the response of the system under the sensorless operating mode to a combination of broken rotor bar and shaft misalignment are provided and analysed.

7.1 Introduction

As stated earlier, dynamic data from external sensors have been gathered for investigation and analysis for the purpose of detecting and diagnosing faults seeded into the test rig's induction motor. These tests explore the effect of a broken rotor bar (BRB), shaft misalignment (MA) and a combination of BRB and MA on the responses of the electrical supply parameters. The test rig's mechanical system, driven by a sensorless variable speed drive (VSD), was used to investigate experimentally measurable changes in these signals that can be correlated with the faults and their levels of severity. Results show that the supply parameters under VSD control obtained from the rig can be correlated with the faults and can be used for an instant diagnosis of change of severity of a fault. In particular, voltage responses are more sensitive to changes in the fault's level as compared to the current since the variable speed drive plays the critical role of regulating the voltage more readily in order to adapt effectively to small load variations or changes that occur due to the presence, or change in level, of a fault. Simultaneous vibration measurements also showed changes which agree with those of the power supply parameters. The test facilities, described earlier, were utilised to replicate real machinery faults that occur in the industry.

All signals available from the Sensorless flux vector drive were collected for the different fault conditions. Changes in signals were compared with each other with the aim of assessing their potential use for fault detection. This chapter discusses and analyses the results obtained from tests by direct comparison between data sets collected under different conditions. The faults may affect current and voltage and generate small changes in these electrical parameters (say, $I+\Delta I$ and $V+\Delta V$), and in the dynamic components (speed, torque) by ($S+\Delta S$) and ($T+\Delta T$), as well as changes in the vibration signal and measured temperature.

7.2 Detection and Diagnosis of BRB in IM using Spectrum Analysis of Electrical Signals

7.2.1 Diagnosis based on Current Signal

In general, a BRB causes peaks in the current and voltage spectrums at frequencies which are multiples of *fs*±*2sfs*.

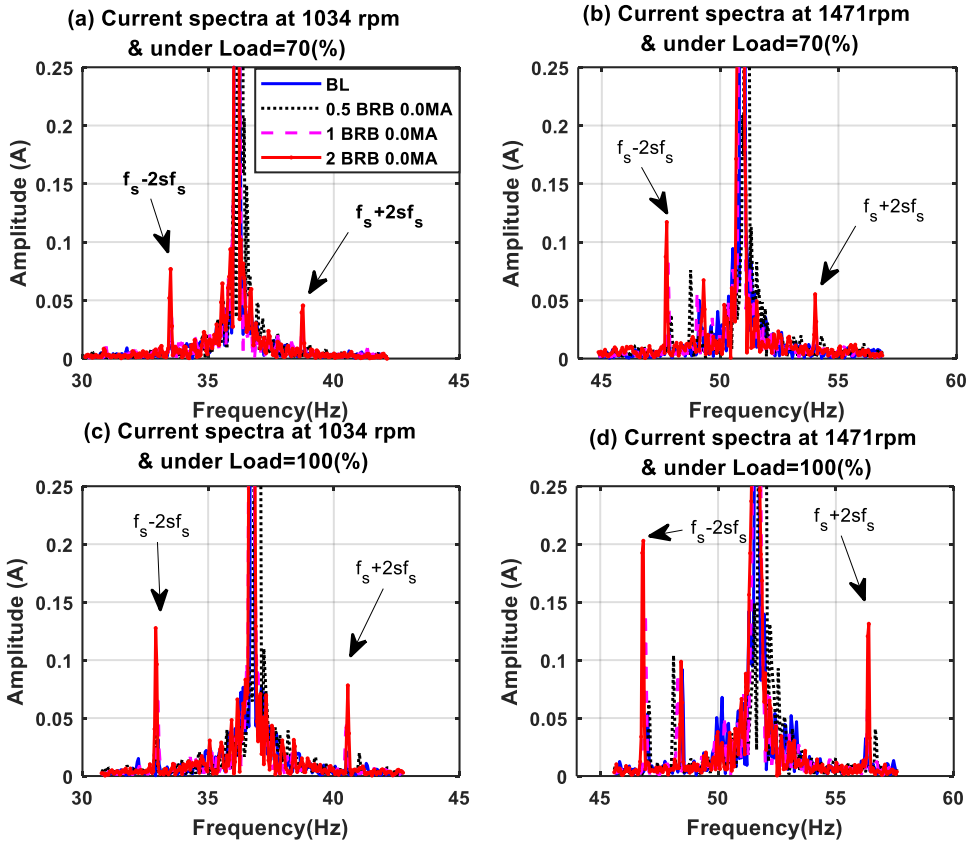

Figure 7-1 Current spectrums for BL and BRB at two speeds & loads showing peaks at Ls& Rs.

Figure 7-1 show phase current signals for a healthy motor and a motor with three levels of BRB fault, 0.5 BRB, 1 BRB and 2 BRB under 70% and 100% of full load, at 1034 rpm and 1471 rpm (70% and 100% of full speed). It can be seen from the figures, that the amplitude of the current spectrums peaks at ($f_s \pm 2sf_s$) increase as the load increases, this may be caused by parameter estimation by VSD, or could be due to motor operating conditions. It is clear that there is some noise included in the measured values with faults

present, that might be because of inverter processor converters when compared with the current value for a healthy motor. When comparing current spectrums with and without BRBs present, the differences can be seen and it is obvious that the amplitude of the current signal in case of 2 BRBs was bigger than of the healthy case, 1 BRB, half broken bar. The amplitudes and sidebands' presence depend upon the BRB's physical position on the rotor fault severity. The locations of the sidebands will shift further away from the central peak, "outwards" as the load and speed is risen. The fault could be better sensed within high loads. It is also noticed that their amplitudes worsen as the BRBs' severity increased in a monotonic manner with fault severity.

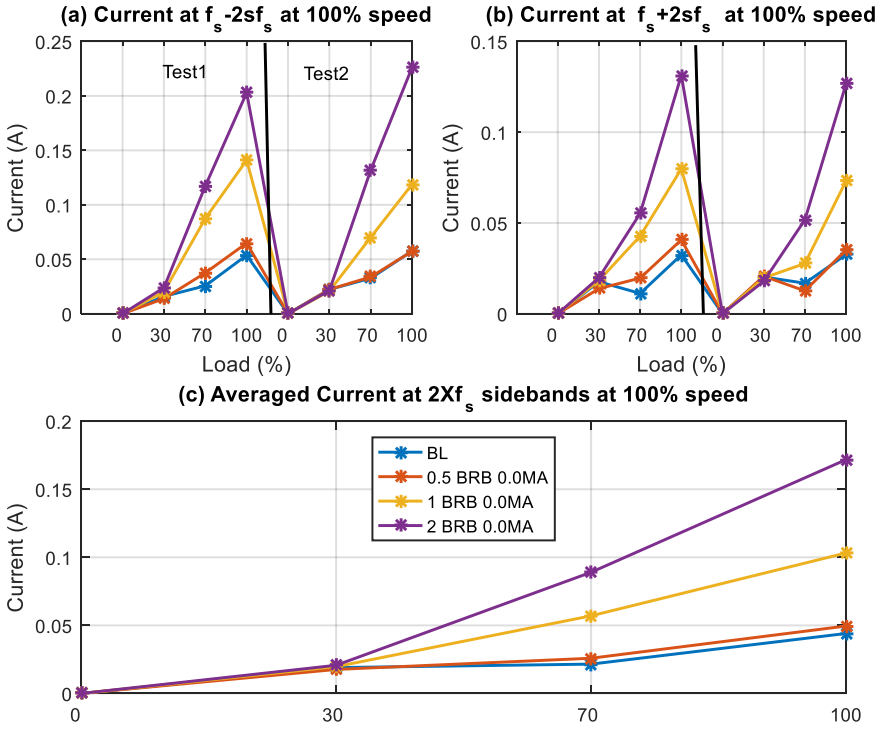

Figure 7-2 The current's average on both upper and lower SB

Figure 7-2 displays the amplitudes of the current at $f_s \pm 2sf_s$ for two sets of tests under different loads (i.e. full load's 0%, 30%, 70%, and 100%) at the speed of 100%. Figure 7-2 (a), shows the amplitudes of the current at *fs-2sfs*, and Figure 7-2 (b) shows the amplitudes of the current at *fs+2sfs*. To ease the diagnosis' exploration procedure for BRBs, the averaging of the amplitudes of the peaks in the current spectrum for both left

and right sidebands are considered. Figure 7-2 (c) presents the current's average at $f_s \pm 2sf_s$. In both the current signal sidebands, the BRBs' diagnosis shows good performance as well as in their severities. There is also an increase in the amplitudes of the current as the BRB severity also increases, and the difference is sufficiently significant to be considered as a fault indicator for changes in the level of the fault. It can therefore be concluded that the current sidebands of $f_s \pm 2sf_s$ observed in the supply frequency is very important in BRBs' diagnosis.

7.2.2 Diagnosis based on Voltage Signal

Figure 7-3 shows phase voltage signals for a BL and motor with the same levels of BRB as shown in Figure 7-1, for the same speed and load conditions.

The sidebands at $f_s \pm 2sf_s$ shown in Figure 7-3 are due to the introduction of the BRB faults into the motor and are a good indication of the presence of a BRB fault. Voltage amplitudes increased as the severity of the BRB fault increased. Furthermore, they are clearly visible in the spectrum under different load tests. It is concluded that the above results are useful for detecting BRBs.

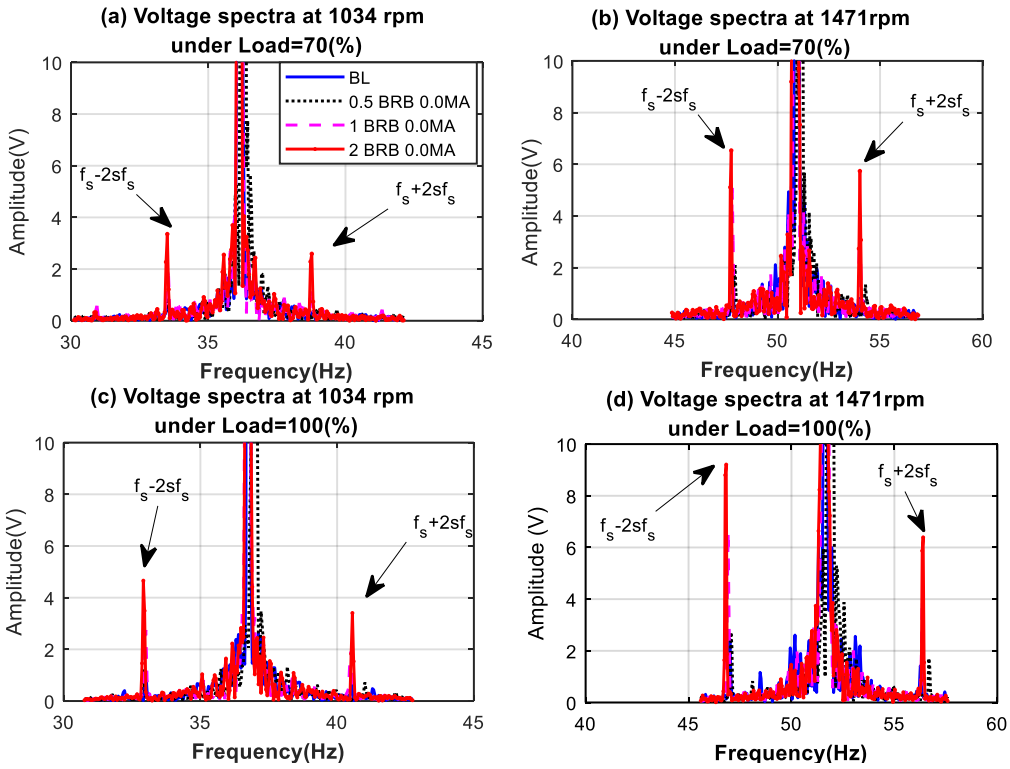

Figure 7-3 Ls and Rs in Voltage spectrums, for two speeds, loads & three levels of BRB

Figure 7-4 displays the voltage amplitudes at sidebands $f_s \pm 2sf_s$ for two sets of tests under different loads (i.e. full load's 0 percent, 3 percent, 70 percent, and 100 percent) at a speed of 100%. Figure 7-4 (a), illustrates the amplitudes of the current at f_s-$2sf_s$, and Figure 7-4 (b) at f_s+$2sf_s$. To ease exploration of the diagnosis of BRBs, averaging of the amplitudes of the peaks in the voltage spectrum for both left and right sidebands is given. Figure 7-4 (c) presents the voltage peaks' average at $f_s \pm 2sf_s$. There is a good performance exhibited by both the sidebands in the BRBs' diagnosis as well as their level of severity. They also exhibit an increase in the amplitudes of the voltage as the BRB also increases in severity, and the difference is sufficiently significant to be considered as an indicator for changes in the level of the fault. To conclude, voltage sidebands of $f_s \pm 2sf_s$ within the supply frequency is crucial in BRBs' diagnosis under sensorless mode.

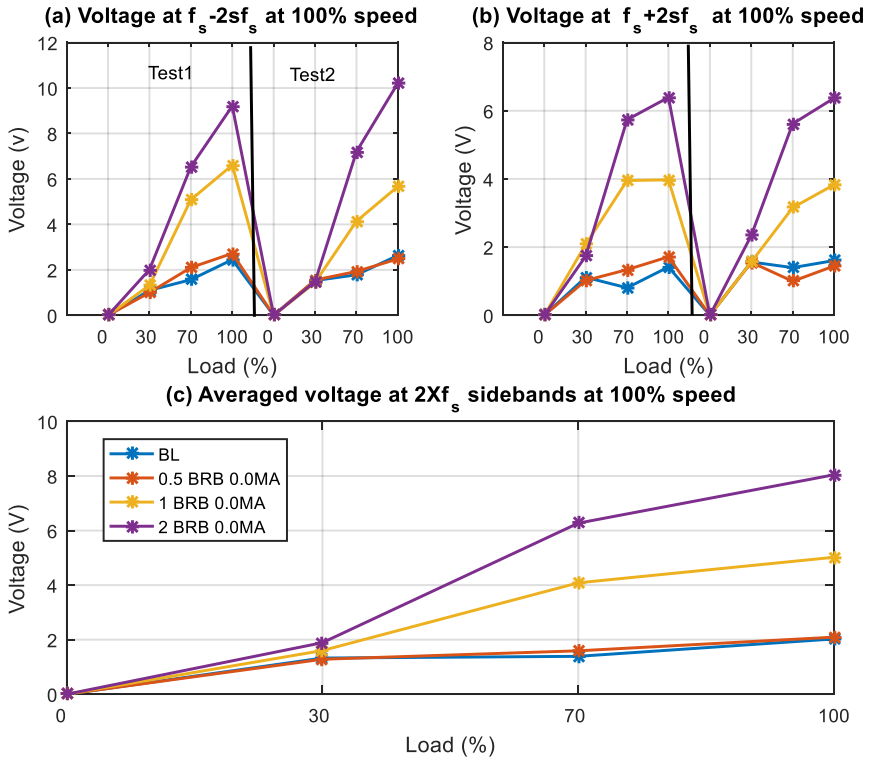

Figure 7-4 The voltage's averaged at both Rs and Ls

7.2.3 Analysis as determined by the Vibration Signals

The discussion above has indicated that the vibration results play a significant role in providing benchmarks in which the voltage and current signals can be investigated. However, in this part, the examination of vibration signals is carried out in order to show a more accurate diagnosis and also for making comparisons, including assessing the vibration responses of BRBs' different severities. Figure 7-5 demonstrates the vibration spectrum in the region of f_r with a change of fault levels at two speeds (1021 rpm and 1451 rpm) and two loads (70% and 100% full load). The figure also illustrates the vibration spectrum's good performance at f_r-$2sf_s$ and also at f_r+$2sf_s$ for the diagnosis of BRB at the different conditions of operations.

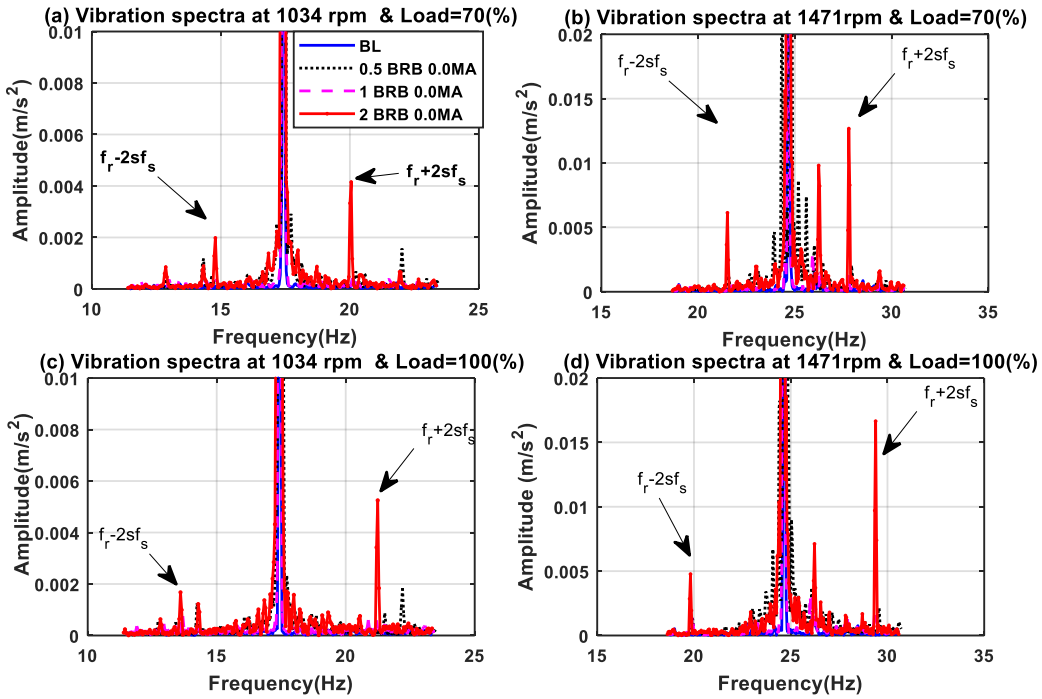

Figure 7-5 Vibration spectrums for BL and three levels of BRB at two speeds and two loads showing peaks at Ls and Rs

Figure 7-6 presents the amplitudes of the vibration peaks' RMS values at f_r-$2sf_s$ and also at f_r+$2sf_s$ for evaluation of tests carried out at full speed based on two different loads (i.e. full speed and 70 and 100 percent). Figure 7-6 (a) shows amplitudes of the vibration peaks' RMS values at f_r-$2sf_s$, and Figure 7-6 (b) shows values of RMS for a peak at f_r+$2sf_s$. It can be seen that these RMS values are effective in separating the severities of BRB faults. It can be noted that the RMS value in 2 BRBS' cases is a little bit higher than for the 0.5 BRB and 1 BRB faults which are at close proximity to each other and also near to the baseline. In addition, it can been seen that the amplitude of the sidebands shows good diagnosis of BRBs in larger faults.

To further explore the performance in detecting BRBs, the vibration amplitudes for both left and right sidebands f_r-$2sf_s$ *and* f_r+$2sf_s$, respectively, have been averaged and the results presented in Figure 7-6 (c). These results confirm the results obtained for the

individual sidebands that the differences in levels of the sideband peaks are an indicator of the presence of a BRB and the level of the fault.

As stated above, the vibration results serve the benchmark purposes particularly in voltage and current investigation.

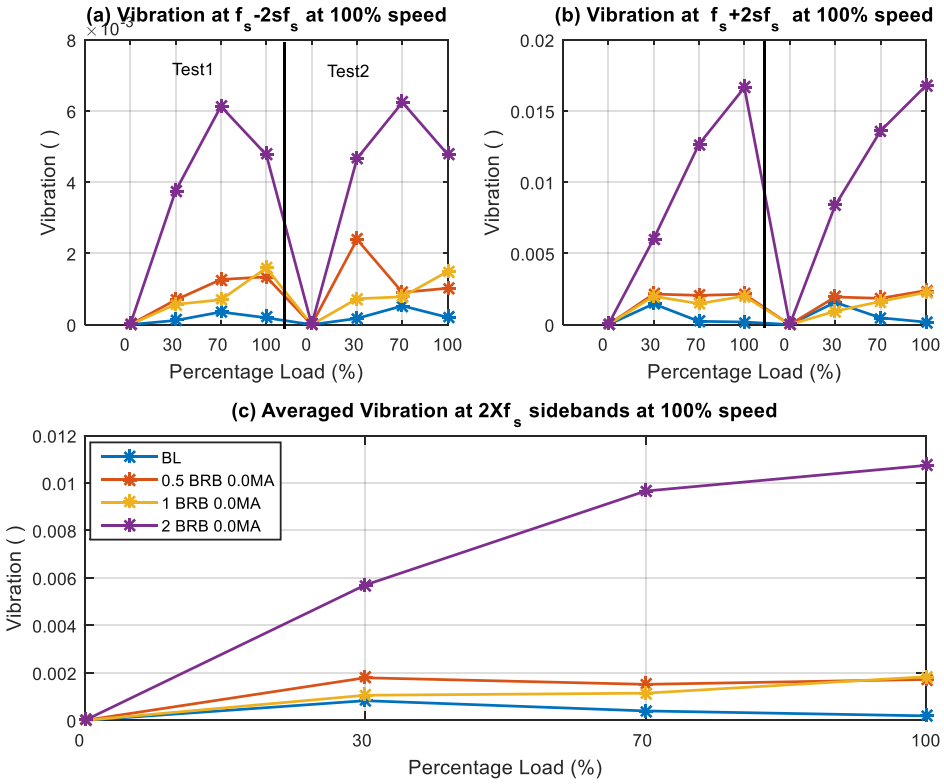

Figure7-6 Averaged vibration at both f_r-$2sf_s$ and f_r+$2sf_s$

7.2.4 Temperature and Speed as Diagnostic Indicators

The temperature was measured using K type thermocouples inside the motor, speed and vibration signals of the ACIM were measured and recorded during the test. Figure 7-7 (a) shows there is considerable change in temperature values during the operation under different load and full speed at two set tests. Obviously, the temperature of the motor increased with the presence and level of a BRB fault. However, the pattern of temperature is surprising. For a seeded fault of 0.5 BRB the temperature increased significantly, but

as the level of the fault increased the temperature gradually decreased almost to the no-fault level.

Figure 7-7 (b) shows that the speed of the induction motor tended to increase with the presence of a seeded BRB fault, but not uniformly. A factor to be considered here is that the fault plays a bigger role of causing speed fluctuations and thus enabling the speed controller to increase the supply parameters in order to control the fault's consequences (Change Y-axis to "Motor Speed, Hz".)

Vibration signals were averaged and the results presented in Figure 7-7 (c) which demonstrates that the fault cases' vibration signals are higher than the baseline's, but do not increase proportionally to the level of the fault. Although there is some overlap, it can be seen that generally the magnitudes can be placed in increasing order as: BL, 0.5 BRB, 2.0 BRB and 1.0 BRB.

This apparent anomaly may be due to temperature changes in the motor which have a significant effect, particularly on the vibration signals as shown by the 2 BRBs' temperature data in Figure 7-7 (a). The rotor bar that is broken by the rotor broken bars' resistance will slightly change as per the changes in temperature. The value of vibration amplitude will also be dependent on the rotor bar's resistance values, which is also dependent on the temperature. Likewise, the change of temperature will affect the frequency, this is because of the change of inductance inside the motor, that is why we cannot ignore this change in temperature in the condition monitoring process.

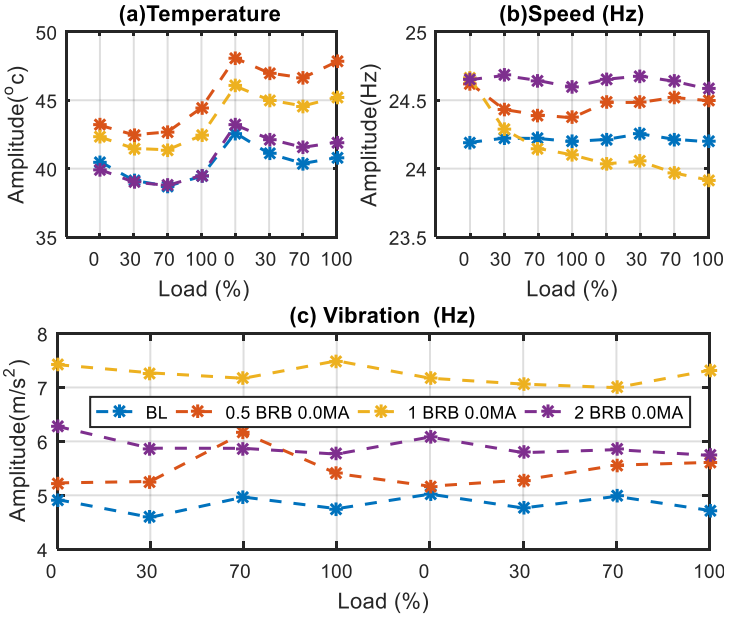

Figure 7-7 Averaged temperature, speed and vibration for IM for BRB

7.3 Detection and Diagnosis of Shaft MA in IM using Spectrum Analysis

7.3.1 Diagnosis based on Current Signal

As has been explained above, sidebands are present in both voltage and current signals in the case of ACIM mechanical faults. Figure 7-8 shows the upper and lower current sidebands around the supply frequency which appear with shaft misalignment.

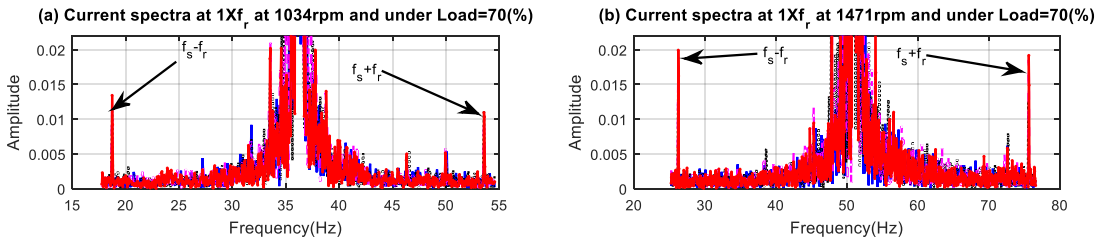

Figure 7-8 Current spectrums for BL and motor with MA at two speeds at 70% full load, showing peaks at Ls and Rs.

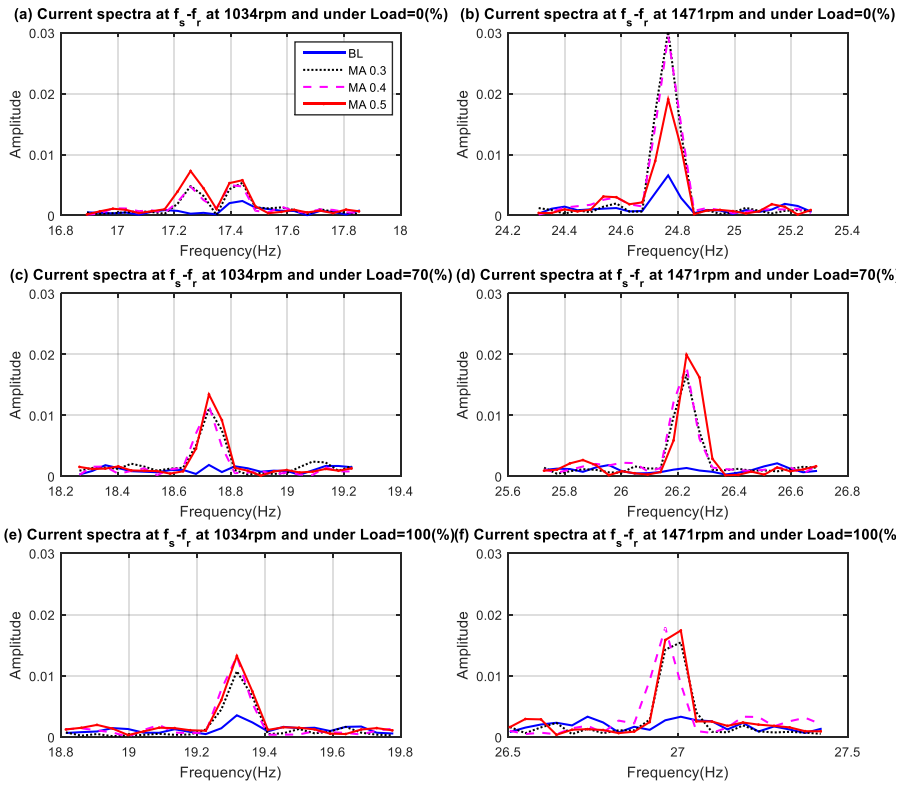

Figure 7-9 Amplitude of current signals at Ls (f_s - f_r) for four levels of MA under 0%, 70% and 100% full load

Figure 7-9 shows the lower sidebands (f_s-f_r), and Figure 7-10 show current signal's upper sidebands (f_s+f_r), at both 70% and 100% under full speed and full load 0%, 70% and 100%. Good misalignment's diagnosis is exhibited by the lower and upper sidebands. Generally, both sidebands' amplitudes increased as misalignment's severity also increased, but there is no clear indication that the amplitude of either sideband increased monotonically by fault severity.

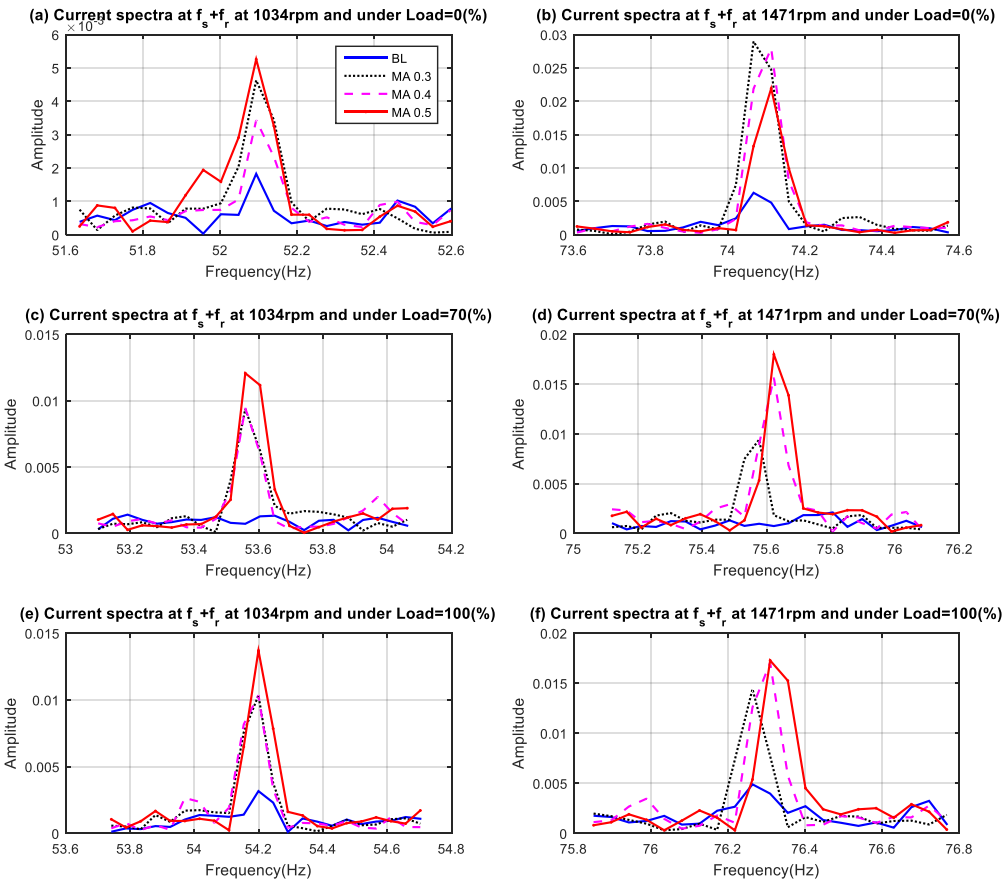

Figure 7-10 Amplitude of current signals at Rs ($f_s + f_r$) for four levels of MA, under 0%, 70% and 100% full load at speeds 1034 rpm and 1471 rpm

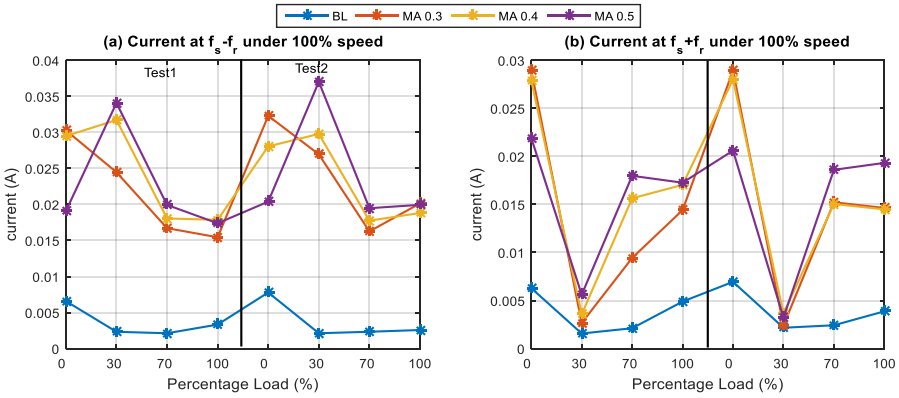

Figure 7-11. The current amplitudes at f_s-f_r and f_s+f_r. for four levels of MA, at full speed, under 0%, 30%, 70% and full load

Figure 7-11 displays the amplitudes of the current at f_s+f_r and f_s-f_r, under varying operational conditions in both Test 1 and Test 2. Figure 7-11 (a) shows the values of the current amplitudes of the lower sideband at f_s-f_r, under varying operational conditions, and Figure 7-11 (b) shows the corresponding values for the upper sideband at f_s+f_r. The lower and upper sidebands' current amplitudes tests were averaged in order to perform a better investigation of misalignment's diagnosis. Figure 7-12 (a) presents the lower sideband's averaged current value at f_s-f_r under the full speed, and Figure 7-12 (b) indicates upper sideband's averaged current value at f_s+f_r. The sidebands indicate a good technique for misalignment's diagnosis. Moreover, increased consumption of current as the misalignment increased is also noted.

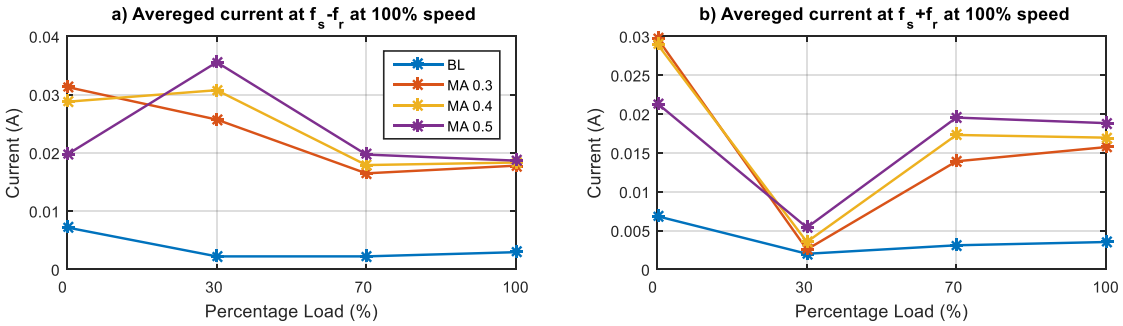

Figure 7-12 Current's averaged at Ls and Rs

7.3.2 Analysis in Voltage Signal

Figure 7-13 show the voltage spectrum in the region of the lower sideband (f_s-f_r) and Figure 7-14 show the voltage spectrum for upper sideband (f_s+f_r). Both figures are for 70% and 100% full speed, and 0%, 70% and 100% full load. The amplitudes of the sidebands (both lower and upper) in the current signal show a good potential for misalignment's diagnosis. Both the sidebands' amplitudes are increased as misalignments' severity increased, but in (f_s-f_r), and (f_s+f_r) for zero load and 1471 rpm, this is due speed ripple.

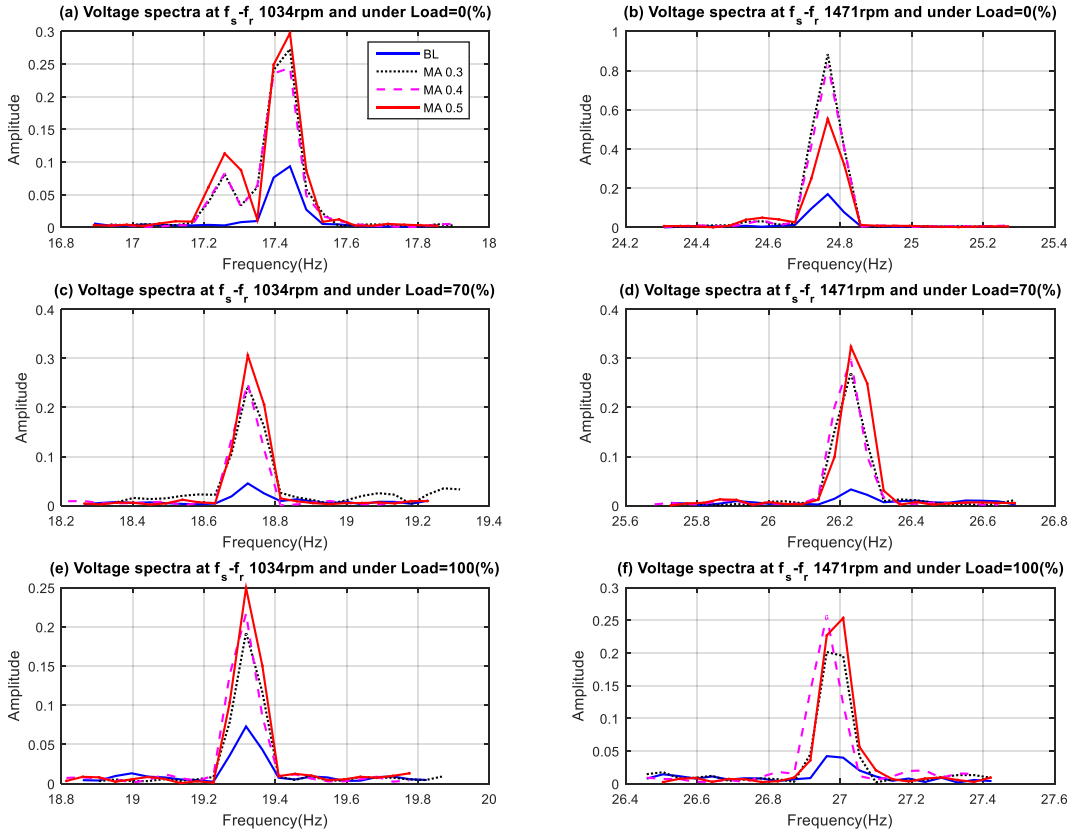

Figure 7-13 Amplitude of voltage signals at Ls (f_s - f_r) for four levels of MA under 0%, 70% and 100% full load at speeds 1034 rpm and 1471 rpm

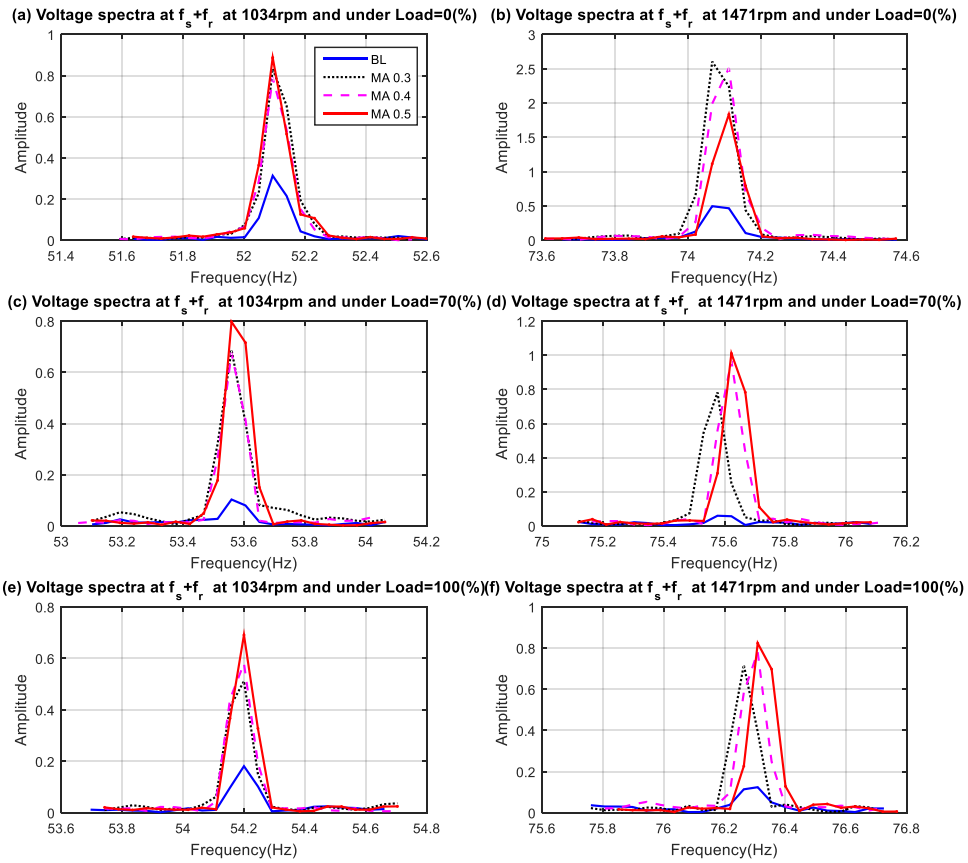

Figure 7-14 Amplitude of voltage signals at Rs ($f_s + f_r$) for four levels of MA under 0%, 70% and 100% full load at speeds 1034 rpm and 1471 rpm

The peaks in the voltage amplitudes at the feature frequencies ($f_s \pm f_r$), at full speed under 0%, 30%, 70% and 100% full load for both sets of tests are presented in Figure 7-15 (a) which shows the RMS values of voltage amplitudes for the lower sideband f_s-f_r. for the given operating conditions. Figure 7-15 (b) presents the upper sideband's voltage amplitudes' RMS values at f_s+f_r, under the same operating conditions. In both tests, upper and lower sidebands' voltage signals showed a better potential for diagnosing misalignment fault. Then, as previously, the voltage amplitudes at the lower and upper sidebands for both tests were averaged. Figure 7-16 shows the averaged voltage signals for both sidebands ($f_s \pm f_r$) at full speed for healthy motor and motor with three levels of misalignment, the sidebands show a good diagnosis of misalignment.

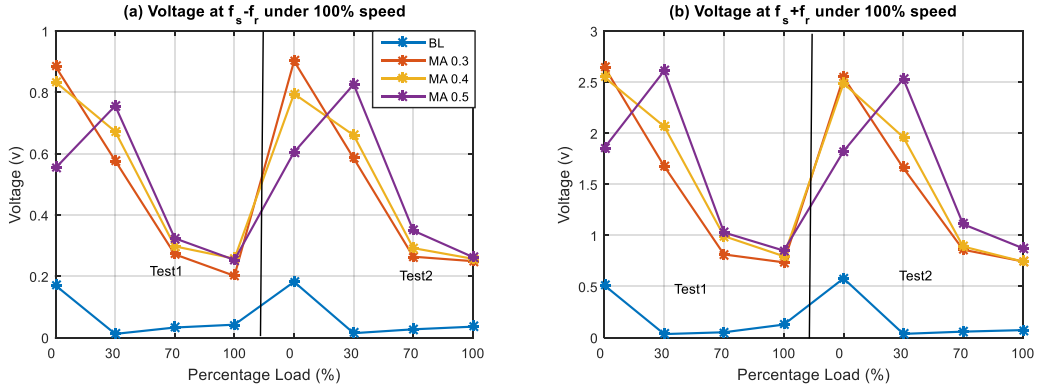

Figure 7-15 Amplitudes of the voltage at f_s-f_r & f_s-f_r with changed conditions

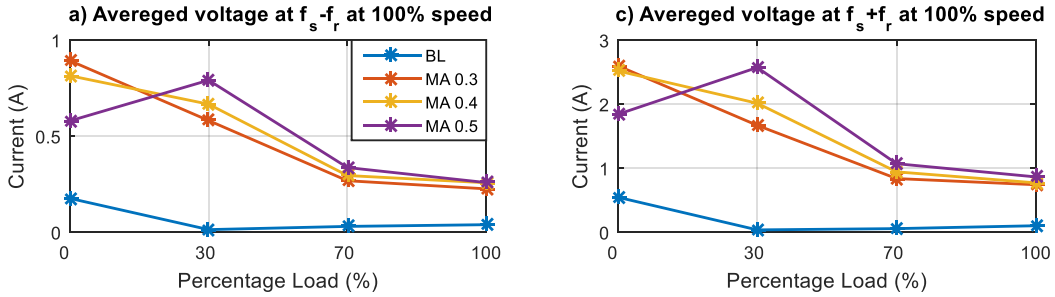

Figure 7-16 Voltage amplitudes at f_s-f_r and f_s+f_r, for four levels of MA at full speed, under 0%, 30%, 70% and full load

Generally, it can be concluded that both current and voltage signals show a good potential for the diagnosis of misalignment faults, with the performance of the current and voltage signals extending to differentiating levels of severity of misalignment. Generally, both sideband signals show an increase in amplitude with a corresponding increase in the degree of misalignment. In conclusion, in the conditioning monitoring process, both signals are key in misalignment fault's diagnosis under sensorless modes.

7.3.3 Diagnosis by Vibration Signals

To serve for benchmarking purposes, the vibration signals of the motor obtained from the accelerometers were analysed for their spectra and utilised to perform the faults' diagnostics.

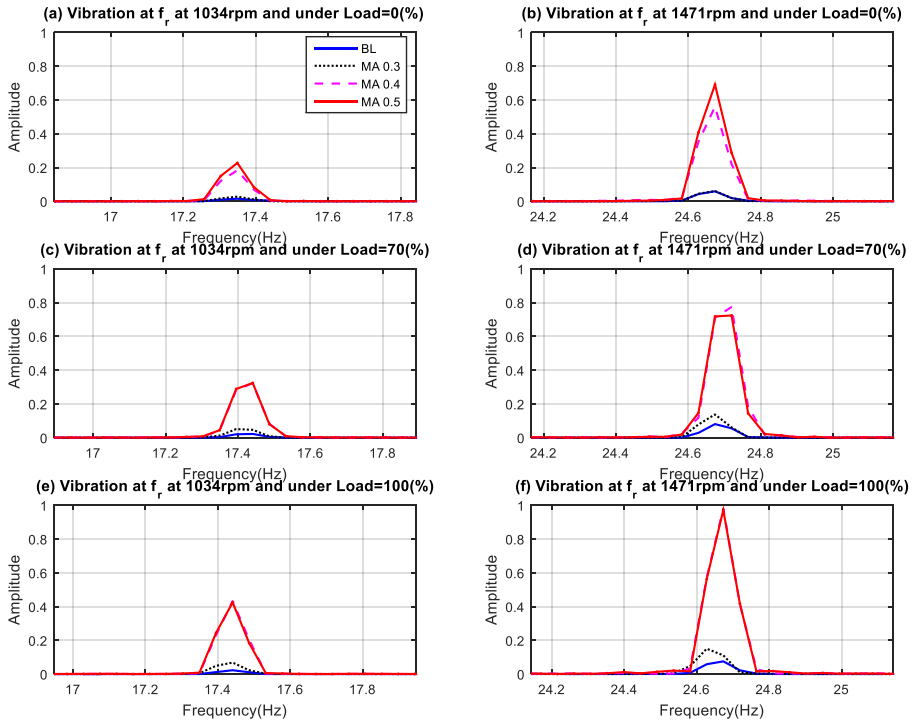

Figure 7-17 Vibration spectrums for BL and three levels of MA at two speeds (1034 rpm and 1471 rpm) and three loads (0%, 70% and 100% full load) showing a peak at f_r

Figure 7-17 shows the vibration spectral peak at f_r. It shows good potential for the vibration signals to diagnose misalignment faults at two speeds (i.e. 70% and 100% full speed) under the given loads. Additionally, there is modulation happening at the rotational frequency's third harmonic as a result of shaft speed. Within the rotation speed's third harmonic ($3f_r$), the vibration spectrum was extracted as indicated in Figure 7-18. Furthermore, this showed a better performance analysis than witnessed in the first harmonic (note difference in scale between Figures 7-17 and 7-18), which also supports the findings in [170]. Therefore, in the performance of misalignment fault's diagnosis, both the vibration at $3f_r$ and f_r are very crucial.

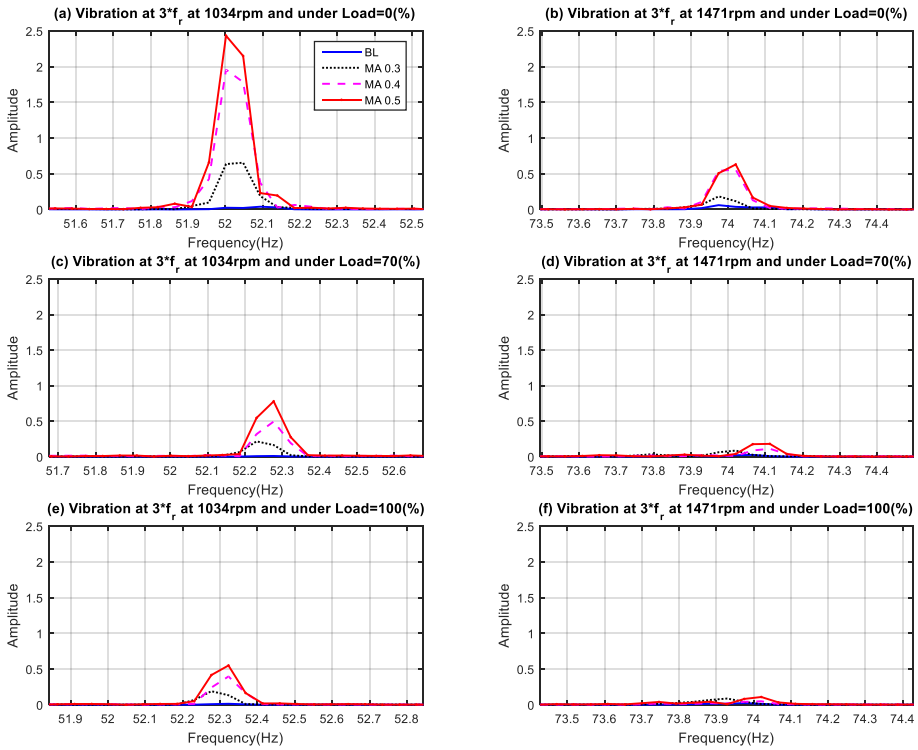

Figure7-18 Vibration spectrums for BL and three levels of MA at two speeds (1034 rpm and 1471 rpm) and three loads (0%, 70% and 100% full load) showing a peak at $3f_r$

Figure 7-19 shows the averaged RMS amplitudes of *fr* and 3*fr* at full speed under 0%, 30%, 70% and 100% full load. Figure 7-19 (a) demonstrates the vibration amplitudes' RMS values at f_r, and Figure 7-19 (b) shows the RMS values at $3f_r$, at two tests. It can be seen that values of RMS at f_r did not provide a good means of separating the different misalignment's severities, and thus the RMS values at $3f_r$ appear to be more suitable for serving the purpose of diagnosing the misalignment's faults than the RMS values of f_r.

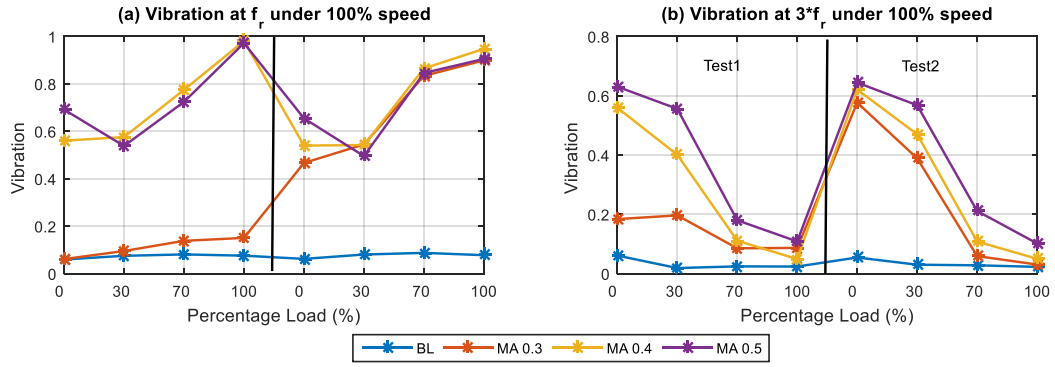

Figure 7-19 RMS vibration amplitudes at f_r and $3f_r$ for healthy motor and three levels of shaft misalignment at full speed and loads 0%, 70% and 100% full load

In the evaluation of the amplitudes of both peaks' diagnostic performances, $3f_r$ and f_r, Figure 7-20 (a) indicates the vibrations average at f_r while Figure 7-20 (b) illustrates the vibration's average at $3f_r$. There is a good analysis of misalignment severities displayed by both harmonics. The results obtained here are used as the standard for the performance of both voltage and current signals.

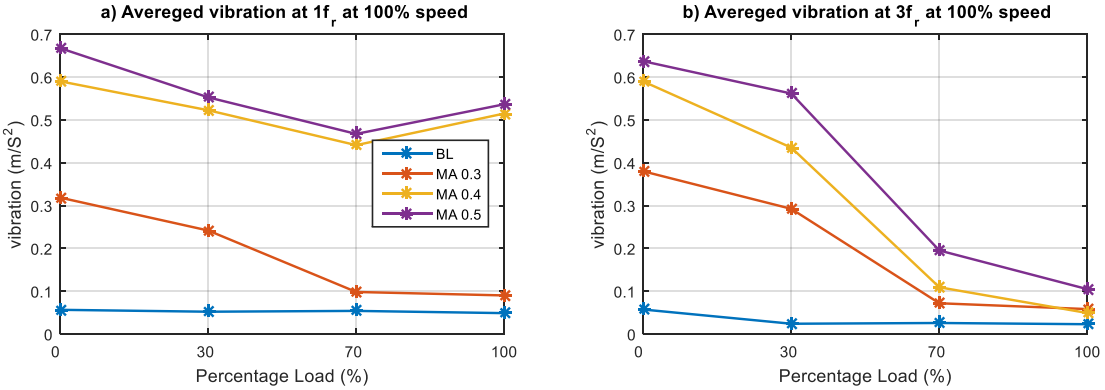

Figure 7-20 Vibration amplitudes (averaged) at f_r and $3f_r$

7.3.4 Temperature and Speed and Responses

As the induction motor runs, the speed and the temperature were recorded. Figure 7-21 shows these values' average when these tests were being conducted. But, for both tests, the temperature values' trends were affected significantly by changes in the shaft alignment as the operation progresses as shown in Figure 7-21 (a). However, there are

small changes shown in the faulty cases as Figure 7-21 (b) shows, capturing the induction motor's speed when compared with the baseline's.

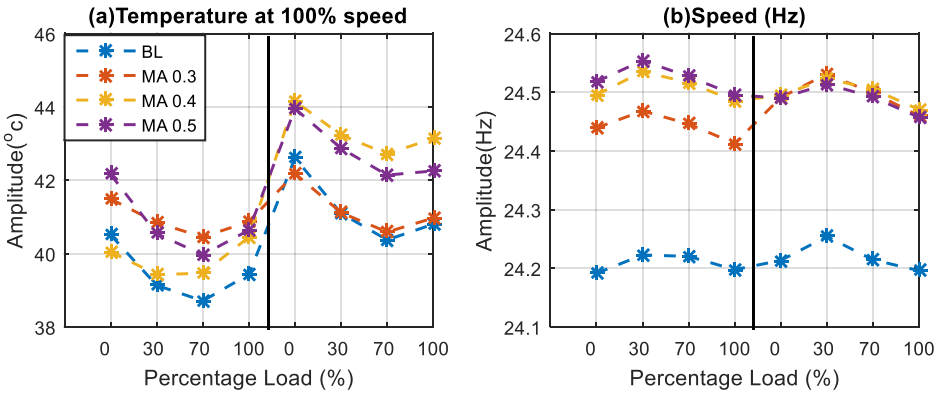

Figure 7-21 Average temperature and speed

7.4 Detection and Diagnosis of Combined Faults using Spectrum Analysis

7.4.1 Impacts of Induced Misalignment on the Features of BRBs

For a better understanding and further clarification of fault detection with a sensorless AC drive control system, this investigation included the response of both current and voltage parameters to simultaneously occurring BRB and MA faults to be able to identify the faults separately. In this case, the benchmarks were the vibration signals.

Results of the vibration signal, voltage and current for both BRB and simultaneous misalignment presented as RMS values. The three signals' spectra features were calculated instead of repeatedly being shown as the signals' spectrums. Additionally, Figures 7-22, 7-23 and 7-24 respectively are used to present the current, voltage, and vibration sidebands amplitudes' averaged RMS values at full speed under the various loads shown above.

7.4.1.1 Diagnosis that is dependent on Current Signal

The average current signals' RMS values are given in Figure 7-22 for shaft misalignments of 0 mm, 0.3 mm, 0.4 mm and 0.5 mm combined in order with zero BRB, 0.5 BRB, 1 BRB and 2 BRB, a total of 16 average RMS values.

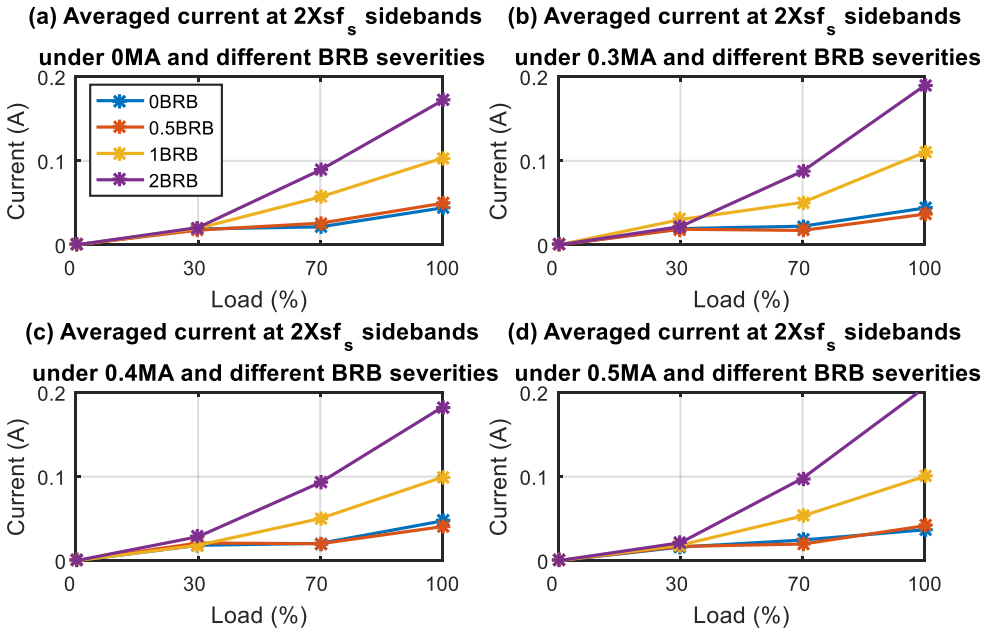

Figure 7-22 Average RMS values of current signals for a spectral peak at 2sf_s, for shaft misalignments of 0 mm, 0.3 mm, 0.4 mm and 0.5 mm combined in order with zero BRB, 0.5 BRB, 1 BRB and 2 BRB

Figure 7-22 confirms that induced misalignment does not impact on the capabilities of current signals to separate BRBs fault severities, likewise the signal features due to BRBs did not show any change.

7.4.1.2 Diagnosis based on Voltage Signal

The average voltage signals' RMS values are given in Figure 7-23, for shaft misalignments of 0 mm, 0.3 mm, 0.4 mm and 0.5 mm combined in order with zero BRB, 0.5 BRB, 1 BRB and 2 BRB, a total of 16 average RMS values. Figure 7-23, indicates

the voltage signals' trend is the same as the current signals' trend. It can be seen here that the misalignment induced does not affect a to change either the BRBs' signal features or the voltage signals' capacity to separate the BRB fault's levels.

The averaged values of RMS show that the misalignment faults' presence had no impact on either the voltage or current's capabilities to separate the different levels of BRB faults or the signal features of the BRBs. However, it should be noted that voltage signals are better able to perform the separation of the BRBs' severities at 30% load as compared with the current signals under the same conditions of load. Nonetheless, a good performance is still demonstrated by both of them and thus can be used to perform sensorless AC drive control system's combination diagnosis.

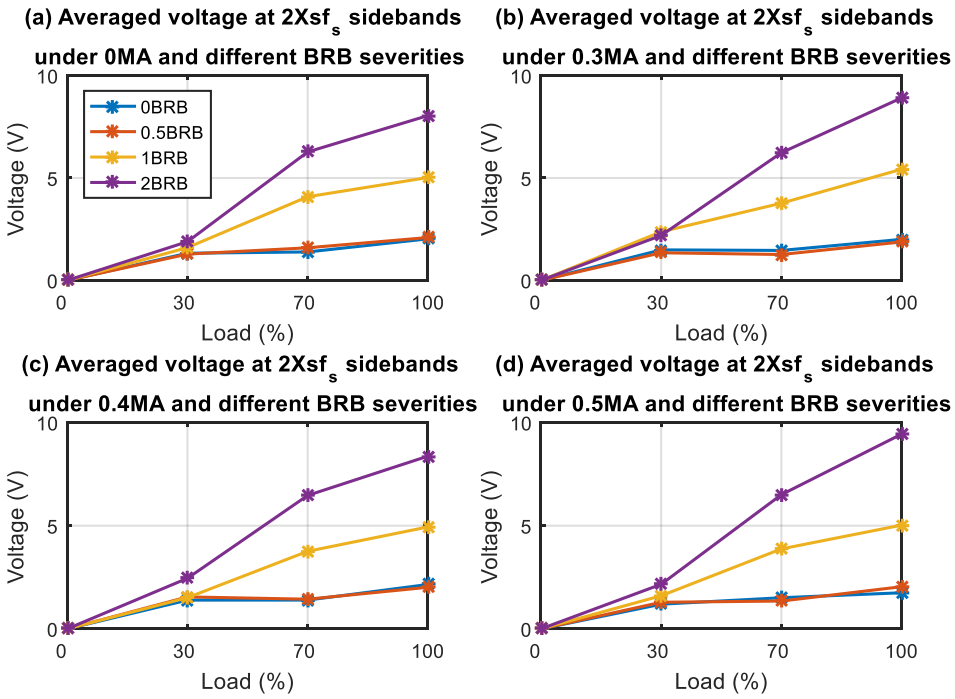

Figure 7-23 Average RMS values of voltage signals for a spectral peak at 2sf_s, for shaft misalignments of 0 mm, 0.3 mm, 0.4 mm and 0.5 mm combined in order with zero BRB, 0.5 BRB, 1 BRB and 2 BRB

7.4.1.3 Diagnosis based on Vibration Signals

Again, vibration signals were utilised as a benchmark with the RMS values of the vibration signals presented for comparison.

Vibration signals were measured under the same test conditions as both the voltage and current signals that were simultaneously collected during the same run. The average vibration signals' RMS values at ($f_r - 2sf_s$) are shown in Figure 7-24, which presents the results for the four different misalignment severities (0 mm, 0.3 mm, 0.4 mm and 0.5 mm) and the four levels of BRB (0, 0.5, 1 and 2) under the usual four loads (0%, 30%, 70% and 100% of full load). It can be seen that misalignment faults affect the vibration signals greatly, leading to an effect on the capability of the vibration analysis to diagnose BRBs' faults. Nevertheless, while the vibration signals are known to wield the ability to detect the faults of BRBs, their ability to separate the faults, particularly the 0.5 BRB as well as the 1 BRB, are not good and is often less effective than either voltage or current signal analysis.

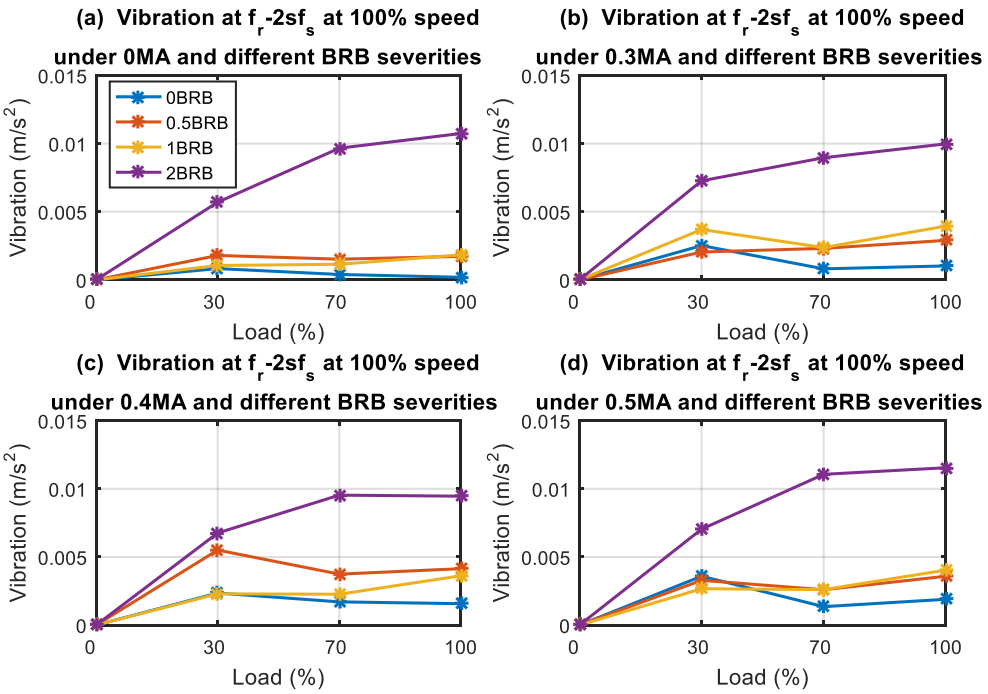

Figure 7-24 RMS vibration signals (average) at $f_r - 2sf_s$

7.4.2 Impacts of BRBs on the Features of Misalignment

It was also essential to ascertain whether the presence of a BRB affected the diagnosis of shaft misalignment under sensorless mode operation. To investigate these faults, the influences of changed BRBs' severities on the features of the misalignment through the use of voltage and current signals were emphasised. Furthermore, vibration signals were analysed as the comparison's benchmark. The determination of the current, voltage, vibration and amplitudes' RMS values at full speed as dictated by the different loads, were as shown in Figures 7-25, 7-26 and 7-28.

7.4.2.1 Analysis of Current Signal

Average RMS values of current signals are given in Figure 7-25, for zero BRB, 0.5 BRB, 1 BRB and 2 BRB, combined, in order, with shaft misalignments of 0 mm, 0.3 mm, 0.4 mm and 0.5 mm, a total of 16 average RMS values.

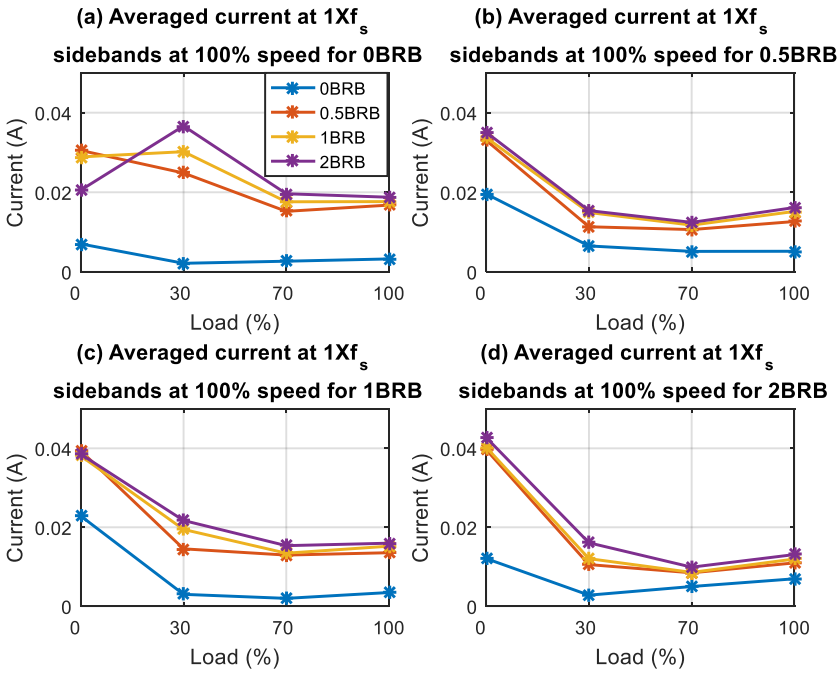

Figure 7-25 Averaged current values for BRBs' effects on different shaft misalignment severities' features

Figure 7-25 demonstrations that the current signals' RMS values for shaft misalignment were not affected by the presence of BRBs faults. There was a good indication shown by the current signals to separate the fault combinations as well as their severities.

7.4.2.2 Diagnosis based on Voltage Signal

The voltage signals' RMS values shown in Figure 7-26 indicates individually the different BRBs severities' effect on the features of shaft misalignment. Figure 7-26, illustrates that the RMS voltage signals were not affected by BRBs faults' presence. There is also a good indication in the voltage signals to separate the fault combinations as well as their severities.

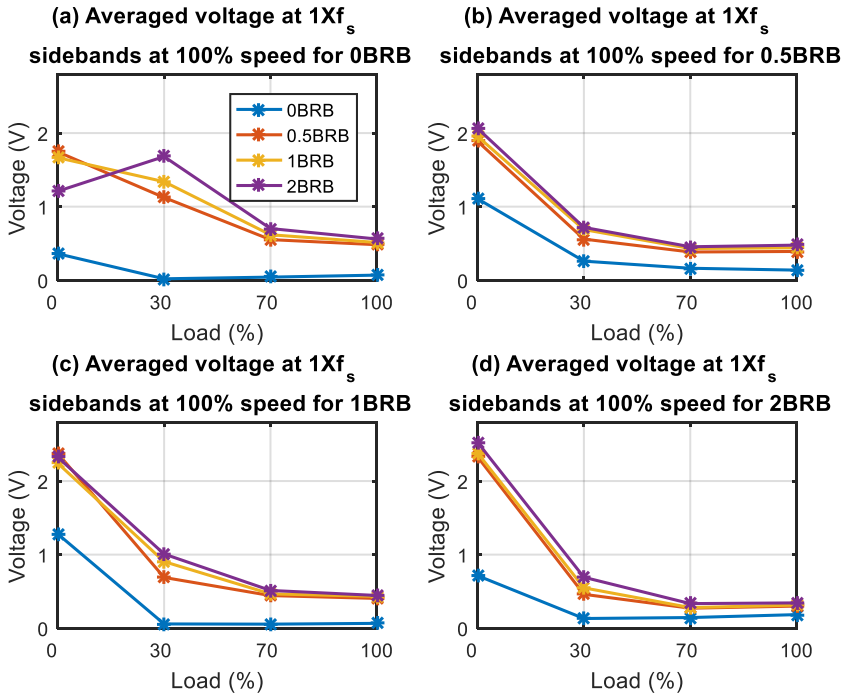

Figure 7-26 Voltages values averaged for the impact of dissimilar BRBs on the features of dissimilar severities of shaft alignment

7.4.2.3 Analysis based on Vibration Signals

As stated previously, vibration signals are utilised for benchmarking. Thus, to evaluate the voltage and current signals' diagnostic performance, the vibration signals, RMS values at $f_r \pm 2sf_s$ have been calculated and demonstrated in Figure 7-27 for comparison.

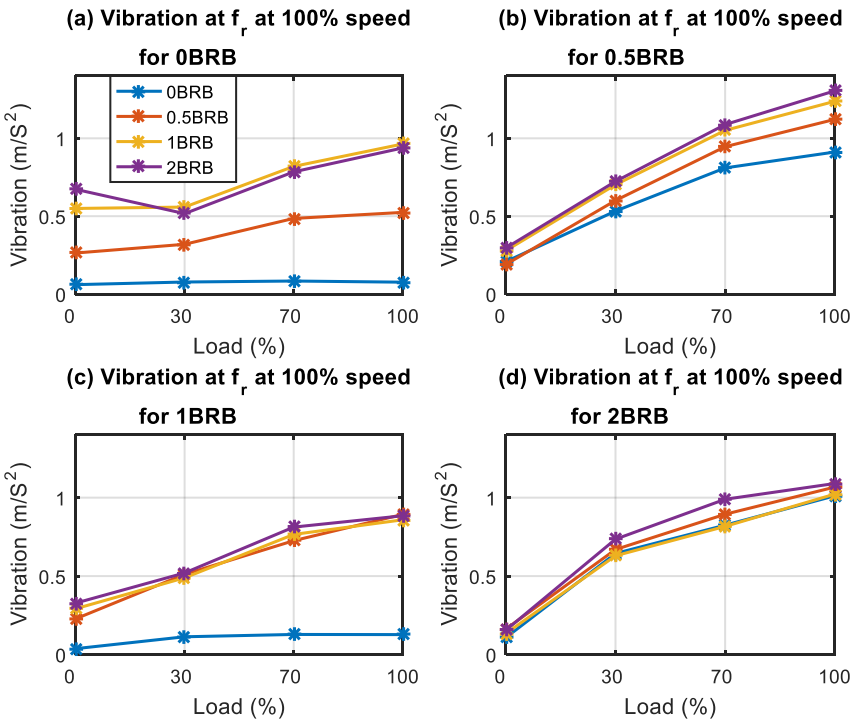

Figure 7-27 RMS of vibration signals for the influences of dissimilar BRBs on different MA

Figure 7-27 clearly show the vibration signals' RMS values. The collection of these vibration signals was carried out simultaneously with the other tests and therefore the conditions were the same as those for the voltage and current signals. The Figure indicates the influences of different BRB severities, i.e. (0 BRB, 0.5 BRB, 1 BRB and 2 BRB) on shaft misalignments 0 mm, 0.3 mm, 0.4 mm and 0.5 mm, in that order. BRBs have a significant effect on the vibration signals obtained for misalignment on their own. In such conditions, the vibration signals are less able to sense misalignment faults and less able than current and voltage signals.

7.5 Summary of Chapter 7

In this chapter, broken rotor bar and/or shaft misalignment are diagnosed based on current and voltage spectrum. The sideband frequencies generated by the presence of BRB or MA faults are proposed as a means of detecting and diagnosing those faults in an electrical system. The results obtained were affected by applied load, motor speed and temperature of sources. However, the sidebands extracted from the signal spectrum at

specific characteristic frequencies contain information on the presence and magnitude of electrical and mechanical faults. Reliable results are obtained by averaging frequency spectrum of the power supply.

Importantly, when using current and voltage signals, it was shown that the presence of one fault (either MA or BRB) did not block the detection of the other (BRB or MA). Nor was diagnosis of the level of severity of the fault impaired.

Chapter 8 Detection and Diagnosis of the Changes in Lubricating Oil Viscosity in Gearbox

To evaluate the performance further, the focus of this chapter is on examining the electrical supply analysis when applied to monitoring the changes of lubricating oils in the downstream gearbox. Particularly three oils with different viscosity values were investigated under different operating conditions. Considering that oils can have both steady and a dynamic loads applied to the rotor system, the power signals, a multiplication of valuates and current signals, are based to diagnose the oils changes.

8.1 Introduction

Gearbox lubricants play a significant role in sustaining effective and efficient operations [171, 172]. Lubricating oils should decrease friction and wear at the contacting surfaces and delineate them for the avoidance of failures and effective operation. Properties of lube oil also have an impact on gear dynamics including heating, power characteristics and vibration [172]. In view of this, frequently tracking lubricant property changes is necessary to avert machine defects [147] and prevent unprecedented malfunctions. Water contamination, particle and oxidation are the main causes of Gearbox lubricant degradation [171]. Generally, lube viscosity is increased by water and oxidation [173, 174]. Research indicates that gearbox performance and behaviour is significantly affected by oil properties, particularly through splashing and churning [175]. Oil churning triggers considerable loss of power within the gearboxes. Notably, a low-speed increase in viscosity increases the rate of churning; however, such losses reduce at high velocity [176]. Additionally, as inferred in [177] viscosity raises temperature because of internal lube friction. Nevertheless, optimal temperature aggravates the formation of ideal tri-biological stratum and chemical activities. Conversely, this in turn reduces viscosity, thus leading to the formation of thinner oil films. Various oil degradation tracking methods have been designed, particularly offline methods [178], however, such methods are rarely used, require additional measuring equipment and implementing them is expensive. The necessity for cost-effective, reliable and easily applicable condition tracking methods are increasingly becoming important to offer a prompt evaluation of the oil qualities.

Current and vibration signature analyses constitute the most extensively utilised diagnosis and condition tracking schemes for detection of faults on different equipment. Although the study on designing methods of detecting degraded oil on the basis of the aforementioned models is scarce, Linilson and Rui [173, 179] investigated the correlation involving vibration signature and viscosity. They discovered that a correlation between oil viscosity and high-frequency vibration properties existed. However, researchers are yet to determine the potential for utilising electrical measurement signatures for detection of degraded lube oil in terms of viscosity[175]. In view of this, the current study explores

how variation of oil viscosities impacts GB transmission systems on the parameter of power supply from varying speed drives (VSDs). Following an investigation of the impact on the gear transmissions processes, a research was conducted using a 10 kilowatt gearbox supply system containing 4 separate oils. The diagnostic ability of dynamic and static properties that are designed on the basis of voltage and current measurements are then investigated for various conditions of operations.

8.2 Effects of Lubrication Properties on Power Losses in Gearboxes

Internal resistance that fluids exert to flow is called viscosity. There is an inverse correlation between temperature and viscosity, whereas a direct correlation exists between pressure and viscosity. Reducing friction between fixed and rotary parts of the machine constitutes the major function of lubricating oil; this increases the efficiency of the machine because of reduced temperature and wear. As determined within gear lubrication methods, increasing the viscosity of oil will retain additional oil on meshing teeth surfaces, thus increasing the likelihood of forming thicker hydro-dynamic films that decrease frictional force. A thick lubricant film is intertwined between moving body surfaces. In contrast, a reduction in viscosity will result in greater friction. In addition, because the presence of meshed teeth constitutes a time-changing event as illustrated through the duration of meshing, there is the likelihood that frictional force changes will change the gearbox responses in terms of meshing frequencies under highest-order harmonics. As stated in the study by Gonçalves, el (2013)[180] the vibration spectra is largely linked to oil viscosity within high frequencies and vary between 2300 Hz -7000Hz on the basis of a 0.34 kilowatt gearbox. Moreover, the components' dynamic reaction linked to gear shaft oscillation frequencies are affected by tri-biological property changes. Similarly, as asserted by de Almeida, Rui Gomes.

Padovese and Linilson Rodrigues (2003)[179], oil density, oil squeezing, and viscosity will result in considerable power losses, this will reflect upon static measurements including power, voltage and mean supply current. In view of this, properties of the lubrication are altered by oil degradation, thus also correspondingly changing the dynamic gear property. Sources of power loss within gear transmission is linked to

different gear parameters including specific sliding, teeth geometry and lube properties. Findings in the study by [147] reveal that using lubricants with ideal viscosity is capable of reducing power loss by 20% [147]. In theory, an increase in viscosity decreases friction, this implies a low consumption of power. The overall power loss P_L within the gearbox has been expressed by [181, 182] [179, 183]:

$$P_L = P_{fr} + P_{spl} + P_{M1} + P_{M0} + P_{sl} \tag{8.1}$$

In the above expression, loss of gear friction is denoted byP_{fr}, loss of gear churning is represented by P_{spl} , which is significantly greater than the remaining three losses namely P_{sl} representing seal power loss, P_{M0} denoting rolling bearing loss, and P_{M1} denoting load dependent rolling bearing loss. Where gear friction power loss P_{fr} is dependent on the load and has a correlation with the teeth quantity of friction co-efficiency (μ_m) and pinion and gear (z_2, z_1) and is expressed as shown[184]:

$$\mathrm{P_{fr}} = \pi\left(\frac{1}{z_1}+\frac{1}{z_2}\right)\left(1-\left(\frac{g_f+g_a}{p_b}\right)+\left(\frac{g_f}{p_b}\right)^2+\left(\frac{g_a}{p_b}\right)^2\right)\mathrm{P_{in}}\mu_m \tag{8.2}$$

In the equation g_a(m) denotes recess path length, g_f(m) represents approach path length, P_{in}(W) represents input power, μ_m represents average friction co-efficient,p_b(m) denotes base pitch. The friction co-efficient $\mu_m$could be computed using the equation below:

$$\mu_m = 0.048\left(\frac{F_{bt}/b}{\nu_{\Sigma C}\,\rho_c}\right)^{0.2}\eta_{oil}^{-0.05}R_a{}^{-0.25}X_L \tag{8.3}$$

$$X_L = \frac{1}{\left(F_{bt}/b\right)^{.0651}} \tag{8.4}$$

Based on Equation (8.3) μ_m is proportionally inversed to velocity v and lube viscosity η_{oil}. Similarly, the churning losses P_{spl} within gears do not depend on load loss;

however, they are dependent on the viscosity, oil density ρ and, geometry and velocity of moving parts dipped in oil, which could be approximated from[180, 184].

Notably, X_LL denotes lubricant factor, b represents face width (in mm), F_{bt} (N) denotes the transverse section of the normal tooth force, $v_{\sum c}$ represents the total pitch point velocity (in m/s), $\mathbf{Re}$ represent Reynolds number, and η_{oil} represents dynamic viscosity of oil (in mPa s). In contrast, load-dependent loss from the bearing is obtained from:

$$P_{spl} = \left(\pi/30\right) n\left[0.5.\rho\left(\left(\pi.n\right)/(30)\right)^2 A_i (0.5.d)^3\right]\left[\left(2.h/d\right)^{0.45}\left(V_{oil}/d\right)^{0.1} F_R^{-0.6}\,\mathrm{Re}^{-0.21}\right] \quad (8.5)$$

The complex effect of velocity and gear geometry on power loss arising from oil splashing and churning is illustrated in Equation (8.5). R_e(Reynolds number) is dependent on the viscosity and density of oil and is expressed as:

$$R_e = \frac{\rho UD}{\eta_{oil}} \quad (8.6)$$

, However, bearing churning loss is dependent on the lubricant viscosity, bearing arrangement, size, and type of bearing [176] and is computed from[180]

$$P_{M0} = \frac{\pi}{30}.n.G_{Br}.{\eta_{oil}}^{2/3}.10^{-3} \quad (8.7)$$

Whereby input power is denoted by P_{in}, approach length is denoted by g_f, recess length is denoted by g_a, Froude number is represented by F_R,roughness is denoted by R_a, base pitch is denoted by p_b, F_{bt} denotes transverse section's normal tooth force, X_L represents a modifiable parameter that relate to all lubricants, b denotes face width, $v_{\Sigma c}$ denotes overall pitch point velocity, ρ_c represents equivalent pitch point curvature radii, ρ represents specific weight, V_{oil} represents the volume of oil, G_{Br} denotes parameters based on the geometry of bearings, n represents input speed (in rpm), D denotes a linear dimension property, U represents the average flow velocity whereas dynamic viscosity is represented by η_{oil}.

Notably, dynamic viscosity η and kinematic viscosity υ constitute the two major forms of viscosities and are expressed using the equation below as:

$$\upsilon = \frac{\eta}{\rho} \tag{8.8}$$

Seemingly, internal gearbox power loss is significantly affected by oil viscosity as illustrated in equations (8.2 & 8.7). Similarly, frictional power losses are inversely proportional towards operating velocity, viscosity values, and lube viscosity as indicated in Equations (8.2 & 8.3). Conversely, Equations (8.4 & 8.7) indicate that an increase in oil viscosity and oil density velocity increases the churning loss. However, churning-induced losses will possibly have higher dominance because the value of fractional power is excessive while the two forms of losses would also change the gear transmission dynamics. Particularly, the effect of churning can escalate the oscillating system's inertia moment and decrease damping effect. In view of this, it results in more rotational system motion. Detailed guidelines regarding the choice of lubricant viscosity for various kinds of gears are examined, as stipulated in the BS PD ISO/TR 18792:2008 whereas the classification of viscosity for industrial fluid lubricants is catered for in BS 4231:1992 ISO 3448:1992. However, like ANSI/AGMA9005-E02 states, gear manufacturer recommendations must be adhered to if they exist, when choosing gear lubricants. Furthermore, standards require manufacturers to give detailed information on the suggested suppliers of oil (Abusaad, Benghozzi, Gu, & Ball, 2013). Generally, the gears' pitch point speed is utilised for identifying the viscosity required. Therefore, viscosity could be determined through the experimental equation below[28]:

$$v_{40} = \frac{7000}{V^{0.5}} \tag{8.9}$$

In the above expression, v_{40} represents the kinematic viscosity of the lube at 40 ^{o}C in (cSt) whereas V denotes the velocity of pitch point operation (in ft/min) and could be computed from [28]

$$V = 0.262\, dn \tag{8.10}$$

In the above expression, *d* represents the diameter of the operating pitch diameter in inches whereas *n* represents the speed of the pinion in (rev/min).

Based on the recommended manufacturers, this experiment used EP 320 as the viscosity of oil within the gearbox, and the suggested manufacturer was Millers Oil Ltd. However, this could be ascertained from equation 8.9 and equation 8.10 and cited standards. The dual-phase helical gearbox features 2 pinions namely the optimum input shaft velocity stands at 1500 rpm shifted to the secondary shaft at the rate of 1.234. Therefore, the secondary shaft's velocity stands at 1851.1 rpm. Based on the gearbox standards and side pinion's highest speed, the pitch point diameter stands at 1.275 in, whereas:

V=618.36

Needed viscosities stands for 40 degrees Celsius will be:

V=618.36

The needed viscosity at 40 ^oC therefore is:

$v_{40} = 7000/618.36^{0.5} = 281.4993 cSt$

By following guidelines in the BS 4231:1992 ISO 3448:1992, the recommended viscosity recommended therefore is ISO VG 320, i.e. EP320.

Based on *the BS 4231:1992 ISO 3448:1992* guidelines, the proposed viscosity will be EP320 (ISO VG 320). From a theoretical perspective, VSD behaviour can reflect such losses of power, especially when there are disturbances in the mechanical systems, for instance, those emanating from changes in viscosity. In such scenario, the VSD modifies the parameters of electric supply to sustain operations at required velocities. Past research has demonstrated that static and dynamic impacts on the downstream machine could be determined within the electric signals. In particular, the dynamic impact could be denoted through sideband component frequencies associated with those of shaft and supply. The changes in amplitude at supply frequencies could be utilised for examining the static impact. In contrast, in sensor-less VSD-driven systems, the control systems adjust the

parameters of supply. It might offer a variety of opportunities for examining such impact instead of merely utilising property frequency components on the basis of changes in high slippage under control techniques of direct voltage Hertz.

8.3 Procedures and Test Facility

8.3.1 Rotary Viscosity Measurements

The viscosity has been determined by an instrument called a rotational viscometer as shown in Figure 8-1.

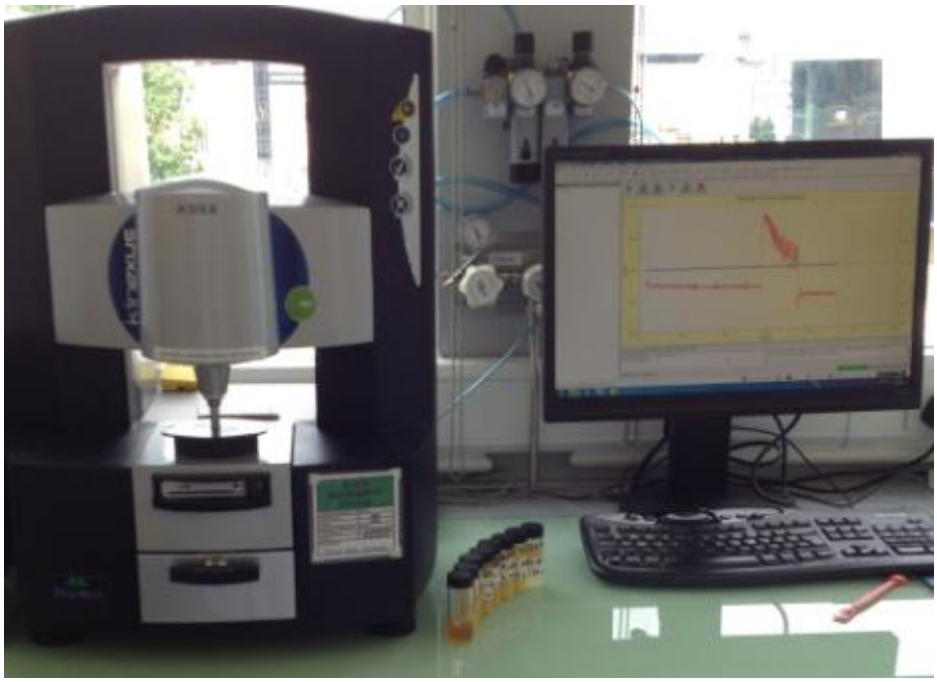

Figure 8-1 Viscosity rotary meter (picture by author)

As shown in Figure 8-2, the sample was placed on at the middle of the plate and covered by an isolated block at variable temperatures, this sample is sheared gap between fixed plate and rotating plate cone. The rate of shear is increase and decrease by selector dial and viscous traction or torque produced on the cone. The viscosity can easily be computed from shear stress (from the torque) and shear rate (from the angular velocity).

The absolute viscosity was specified in centipoise (cP), equivalent to Pa·s in SI units[183].

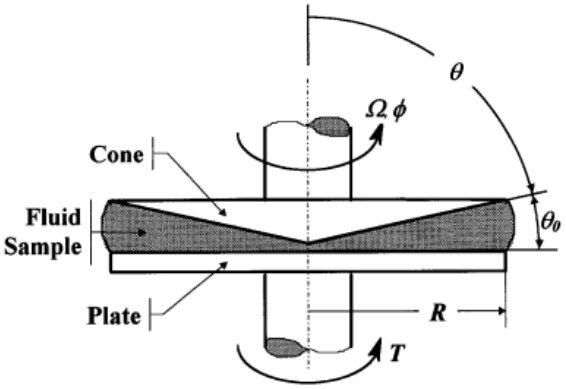

Figure 8-2 Cone-Plate rotary viscometer[28]

8.3.2 Test Rig Facilities

The testing rig utilised in the chapter enables operators to conduct deterministic, recurrent test sequences and gather data on the tests in various fault and load conditions, and different velocity. Repetition of tests could be undertaken identically for fault and health conditions. Additionally, the severe nature of faults could be altered under similar testing parameters and conditions. The design of the testing rig is done in a manner that replicates actual industrial use. The analysis performed on experimental data within the chapter was gathered from a gearbox testing rig indicated in Figure 8-3. The gearbox testing rig features electrical and mechanical control systems. The mechanical component has a flexible spider-rubber coupling that connects elements, a tachometer connected to direct current motor, encoder connected to the alternating current motor shaft, direct current motor, and 2 gearboxes linked back-to-back through flexible coupling.

The initial gearbox functions as the speed governor that regulates the velocity whereas the remaining gearbox functions as the speed accelerator; this enables the system to maintain enough speed, thus allowing the load generators to generate enough loads towards the alternating current motor via the 2 gearboxes.

Notably, a system that obtains data at high-speed from the sensors that measure vibration, gearbox temperatures, and three-phase voltages and currents, transmits the data into

personal computers for Matlab processing and evaluation. The use of dynamic information involves evaluating how traditional analysis techniques for diagnosing and detecting varied oil viscosities function.

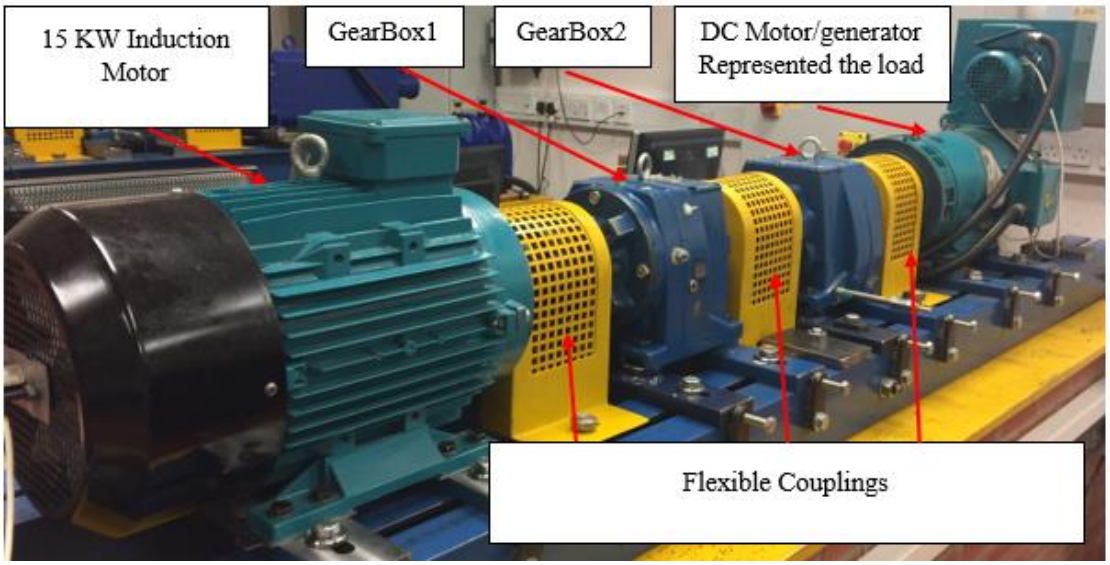

Figure 8-3 Photograph of mechanical part of the test rig

8.3.1 Test Rig Operation

For simulation of variable speed and variable load operating circumstances of ordinary industrial machines, tests were undertaken on the basis of shifting applied loads whereas the alternating current motor velocity was fixed. Nevertheless, a repetition of similar velocity cycle is initiated for each load. The testing conditions are presented below:

- The alternating current undergoes a 3-minute operation for initial cycle followed by testing of all cycles for 2 minutes. In the cycle, configurations of the load are at 0%, 30%, 70% and 100% of maximum load, each operating at 40 seconds, whereas in the cycle the velocity is fixed.
- The value of the speed limit is altered for each cycle and assumes this sequence: 50%, 75%, and 100%. There is a repetition of all cycles for all speed values.
- The collection of data is undertaken at each run. All tests undergo a 5-time repetition for the collection of repetitive results.

- Firstly, the testing rig is subjected to calibration to ensure all signals and parameters lie in calibration thresholds.
- Afterwards, varying viscosities including EP 1000, EP 650, EP 320, and EP 100 are introduced to the testing rig through purged holes at the bottom and top part of the gearbox. This operation ensures that the gearbox remains in the same misalignment condition and position.
- Later, a collection of data for varying conditions of oil viscosity namely EP 1000, EP 650, EP 320, and EP 100 is undertaken.
- Then all oil viscosity changes are contrasted.
- A typical testing speed variation cycle based on one load condition that was conducted at every testing run is illustrated in figure 8-4 below:

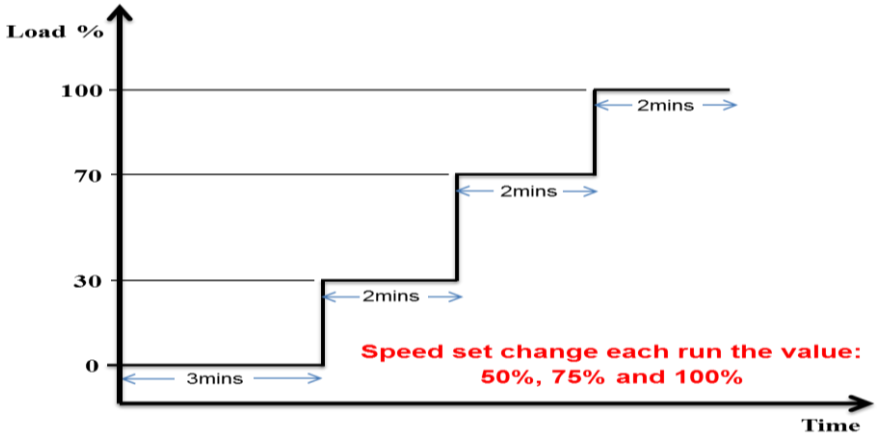

Figure 8-4 Typical test cycle (by Author)

Notably, the manufacturer of the gearbox proposes EP 320. The laboratory manufacture of EP 650 was achieved through combining 39% EP 100 with 61% EP 1000, whereas the gearbox recommended the manufacturer supplied the other types.

8.4 Results and Discussion

Seemingly, a collection of the vibration signals from practical gearbox experiment was undertaken while the gearbox rigs were running on four oil viscosity circumstances (EP

1000, EP 650, EP 320, and EP 100), three varying speeds of 100%, 75%, and 50%, and four varying loads.

8.4.1 Results of Viscosity Measurement

Measurements were taken for each oil type viscosity prior to testing. The rotary viscometer testing method formed the basis for measurement. From Figure 8-5 the presentation of the results is in the form of absolute dynamic viscosities within centipoises; in terms of SI units, this equals to Pas. Viscosity value differences are defined by clarity between the oils subjected to testing and as the increase in temperature occurs they decrease in size.

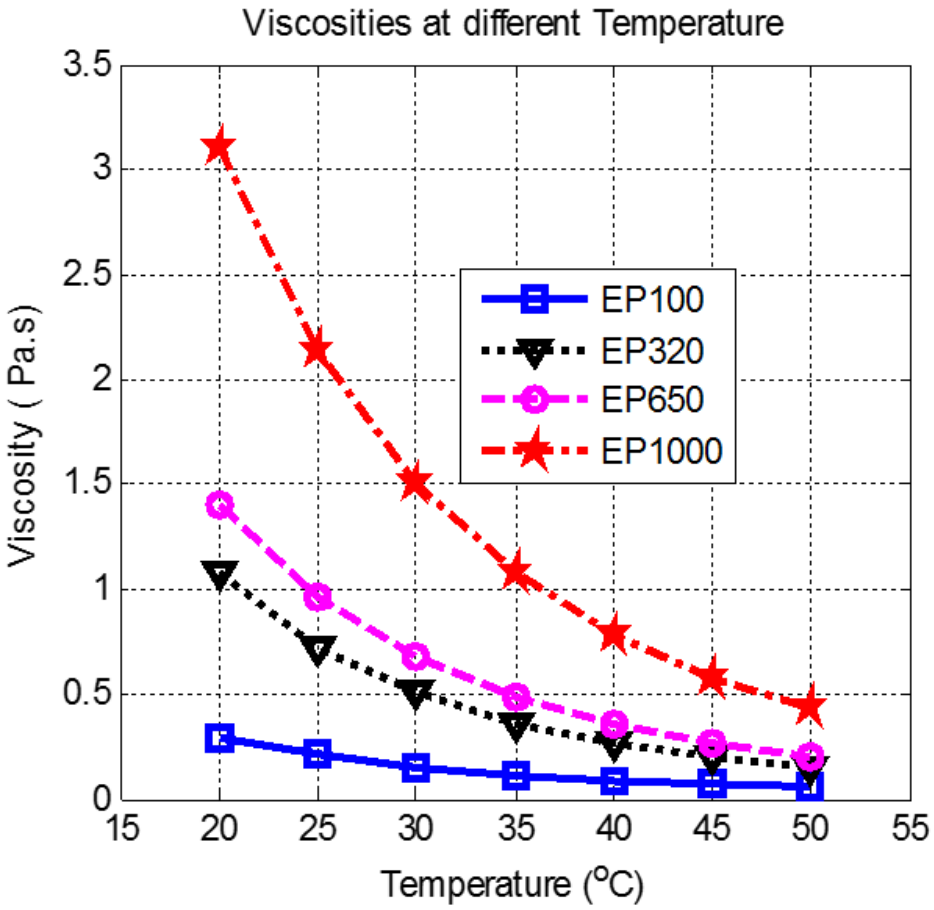

Figure 8-5 Tested oil viscosity values at varying temperatures

8.4.2 Effect of Temperature

Comparatively, it could be inferred that in Figure 8-6 (a) and (b) there is a gradual increase of GB2 and GB1 temperatures which attains stability by the third test after the system has become stable. Notably, temperature value differences between various lubricants within GB1 denote the lubricants' viscosity values. Besides, the same trends in temperature within GB2 indicate that consistency between varying tests existed, thus indicating that churning losses exceed the friction losses.

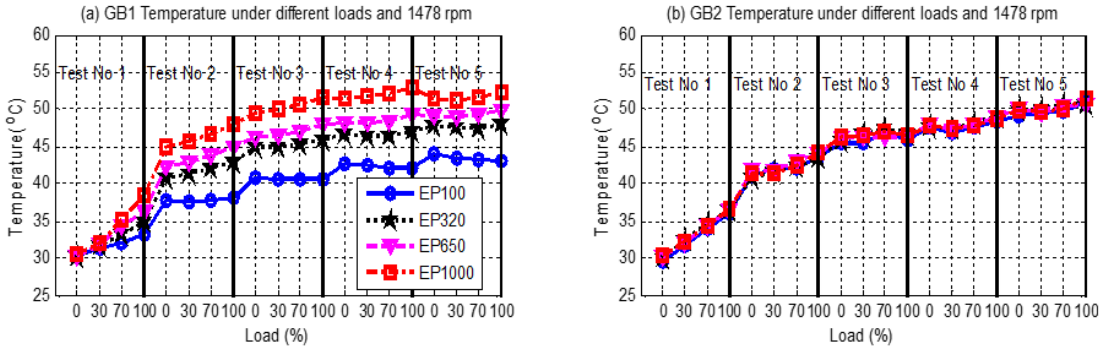

Figure 8-6 Temperature under varying viscosity and load in 5 operations

Speed has been averaged and tabulated under similar circumstances in the test. Figure 8-7 indicates similar properties in varying speeds, in the sense that the systems have stabilised from third testing runs. Additionally, Figure 8-7 indicates that altering the viscosity of oil did not have a significant effect on the speed of the system. Notably, drives compel the supply parameters of induction motors to retain stable speed.

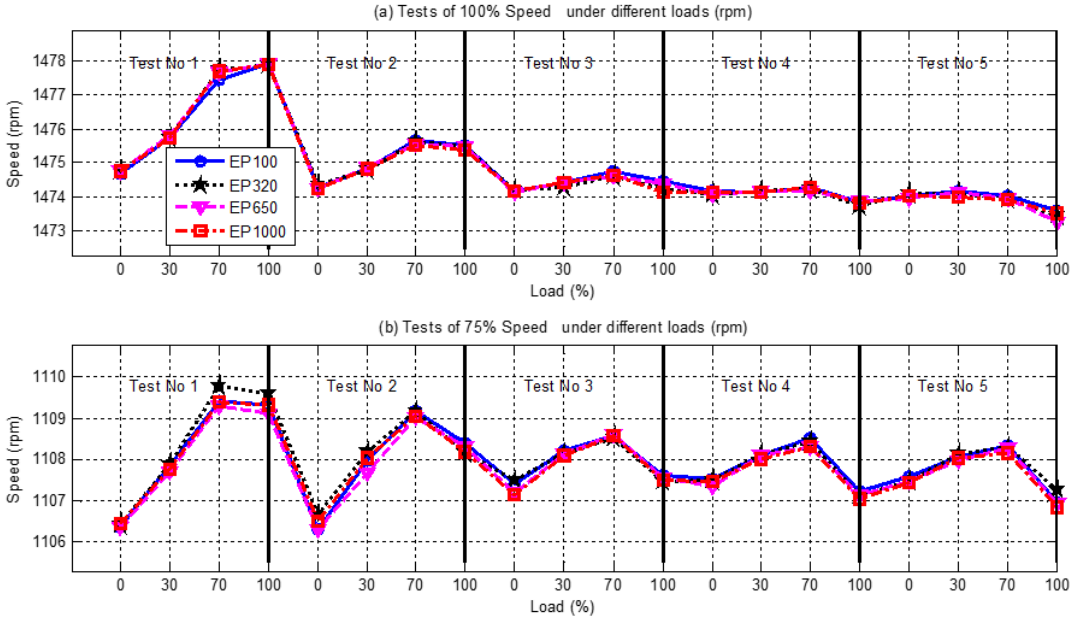

Figure 8-7 Speed comparison under different operating conditions

The negligible changes that occur when speeding will stabilise the temperatures across all scenarios. Furthermore, the speed signals have a significant effect on direct current and alternating current motors, that is, a significant correlation exists between temperature and the motor winding resistors. Therefore, this property might be utilised for accurate detection of viscosity faults.

8.4.3 Analysis through Vibration

Notably, lubricant properties have a significant effect on the gearbox. For instance, EP 100 that constitutes the lowest viscosity of oil indicates the highest levels of vibration under varying local circumstances and speed. It can be attributed to the notion that lower viscosity of oil results in a thinner thickness of the film and higher friction, thus causing greater levels of vibration. Seemingly, EP 320 produces the lowest vibrations; the company recommends the use of this viscosity. Besides, EP 100 viscosity has more vibration. Additionally, when an increase of the load occurs, vibration will escalate across all oil viscosities. Under this frequency, the highest vibration is recorded in EP 100 whereas the lowest vibration is experienced for EP 320. In contrast, the lowest values of vibration were reflected by EP 1000, thus showing the viscosities' damping effect. For

an explanation of this, Figures 8-8, and 8-9 illustrate that EP320 can be considered the most ideal viscosity for decreasing vibration

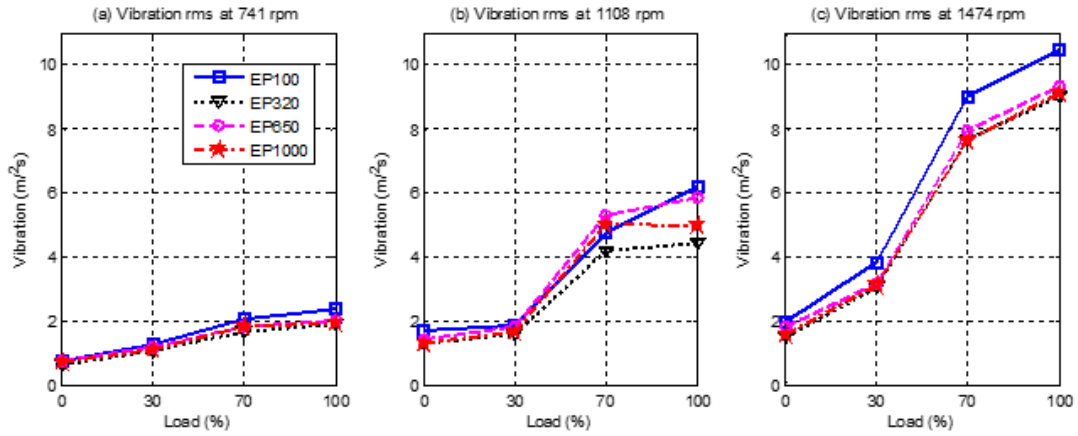

Figure 8-8 Vibration comparison in varying operating circumstances

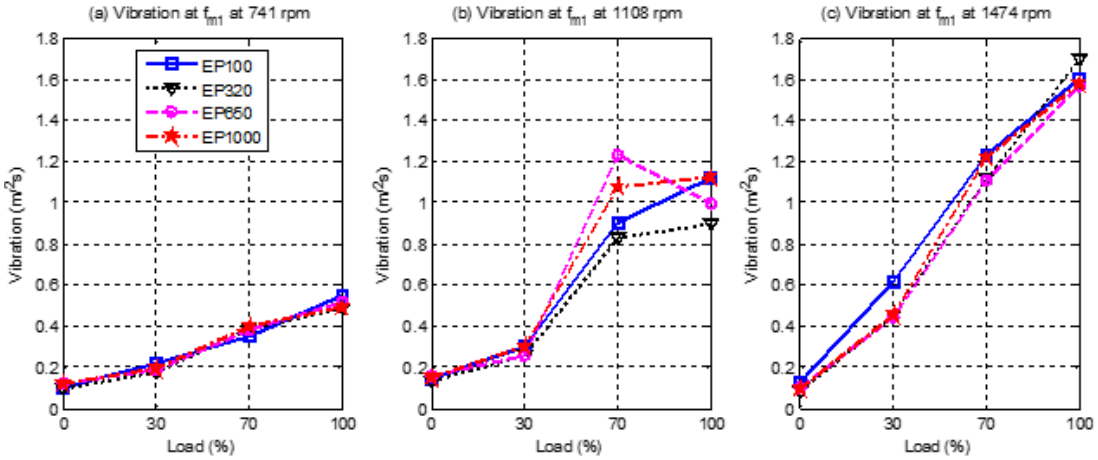

Figure 8-9 Vibration at f_{m1} comparison in varying circumstances of operation

8.4.4 Analysis using Electrical Signals

Figure 8-10 below indicates that viscosity changes influenced the drive's reaction that supplied the motors with additional voltage for torque expansion. The drive maintained reference speed and reacted accurately to changes in reference, thus maintaining the speed of the motor at required values. Test signal comparison at 100% speed for varying

loads at 5 operations is given. There was a decrease in voltage at 30% of load, and afterwards, it increased in the range of 70%-100% in all varying viscosities for each operation, this was attributed to the existence of the drive. Therefore, this property might be utilised to accurately locate viscosity fault.

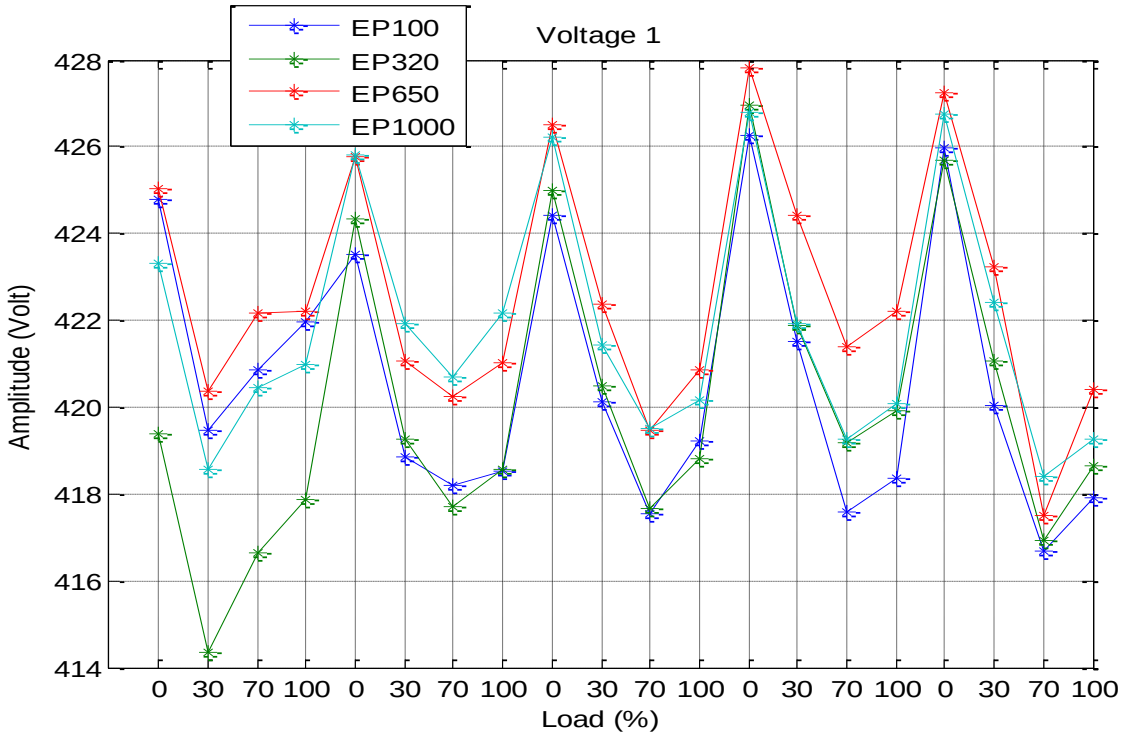

Figure 8-10 Voltage under varying viscosity, varying load in 5 operations at 100% speed

The statistical parameter of the RMS has been undertaken to investigate the form accurately. Figure 8-11 illustrates the current of load and viscosity change for 5 operations, which increase gradually with a load in all instances of viscosity change, under varying loads; however, a negligible variation exists but the variation is insufficient to be regarded as an indicator of fault for viscosity changes.

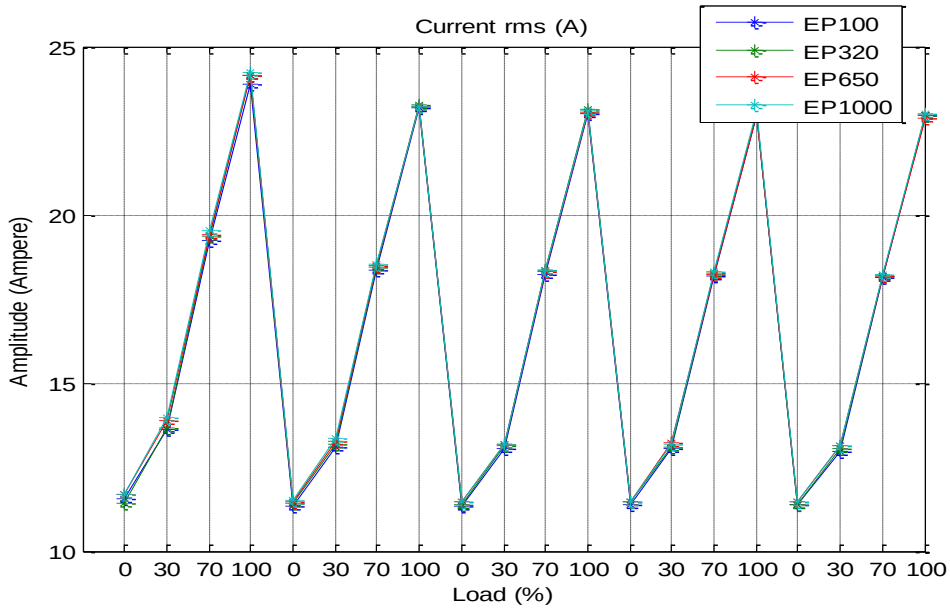

Figure 8-11 Varying viscosity, varying load, and current in 5 operations at 100% speed

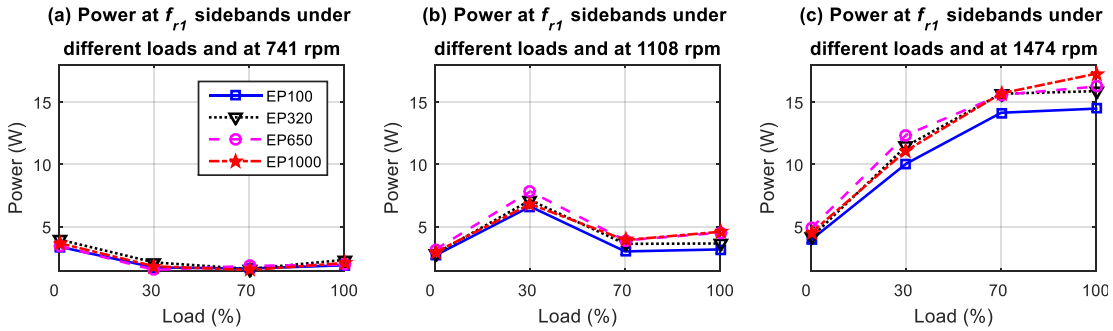

Figure 8-12 Power amplitudes at f_{r1} sidebands in varying load and speed

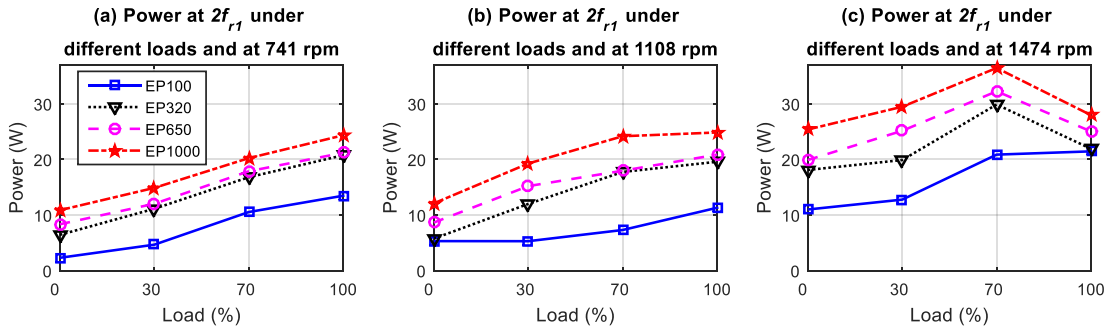

Figure 8-13 Comparison of power signal with varying oil viscosity

The inspection of the power spectrum was undertaken to determine the impact of viscosity change for identification and assessment of faults. Figure 8.12 illustrates the frequencies of properties associated with f_{r1}, and particularly shaft frequency sidebands ($f_s \pm f_{r1}$). Based on the illustration, sidebands at the specified frequency component lack clear viscosity changes. However, in Figure 8-13 the power signals at $2f_{r1}$ reveals clear oil viscosity changes, symbolising the possibility of employing them in diagnosis. Additionally, it shows that velocity has a significant impact, where increased velocity implies the circulation of additional mass with gears resulting in significant fluctuations. When gear parts oscillate, circulation of a huge amount of oil occurs with the movement of the gear and oil quantity created escalating with speed. The impact will reduce the level of oil within the reservoir of the gearbox and consequently reduce the effect of damping for the removed mass. Similarly, the mass created is largely dependent upon the properties of oil, especially density and viscosity. The efficient inertia moment could differ because the oscillating oil shape is not balanced because of the uneven mass and inherent eccentricity. It produces additional torsional rotations at the frequency of the shaft, thus modulating the power system's supply component. Nevertheless, the frequency components for the second and third shafts reveal indistinguishable viscosity changes.

8.5 Summary of Chapter 8

This chapter presented an analysis of the results on the use of traditional methods for fault detection, especially oil viscosity changes within gearboxes downstream the driving motor. A recap of the findings indicates that a correlation exists between supply signal and oil viscosity changes. The correlation is premised on frictional changes within the gearbox that in turn affects speed and torque. Additionally, the temperature will influence the viscosity of the oil. Notably, a correlation existed between oil viscosity change and the external measurements and control of the VSD. Furthermore, it controls the voltage for adjustment of tiny changes in load caused by temperature, vibration, and oil viscosity changes. The results indicate a clear variation between other cases and baseline in electrical signals. The signal of the voltage has higher sensitivity compared to that for

current, thus showing that VSD controls the voltage of adapting changes in load because of viscosity change, hence the instant changes in power. The result illustrates the effective nature of VSD voltage power signals to locate oil viscosity changes.

Chapter 9 Conclusions and Future Work

In this chapter, a summary of the achievements of this study is provided. The chapter also provides a description of the objectives as provided in the first chapter of the study. The summary is inclusive of the key conclusions and the author's contribution to this knowledge field. Additionally, the author also provides the conclusion of the study on motor condition monitoring using the MCSA and MVSA in sensorless mode operation. Finally, the study provides its recommendation for future work in this topic of study.

9.1 Review of Aim, Objectives and Achievements

Aim: The primary aim of this research was the detection and diagnosis of faults in ACIM using MCSA and MVSA of the AC induction motor under sensorless variable speed drive mode. Using these techniques, the objective of the study was met and the author was able to show that MCSA is a potential and suitable method for the detection and distinguishing of the most common electrical and mechanical faults in ACIM. The study objectives were attained by conducting an experimental study on ACIM in sensorless VSD operation. With different levels of severity, two different types of faults were used. For benchmarking and comparison purposes, the vibrational analysis was used in parallel with MCSA and MVSA.

In the paragraphs that follow, this study achievement of this research is aligned with the study objectives which were highlighted in Section 1.4.1 of the first chapter.

Objective 1: To perform a study and literature review of condition monitoring in rotating machinery as well as performing a literature review of theory and application of condition monitoring systems to electrical and mechanical machines using sensorless modes and identifying gaps in the knowledge.

Achievement 1: A thorough review of previous studies was conducted and included theoretical development and history in the field of study. A critical discussion of vital studies on the topic of the study is provided in Chapter 2. The importance of maintenance procedures and fault detection is also discussed. Conventional condition monitoring techniques of rotating machinery have been discussed in Chapter 2, as well as industrial applications of control systems and techniques used when the induction motor is controlled with sensorless VSDs. This review found a clear gap in the use of tools and data available from supply parameters under the sensorless mode for electrical and mechanical fault detection and diagnosis. It is determined the direction of this study is to address this issue and hopefully make a unique and significant theoretical contribution to knowledge.

Objective 2: To review the literature and explain the most common techniques utilised for condition monitoring of electrical and mechanical system under sensorless VSDs and speed control schemes, as well as describe the principles of ACIM and control systems, including field oriented control (FOC).

Achievement 2: A general literature review was carried out into the understanding of control systems in Chapter 2. A discussion is presented covering techniques used for control system based condition monitoring and details of induction motor condition monitoring is presented. The review is extended in Chapter 3 where the detailing of motors (ACIM) working principles are provided as well their construction; a discussion of theory and concepts of control systems is also provided in addition to describing ACIM under sensorless VSD. FOC was then presented after the discussion of the theories. An explanation of the principle of the sensorless drive is also provided. Lastly, how electrical and mechanical faults impact on supply parameters and the sensorless VSD response is also provided.

Objective 3: To describe the principles of motor faults, including electrical and mechanical faults and parameters under healthy and faulty conditions.

Achievement 3: The detail of electrical and mechanical faults in induction motors has been presented, including broken rotor bars, open-circuits in the windings of the stator, faults in the bearing of the motor, air-gap eccentricity, and shaft misalignment. A review is presented of electrical parameters under a healthy and faulty condition in an induction motor. Moreover, an explanation is given of the physical phenomena associated with faulty induction motors.

Objective 4: In this objective, experiments were designed and performed with the aim of testing the performance of a mechanical system, together with the control system under healthy conditions for different applied loads and speeds, to facilitate the setup characteristics and baseline evaluation.

Achievement 4: The developed test rig facility is detailed in Chapter 6. It was operated numerous times under different loads and speeds to confirm its reliability and ability to replicate data under sensorless mode. The test rig consists of the following parts, a 4 kW

1420 RPM three phase ACIM, a variable speed controller, coupling and links, and a DC generator (acted as a mechanical load). Four ACIM's were used and had the same specification and different health conditions. Therefore, the data was collected in an environment similar to that found in the industry and simulated the real-life application of induction motors. The motor function was monitored using several measuring devices in the test rig. Lastly, the motor test rig designs were shared to be used in other projects.

Objective 5: To allow the experiments to reproduce common mechanical and electrical faults with varying severities, under different load operating conditions and speed.

The ACIM faults were to include both mechanical and electrical under VSD such as shaft misalignment, and/or broken rotor bar and also to investigate the effects of gear lubrication oil viscosity.

Achievement 5: Two different common faults in induction motor were successfully tested which were broken rotor bar, shaft misalignment, and combinations of both. In another rig, lubrication oil with different viscosities was tested, more information is given on this in Chapter 8. Each fault was applied with different degrees of severity under different loads and speeds.

Objective 6: To analyse the influence of an external fault on the diagnosis of an internal fault, and perform successful data analysis to investigate the possibility of detecting the examined faults under a VSD system without requiring any more resources than normally needed when advanced and complex analysis is undertaken. Conventional spectrum analysis will be applied to the dynamic data.

Achievement 6: Spectrum analysis was conducted on the electrical supply signals including motor nameplate parameters such as power, current, and voltage. Others included the detection/analysis of vibration and broken rotor bars diagnosis and/or the misalignment of the shaft. These analyses were conducted with high accuracy but low cost. Results from the broken rotor bar and/or misalignment tests allowed a comparison between the detection performances of both current and voltage signals under sensorless operating control mode.

Objective 7: To develop mathematical models and simulations to better help understand the behaviour of the AC induction motor with sensorless VSD for healthy and faulty conditions, when operating under different speed and load conditions.

Achievement 7: Ready-to-use modules in the Matlab/Simulink software was used in the achievement of this objective. The modules were instrumental in characterising the various changes in electrical and dynamic properties of the motors due to various faults by helping in a measurement setup, selection of data processing and diagnosis rule and development. The response of the model is examined under different speeds and load oscillating amplitude conditions. The control system was first tuned to achieve stable and correct speed control. The results from the model were then compared to the rig data to verify that the model reasonably represented real motor operations. Results obtained from the model confirm that the broken rotor bar and/or shaft misalignment have important effects on the electrical supply parameters of the AC motor. These results from the model were then compared to the rig data to verify that the model reasonably represented real motor operations. The details of the model operation and verifications are presented in Chapter 5.

Objective 8: To perform an analysis of the response exhibited by sensorless VSD driven systems under varying fault conditions as well as perform an investigation on the capabilities of detecting and diagnosing faults under this mode of operation.

Achievement 8: In chapter 7, the response of the sensorless variable speed driven system under varying fault conditions was studied. Two main levels of degrees of fault were found for each of the two faults that were introduced into the system under test. These were shaft misalignment and/or broken rotor bar. A presentation of the abilities of voltage and current signals in the detection of each individual fault was made. For purposes of benchmarking and comparison, vibration signals were also obtained. It was found that induced faults under sensorless VSD driven systems can be detected using both current and voltage signal though, in some instances, the voltage has a greater potential for the diagnosis of faults as presented in the results.

Objective 9: To implement experiments to replicate common mechanical faults in the

gear transmission, based on different degrees of severities and under different operating conditions of speed and load.

Achievement 9: Oil with different viscosities and faults in the gear transmission system were tested: Each oil viscosity was used under different load and speed conditions. The results were investigated based on the feature frequencies found in their spectra; viscosity can be separated by dynamic feature for all the tested cases.

Objective 10: To provide suggestions and recommendations for further research in this area of study.

Achievement 10: Several suggestions for future research projects are provided as shown in section 9.4. These suggestions provide basic guidance on further studies on condition monitoring in ACIM using the techniques developed in this study.

9.2 Conclusions

A summary of the key findings is provided here based on the experiments that were described in the chapters above:

1): Broken rotor bars, shaft misalignments, change in gearbox lubricants, and combined broken rotor bar with shaft misalignment faults have been detected and diagnosed using power supply signals under VSD systems.

2): Under different operating conditions (speed and load), with different degrees of severities using sensorless mode, reliable information about the health and faulty condition of the system can be extracted from electrical supply parameters. Based on the analysis of electrical supply signals in the frequency, it has been attained the following conclusions:

3): Conclusions from the broken rotor bar results can be summarised as:

- Asymmetric sidebands at frequencies ($f_s \pm 2sf_s$) in the current and voltage spectrum show around the supply frequency in a power spectrum.
- The spectrums of stator current and voltage signatures show that the amplitude of sidebands increases with increasing level of BRB fault and load.

- The voltage spectrum displayed better results than current spectrum, which shows that, the VSD adjusted the voltage to changes in the speed in response to a change in load caused by fault.

4): Conclusions from the misalignment results can be summarised as:

- Additional friction is generated by shaft misalignment and this increases the static load of the system, increasing the required electrical power that is needed to overcome this.
- Misalignment faults can be detected on a sensorless drive, with spectral peaks at $f_s \pm f_r$ of shaft running speed, which MA detection can be extracted because these components consist of both rotational and lateral vibrations.
- Around the rotor frequency, the amplitude of the sidebands is shown to increase with the increase in the level of the load as well as with misalignment. This information is shown by the spectrums of stator current and voltage signatures.

5): Conclusions from broken rotor bar and misalignment results as:

- Evaluation outcomes demonstration that the combined faults lead to an additional rise in the sideband amplitude and this increase can be detected in both the current and voltage signals under the sensorless mode.
- The impact of misalignment faults on broken rotor bar detection and the diagnosis was small in high loads, but there is no effect in small loads when using the power supply spectrum.
- The impact of the broken rotor bar on the detection and diagnosis of shaft misalignment was small in high loads. Nevertheless there is no effect in small loads when using the power supply spectrum.

6): Conclusions from oil viscosity changes

- The degradation in the oil which causes a change in viscosity is shown to cause a change in static power consumption and the dynamic behaviour of the gearbox transmission system.

- ❖ Oil degradation also causes a change in the dynamic behaviour of the gear transmission system as it adversely affects the damping effects as well as increasing inertia moments of imbalance. These effects cause the rotating system to experience higher oscillations as demonstrated by the increasing sidebands around the frequency of the supply.
- ❖ The expected diagnostic performance was shown by the dynamic power characteristics. That is at all tested speed and load ranges, viscosities can be distinguished at the peak in the power spectrum at $2f_{r1.}$
- ❖ In comparison, less effective performance in detecting the changes in viscosity is shown by vibration signals than that of electrical and control parameters.

9.3 Contributions of this Research Project to Knowledge

This research project has contributed in its own way to this field of electrical signal analysis, particularly the analysis of electrical and vibration signals to facilitate accurate detection and diagnosis of both mechanical and electrical signals. It has provided new knowledge and understanding not found in any other study. The following are the key knowledge contribution areas:

Contribution 1:

To the best of the author's knowledge, the study work in this thesis is first to examine the impact on the motor current and motor voltage signal spectrum due to fluctuations in motor performance that take place when a fault happens in the rotor shaft and/or rotor bar.

Contribution 2:

New knowledge has been produced in relation to the development of a performance study based on fault detection and diagnosis under sensorless VSD with a broken rotor bar and mechanical shaft misalignment. The study includes dynamic data responses under different operating conditions of load and speed. Importantly, when using the spectrums of voltage and/or current signals it was shown that the presence of one fault (either MA or BRB) did not block the detection of the other (BRB or MA), nor was a diagnosis of

the level of severity of the fault impaired. The influence the diagnostic accuracy of misalignment on the diagnosis of BRB is as a result of the load and speed oscillation. However, the performance of the detection is lower due to drive compensation of oscillation and noise contamination

Contribution 3:

New use of dynamic data voltage and current, together with conventional MCSA and MVSA methods for detecting and diagnosing gear oil viscosity changes has been implemented. To the best of the author's knowledge, this approach has not been presented in prior research. The detection and diagnosis of changes in gear lubrication oil viscosity depend on consequent changes in the power supply. No research was found describing in any detail the potential of detecting and diagnosing gear oil viscosity changes using electrical power supply parameters under sensorless VSDs. There is a relationship between the change of oil viscosity and supply signals. This relation is due to the change of friction in the gearbox which will affect both torque and speed. Moreover, the oil viscosity will be influenced by temperature. The VSD control data and external measurements correlated with the change of oil viscosity.

9.4 Suggestions for Future Work

For thorough and successful monitoring of ACIM using MCSA, development of sophisticated techniques for the detection of various types of faults with different levels of severity is needed. In motors supplied through a VSD, this study has shown that electrical signals are suitable in fault detection and can therefore be relied upon to provide sufficient information for condition monitoring of induction motors. It is the ultimate desire of the authors that this study will provide enough simulation to readers to generate new ideas that will significantly contribute to the further development of technologies used in condition monitoring of machines. Additionally, there is a need for detailed analysis for initial faults detection and identification for ACIM under sensorless control mode operation. In line with this study's findings, the following recommendations for research will be important in enhancing condition monitoring of ACIM.

Recommendation 1:

There is a need for more experiments to be conducted on a number of ACIM to get an accurate image and information on the reliability, accuracy and sensitivity of the CM techniques employed in this study. Further experiments should also include other types of faults (both mechanical and electrical) with different levels of severity. These other faults may include the breakage of the tooth of a gear, gear pitting, and flexible coupling problems.

Recommendation 2:

This research should also be applied to other machinery with motor-driven systems such as diesel engines, compressors, and pumps.

Recommendation 3:

Effective performance in the detection of the faults can be provided by static data and electrical power supply parameters. Successful application of spectral analysis of dynamic data was done in this study, but there is a need for more advanced signal processing techniques which could provide more accurate and valuable information. These techniques may include the use of time-frequency analysis, modulation signal bispectrum, and/or wavelets. Furthermore, static data response from sensorless VSDs could be analysed using neural networks, fuzzy logic, and artificial intelligent systems.

Recommendation 4:

Further investigation of sensorless VSD under different fault conditions is needed, this will go a long way in helping in the assessment of the performance of current residuals in such conditions. It will also be interesting to deal with a combination of mechanical faults such as small amount of misalignment, gearbox faults, unbalance, and faulty couplings, this is because these faults produce a change in electrical current signals at the components of shaft frequency.

Recommendation 5:

The amplitude of lower sideband $fs\text{-}2sf_s$ is noticeably different than upper sideband $fs+2sf_s$. There may be a reason for this that might aid fault identification.

Schemes could be used to extract further valuable information; this may involve the use of different techniques which could be applied to analyse the static data response from sensorless VSDs. Additional experiments are recommended to investigate the sensorless VSD response to other types of faults.

References

1. Riera-Guasp, M., J.A. Antonino-Daviu, and G.-A. Capolino, *Advances in Electrical Machine, Power Electronic, and Drive Condition Monitoring and Fault Detection: State of the Art.* IEEE Trans. Industrial Electronics, 2015. **62**(3): p. 1746-1759.

2. Siddiqui, K.M., K. Sahay, and V. Giri, *Health monitoring and fault diagnosis in induction motor-a review.* International Journal of Advanced Research in Electrical, Electronics and Instrumentation Engineering, 2014. **3**(1): p. 6549-6565.

3. Siddique, A., G. Yadava, and B. Singh, *A review of stator fault monitoring techniques of induction motors.* IEEE transactions on energy conversion, 2005. **20**(1): p. 106-114.

4. Karmakar, S., et al., *Induction motor and faults*, in *Induction Motor Fault Diagnosis*. 2016, Springer. p. 7-28.

5. Iorgulescu, M. and R. Beloiu. *Faults diagnosis for electrical machines based on analysis of motor current*. in *Optimization of Electrical and Electronic Equipment (OPTIM), 2014 International Conference on*. 2014. IEEE.

6. Engineering, C.P.M., *Only 1% of an electric motor's lifecycle costs are spend on maintenance.* 2015.

7. Research, V.M., *Electric Motor Market Overview.* Global Electric Motor Market, 2015.

8. Huang, X., T.G. Habetler, and R.G. Harley, *Detection of rotor eccentricity faults in a closed-loop drive-connected induction motor using an artificial neural network.* IEEE Transactions on Power Electronics, 2007. **22**(4): p. 1552-1559.

9. Nandi, S., H.A. Toliyat, and X. Li, *Condition monitoring and fault diagnosis of electrical motors—A review.* IEEE transactions on energy conversion, 2005. **20**(4): p. 719-729.

10. Rao, B., *Handbook of condition monitoring*. 1996: Elsevier.

11. Marais, H.-J., G. van Schoor, and K.R. Uren, *An Energy-based approach to condition monitoring of industrial processes.* IFAC-PapersOnLine, 2015. **48**(21): p. 772-777.

12. Ahmad, R. and S. Kamaruddin, *An overview of time-based and condition-based maintenance in industrial application.* Computers & Industrial Engineering, 2012. **63**(1): p. 135-149.

13. Ilonen, J., et al., *Diagnosis tool for motor condition monitoring.* Industry Applications, IEEE Transactions on, 2005. **41**(4): p. 963-971.

14. Chaari, F., et al. *Advances in Condition Monitoring of Machinery in Non-Stationary Operations*. in *Proceedings of the Fourth International Conference on Condition Monitoring of Machinery in Non-Stationary Operations, Lyon, France*. 2014. Springer.

15. Mikami, H., et al., *Historical evolution of motor technology*. 2011. **60**(1): p. 39.

16. Alger, P.L. and R.J.P.o.t.I. Arnold, *The history of induction motors in America.* 1976. **64**(9): p. 1380-1383.

17. Bonnett, A.H. and T. Albers. *Squirrel cage rotor options for AC induction motors*. in *Pulp and Paper Industry Technical Conference, 2000. Conference Record of 2000 Annual*. 2000. IEEE.

18. Parekh, R., *AC Induction Motor Fundamentals.* Microchip Technology Inc, 2003.

19. Su, H., et al., *Induction Machine Condition Monitoring Using Neural Network Modeling.* IEEE Transactions on Industrial Electronics, 2007. **54**(1): p. 241-249.

20. Gao, Z., et al., *A Frequency Demodulation Approach to Induction Motor Speed Detection.* IEEE Transactions on Industry Applications, 2011. **46**(4): p. 1632-1642.

21. Tavner, P., L. Ran, and J. Penman, *Condition monitoring of rotating electrical machines*. Vol. 56. 2008: IET.

22. Vas, P., *Parameter estimation, condition monitoring, and diagnosis of electrical machines*. 1993: Oxford University Press.

23. Han, Y. and Y. Song, *Condition monitoring techniques for electrical equipment-a literature survey.* IEEE Transactions on Power delivery, 2003. **18**(1): p. 4-13.

24. Capolino, G.-A., J.A. Antonino-Daviu, and M. Riera-Guasp, *Modern diagnostics techniques for electrical machines, power electronics, and drives.* IEEE Transactions on Industrial Electronics, 2015. **62**(3): p. 1738-1745.

25. Seera, M., et al., *Condition monitoring of induction motors: A review and an application of an ensemble of hybrid intelligent models.* Expert Systems with Applications, 2014. **41**(10): p. 4891-4903.

26. Hughes, A. and B. Drury, *Electric motors and drives: fundamentals, types and applications*. 2013: Newnes.

27. Trigeassou, J.-C., *Electrical Machines Diagnosis*. 2013: John Wiley & Sons.

28. Abu Saad, S., *The Untilisation of Information Available in a Sensorless Control System of an AC Induction Motor for Condition Monitoring (Phd Thesis)*, in *Centre for Efficiency and Performance Engineering*. 2015, University of Huddersfield: University of Huddersfield p. 265.

29. Hou, Z., et al. *Rotor faults diagnosis in rotor field oriented controlled induction motors based on torque current*. in *Electrical Machines and Systems (ICEMS), 2014 17th International Conference on*. 2014. IEEE.

30. Patton, R. and J. Chen, *Observer-based fault detection and isolation: Robustness and applications.* Control Engineering Practice, 1997. **5**(5): p. 671-682.

31. Rgeai, M.N., *Helical gearbox fault detection using motor current signature analysis(Phd Thesis)*, in *Mechanical, Aerospace and Civil Engineering*. 2007, University of Manchester: School of Mechanical, Aerospace and Civil Engineering.

32. Lane, M., et al., *Investigation of reductions in motor efficiency and power factor caused by stator faults when operated from an inverter drive under open loop and sensorless vector modes.* Systems Science & Control Engineering, 2017. **5**(1): p. 361-379.

33. Hamad, N., et al. *An investigation of electrical motor parameters in a sensorless variable speed drive for machine fault diagnosis*. in *Automation and Computing (ICAC), 2016 22nd International Conference on*. 2016. IEEE.

34. Shaeboub, A., et al. *Detection and diagnosis of compound faults in induction motors using electric signals from variable speed drives*. in *Automation and Computing (ICAC), 2016 22nd International Conference on*. 2016. IEEE.

35. Fournier, E., et al., *Current-based detection of mechanical unbalance in an induction machine using spectral kurtosis with reference.* IEEE Transactions on Industrial Electronics, 2015. **62**(3): p. 1879-1887.

36. Moore, R., et al., *The Reliability-based maintenance strategy: a vision for improving industrial productivity*. 1993, CSI Industry Report No. AN-GM-00I-09.09. 93.

37. Abdusslam, S.A., *Detection and diagnosis of rolling element bearing faults using time encoded signal processing and recognition (PhD Thesis)*. 2012, University of Huddersfield.

38. Saleh, A., *Detection and Diagnosis of Electrical Faults in Induction Motors Using Instantaneous Phase Variation.(PhD Thesis)*, in *Mechanical Engineering*. 2005, University of Manchester: University of Manchester.

39. Grimmelius, H.T., et al., *Three state-of-the-art methods for condition monitoring.* IEEE Transactions on Industrial Electronics, 1999. **46**(2): p. 407-416.

40. Yang, S., et al., *Condition monitoring for device reliability in power electronic converters: A review.* IEEE Transactions on Power Electronics, 2010. **25**(11): p. 2734-2752.

41. Shaeboub, A., *The Monitoring of Induction Machines Using Electrical Signals from the Variable Speed Drive(PhD Thesis)*. 2018, University of Huddersfield.

42. Davies, A., *Handbook of Condition Monitoring: Techniques and Methodology*. 1997: Springer Netherlands.

43. Beebe, R.S., *Predictive maintenance of pumps using condition monitoring*. 2004, UK: Elsevier.

44. Mobley, R.K., *An introduction to predictive maintenance*. 2002: Butterworth-Heinemann.

45. Payne, B.S., *Condition monitoring of electric motors for improved asset management(PhD Thesis)*. 2003, University of Manchester: University of Manchester.

46. Toutountzakis, T. and D. Mba, *Observations of acoustic emission activity during gear defect diagnosis.* NDT & E International, 2003. **36**(7): p. 471-477.

47. Elmaleeh, M.A., N. Saad, and M. Awan. *Condition monitoring of industrial process plant using acoustic emission techniques*. in *Intelligent and Advanced Systems (ICIAS), 2010 International Conference on*. 2010. IEEE.

48. Tan, C.K. and D. Mba, *Limitation of acoustic emission for identifying seeded defects in gearboxes.* Journal of Nondestructive Evaluation, 2005. **24**(1): p. 11-28.

49. Sullivan, G., et al., *Operations & Maintenance Best Practices.* A guide to achieving operational efficiency, Release, 2004. **2**.

50. Nham, T.T. and R.M. Bombelka, *Determination of metals in lubricating oil by ICP-AES.* Varian-Instruments at work, ICP-2, 1991.

51. Kessissoglou, N.J. and Z. Peng, *Integrating vibration and oil analysis for machine condition monitoring.* Practicing Oil Analysis Magazine, 2003.

52. Rao, S., *Mechanical Vibrations 3rd Edition*. 1995: Addison-Wesley Publishing Company, Reading, MA.

53. Kia, S.H., H. Henao, and G.-A. Capolino, *Gear tooth surface damage fault detection using induction machine stator current space vector analysis.* IEEE Transactions on Industrial Electronics, 2015. **62**(3): p. 1866-1878.

54. Nandi, A., *Vibration based fault detection-features, classifiers and novelty detection.* Condition Monitoring and Diagnostic Engineering Management, COMADEM International, 2002.

55. Seera, M., et al., *Fault detection and diagnosis of induction motors using motor current signature analysis and a hybrid FMM–CART model.* IEEE transactions on neural networks and learning systems, 2012. **23**(1): p. 97-108.

56. Benbouzid, M.E.H., *A review of induction motors signature analysis as a medium for faults detection.* IEEE transactions on industrial electronics, 2000. **47**(5): p. 984-993.

57. Bellini, A., et al., *Advances in diagnostic techniques for induction machines.* IEEE Transactions on industrial electronics, 2008. **55**(12): p. 4109-4126.

58. Mehrjou, M.R., et al., *Rotor fault condition monitoring techniques for squirrel-cage induction machine—A review.* Mechanical Systems and Signal Processing, 2011. **25**(8): p. 2827-2848.

59. Thorsen, O. and M. Dalva, *Methods of condition monitoring and fault diagnosis for induction motors.* European transactions on electrical power, 1998. **8**(5): p. 383-395.

60. Gu, F., et al., *Electrical motor current signal analysis using a modified bispectrum for fault diagnosis of downstream mechanical equipment.* Mechanical Systems and Signal Processing, 2011. **25**(1): p. 360-372.

61. Alwodai, A., *Motor Fault Diagnosis Using Higher Order Statistical Analysis of Motor Power Supply Parameters (Phd Thesis)*, in *Centre for Efficiency and Performance Engineering*. 2015, University of Huddersfield: University of Huddersfield.

62. Gao, Z., C. Cecati, and S. Ding, *A Survey of Fault Diagnosis and Fault-Tolerant Techniques Part II: Fault Diagnosis with Knowledge-Based and Hybrid/Active Approaches.* 2015.

63. Ghorbanian, V. and J. Faiz, *A survey on time and frequency characteristics of induction motors with broken rotor bars in line-start and inverter-fed modes.* Mechanical Systems and Signal Processing, 2015. **54**: p. 427-456.

64. Cecati, C., *A survey of fault diagnosis and fault-tolerant techniques—part II: fault diagnosis with knowledge-based and hybrid/active approaches.* IEEE transactions on industrial electronics, 2015.

65. Gao, Z., C. Cecati, and S.X. Ding, *A survey of fault diagnosis and fault-tolerant techniques—Part I: Fault diagnosis with model-based and signal-based approaches.* IEEE Transactions on Industrial Electronics, 2015. **62**(6): p. 3757-3767.

66. Abusaad, S., et al., *The Detection of Shaft Misalignments Using Motor Current Signals from a Sensorless Variable Speed Drive*, in *Vibration Engineering and Technology of Machinery*. 2015, Springer. p. 173-182.

67. Kar, C. and A. Mohanty, *Monitoring gear vibrations through motor current signature analysis and wavelet transform.* Mechanical systems and signal processing, 2006. **20**(1): p. 158-187.

68. Benbouzid, M.E.H., M. Vieira, and C. Theys, *Induction motors' faults detection and localization using stator current advanced signal processing techniques.* Power Electronics, IEEE Transactions on, 1999. **14**(1): p. 14-22.

69. Haram, M., et al. *Electrical motor current signal analysis using a modulation signal bispectrum for the fault diagnosis of a gearbox downstream*. in *Journal of Physics: Conference Series*. 2012. IOP Publishing.

70. Kar, C. and A. Mohanty, *Multistage gearbox condition monitoring using motor current signature analysis and Kolmogorov–Smirnov test.* Journal of Sound and Vibration, 2006. **290**(1): p. 337-368.

71. Zhang, J., J. Dhupia, and C. Gajanayake, *Stator Current Analysis from Electrical Machines Using Resonance Residual Technique to Detect Faults in Planetary Gearboxes.* 2015.

72. Lane, M., et al., *Investigation of Motor Current Signature Analysis in Detecting Unbalanced Motor Windings of an Induction Motor with Sensorless Vector Control Drive*, in *Vibration Engineering and Technology of Machinery*. 2015, Springer. p. 801-810.

73. Benghozzi, A., et al., *The diagnosis of a gearbox transmission system using electrical control parameters*. 2012, IEEE.

74. Ben-Ghozzi, A.A., *Plant condition monitoring using the sensorless control data from an electrical motor drive (PhD Thesis)*, in *Centre for Efficiency and Performance Engineering*. 2016, University of Huddersfield.

75. Cunha, C.C.M., et al. *Detection of rotor faults in torque controlled induction motor drives*. IEEE.

76. Bellini, A., et al., *Closed-loop control impact on the diagnosis of induction motors faults.* Industry Applications, IEEE Transactions on, 2000. **36**(5): p. 1318-1329.

77. Kim, K., A.G. Parlos, and R. Mohan Bharadwaj, *Sensorless fault diagnosis of induction motors.* IEEE Transactions on Industrial Electronics, 2003. **50**(5): p. 1038-1051.

78. Kołodziejek, P. and E. Bogalecka, *Broken rotor bar impact on sensorless control of induction machine.* COMPEL - The International Journal for Computation and Mathematics in Electrical and Electronic Engineering, 2009. **28**(3): p. 540-555.

79. Kołodziejek, P. and E. Bogalecka, *Broken rotor symptoms in the sensorless control of induction machine.* COMPEL: The International Journal for Computation and Mathematics in Electrical and Electronic Engineering, 2012. **31**(1): p. 237-247.

80. Ochoa, S.D. and M. Pacas. *Rotor asymmetries detection in induction motors driven by a sensorless field oriented control*. IEEE.

81. Kral, C., et al., *Sequences of field-oriented control for the detection of faulty rotor bars in induction machines-the Vienna Monitoring Method.* IEEE Transactions on Industrial Electronics, 2000. **47**(5): p. 1042-1050.

82. Cruz, S. and A. Cardoso. *Fault indicators for the diagnosis of rotor faults in FOC induction motor drives*. in *Electric Machines & Drives Conference, 2007. IEMDC'07. IEEE International*. 2007. IEEE.

83. Lane, M., *Using AC Motor as a Transducer for Detecting Electrical and Electromechanical Faults.* MRes Thesis, University of Huddersfield, 2011.

84. Toliyat, H.A. and G.B. Kliman, *Handbook of electric motors*. Vol. 120. 2004: CRC press.

85. Polka, D., *Motors and Drives: A Practical Technology Guide*. 2003: ISA.

86. Hughes, A., *Electric motors and drives: fundamentals, types and applications*. 2006, Oxford: Newnes / Elsevier.

87. A. E. Fitzgerald, et al., *Electric Machinery.* London: McGraw-Hill Education - Europe, 2003.

88. Theodore, W., *Electrical machines, drives and power systems, 6/E*. 2007: Pearson Education India.

89. Machines, E., *Drives, and Power Systems.* Autor: Theodore Wildi, 2006.

90. Fitzgerald, A.E., et al., *Electric machinery*. Vol. 5. 2003: McGraw-Hill New York.

91. Instruments, T., *Implementation of a speed field orientated control of three phase AC induction motor using TMS320F240.* BPRA076, 1998. **4**: p. 40-46.

92. Seibel, B., T. Rowan, and R. Kerkman. *Field oriented control of an induction machine with DC link and load disturbance rejection*. in *Applied Power Electronics Conference and Exposition, 1996. APEC'96. Conference Proceedings 1996., Eleventh Annual*. 1996. IEEE.

93. Bunte, A., H. Grotstollen, and P. Krafka. *Field weakening of induction motors in a very wide region with regard to parameter uncertainties*. in *Power Electronics Specialists Conference, 1996. PESC'96 Record., 27th Annual IEEE*. 1996. IEEE.

94. Yu, Z. and D. Figoli, *AC Induction Motor control using constant V/Hz principle and Space Vector PWM technique with TMS320C240.* Texas Instruments: Houston, TX, 1998.

95. Anand, A., *Newnes Electrical Power Engineer's Handbook umar Control Systems.* 2 ed. 2007, New Delhi.: PHI Learning Private Limited.

96. Bose, B.K., *Power electronics and variable frequency drives: technology and applications*. 1997, Piscataway, NJ: IEEE Press.

97. Drury, B., *The Control Techniques Drives and Controls Handbook, Second Edition*. 2009: The Institution of Engineering and Technology.

98. Muñoz, O.D., *Design Strategy for a 3-Phase Variable Frequency Drive (VFD).* 2011.

99. Saidur, R., et al., *Applications of variable speed drive (VSD) in electrical motors energy savings.* Renewable and Sustainable Energy Reviews, 2012. **16**(1): p. 543-550.

100. Buja, G.S. and M.P. Kazmierkowski, *Direct torque control of PWM inverter-fed AC motors-a survey.* IEEE Transactions on industrial electronics, 2004. **51**(4): p. 744-757.

101. Crowder, R., *Electric Drives and Electromechanical Systems: Applications and Control*. 2006: Newnes.

102. Menaa, M., et al. *Vector control of induction motor by a spiral vector theory*.

103. Abu-Rub, H., A. Iqbal, and J. Guzinski, *High performance control of AC drives with MATLAB/Simulink models*. 2012, Chichester: Wiley.

104. Ma, Z. and S. Wang, *Online fault detection and robust control of condenser cooling water systems in building central chiller plants(PhD Thises).* Energy and buildings, 2011. **43**(1): p. 153-165.

105. Smart, E., *Detecting abnormalities in aircraft flight data and ranking their impact on the flight(PhD Thises)*, in *Institute of Industrial Research*. 2011, University of Portsmouth: University of Portsmouth.

106. Ahmed, A.H.O., *Speed Sensorless Vector Control of Induction Motors Using Rotor Flux based Model Reference Adaptive System.* SUST Journal of Engineering and Computer Science (JECS), 2015. **16**(3).

107. Jeong, I.-W., W.-S. Choi, and K.-H. Park, *Sensorless Vector Control of Induction Motors for Wind Energy Applications Using MRAS and ASO.* Journal of Electrical Engineering & Technology, 2014. **9**(3): p. 873-881.

108. Paladugu, A. and B.H. Chowdhury, *Sensorless control of inverter-fed induction motor drives.* Electric Power Systems Research, 2007. **77**(5): p. 619-629.

109. Ravi Teja, A., et al., *A new model reference adaptive controller for four quadrant vector controlled induction motor drives.* Industrial Electronics, IEEE Transactions on, 2012. **59**(10): p. 3757-3767.

110. Gadoue, S.M., D. Giaouris, and J.W. Finch, *Sensorless control of induction motor drives at very low and zero speeds using neural network flux observers.* Industrial Electronics, IEEE Transactions on, 2009. **56**(8): p. 3029-3039.

111. Harnefors, L. and M. Hinkkanen, *Complete stability of reduced-order and full-order observers for sensorless IM drives.* Industrial Electronics, IEEE Transactions on, 2008. **55**(3): p. 1319-1329.

112. Demenko, A., P. Kolodziejek, and E. Bogalecka, *Broken rotor bar impact on sensorless control of induction machine.* COMPEL-The international journal for computation and mathematics in electrical and electronic engineering, 2009. **28**(3): p. 540-555.

113. Hajian, M., et al., *Adaptive nonlinear direct torque control of sensorless IM drives with efficiency optimization.* Industrial Electronics, IEEE Transactions on, 2010. **57**(3): p. 975-985.

114. Kliman, G.B., et al., *Sensorless, online motor diagnostics.* Computer Applications in Power, IEEE, 1997. **10**(2): p. 39-43.

115. Siddiqui, K.M. and V. Giri. *Broken rotor bar fault detection in induction motors using wavelet transform*. in *Computing, Electronics and Electrical Technologies (ICCEET), 2012 International Conference on*. 2012. IEEE.

116. Bonnett, A.H. and G.C. Soukup, *Analysis of rotor failures in squirrel-cage induction motors.* IEEE Transactions on Industry Applications, 1988. **24**(6): p. 1124-1130.

117. Didier, G., H. Razik, and A. Rezzoug. *On the experiment detection of incipient rotor fault of an induction motor*. in *Electric Machines and Drives Conference, 2003. IEMDC'03. IEEE International*. 2003. IEEE.

118. Liu, Z., et al. *On-line squirrel cage induction motors' rotor mixed fault diagnosis approach based on spectrum analysis of instantaneous power*. in *Intelligent Control and Automation, 2004. WCICA 2004. Fifth World Congress on*. 2004. IEEE.

119. Oumaamar, M., et al. *Neutral voltage analysis for broken rotor bars detection in induction motors using Hilbert transform phase*. in *Industry Applications Conference, 2007. 42nd IAS Annual Meeting. Conference Record of the 2007 IEEE*. 2007. IEEE.

120. Wu, L., T.G. Habetler, and R.G. Harley. *A review of separating mechanical load effects from rotor faults detection in induction motors*. in *Diagnostics for Electric Machines, Power Electronics and Drives, 2007. SDEMPED 2007. IEEE International Symposium on*. 2007. IEEE.

121. Supangat, R., et al. *Detection of broken rotor bar faults and effects of loading in induction motors during rundown*. in *Electric Machines & Drives Conference, 2007. IEMDC'07. IEEE International*. 2007. IEEE.

122. Hu, N.Q., et al., *A novel transform demodulation algorithm for motor incipient fault detection.* IEEE Transactions on Instrumentation and measurement, 2011. **60**(2): p. 480-487.

123. Ozelgin, I., *Analysis of magnetic flux density for airgap eccentricity and bearing faults.* International Journal of Systems Applications, Engineering & Development, 2008. **2**(4): p. 162-169.

124. Vitek, O., et al. *Detection of eccentricity and bearings fault using stray flux monitoring*. in *Diagnostics for Electric Machines, Power Electronics & Drives (SDEMPED), 2011 IEEE International Symposium on*. 2011. IEEE.

125. Morinigo-Sotelo, D., et al., *Practical aspects of mixed-eccentricity detection in PWM voltage-source-inverter-fed induction motors.* IEEE Transactions on Industrial Electronics, 2010. **57**(1): p. 252-262.

126. Hong, J., et al., *Offline monitoring of airgap eccentricity for inverter-fed induction motors based on the differential inductance.* IEEE Transactions on Industry Applications, 2013. **49**(6): p. 2533-2542.

127. Liu, W., J. Han, and J. Jiang, *A novel ball bearing fault diagnosis approach based on auto term window method.* Measurement, 2013. **46**(10): p. 4032-4037.

128. Schoen, R.R., et al., *Motor bearing damage detection using stator current monitoring.* IEEE transactions on industry applications, 1995. **31**(6): p. 1274-1279.

129. Alwodai, A., et al., *A study of motor bearing fault diagnosis using modulation signal bispectrum analysis of motor current signals.* Journal of Signal and Information Processing, 2013. **4**(03): p. 72.

130. Thomson, W.T. *On-line MCSA to diagnose shorted turns in low voltage stator windings of 3-phase induction motors prior to failure*. in *Electric Machines and Drives Conference, 2001. IEMDC 2001. IEEE International*. 2001. IEEE.

131. Cusidó, J., et al., *Signal injection as a fault detection technique.* Sensors, 2011. **11**(3): p. 3356-3380.

132. Alwodai, A., et al. *Inter-turn short circuit detection based on modulation signal bispectrum analysis of motor current signals*. in *Automation and Computing (ICAC), 2013 19th International Conference on*. 2013. IEEE.

133. Moghe, S. and A. Mahure, *Study of Vibration Response of Coupling under Misalignment Condition-A Review.*

134. Arebi, L., F. Gu, and A. Ball. *A comparative study of misalignment detection using a novel Wireless Sensor with conventional Wired Sensors*. in *Journal of Physics: Conference Series*. 2012. IOP Publishing.

135. Kumar, C., G. Krishnan, and S. Sarangi. *Experimental investigation on misalignment fault detection in induction motors using current and vibration signature analysis*. in *Futuristic Trends on Computational Analysis and Knowledge Management (ABLAZE), 2015 International Conference on*. 2015. IEEE.

136. Patel, T.H. and A.K. Darpe, *Experimental investigations on vibration response of misaligned rotors.* Mechanical Systems and Signal Processing, 2009. **23**(7): p. 2236-2252.

137. Nagrani, S., S. Pathan, and I. Bhoraniya, *Misalignment fault diagnosis in rotating machinery through the signal processing technique-signature analysis.* Int J Adv Eng Res Stud E-ISSN, 2012: p. 2249-8974.

138. Jalan, A.K. and A. Mohanty, *Model based fault diagnosis of a rotor–bearing system for misalignment and unbalance under steady-state condition.* Journal of Sound and Vibration, 2009. **327**(3): p. 604-622.

139. Wongsuwan, T., et al. *Motor misalignment detection based on hidden markov model*. in *Communications and Information Technologies, 2006. ISCIT'06. International Symposium on*. 2006. IEEE.

140. Blodt, M., et al. *Detection of mechanical load faults in induction motors at variable speed using stator current time-frequency analysis*. in *Diagnostics for Electric Machines, Power Electronics and Drives, 2005. SDEMPED 2005. 5th IEEE International Symposium on*. 2005. IEEE.

141. Obaid, R.R., T.G. Habetler, and R.M. Tallam. *Detecting load unbalance and shaft misalignment using stator current in inverter-driven induction motors*. in *Electric Machines and Drives Conference, 2003. IEMDC'03. IEEE International*. 2003. IEEE.

142. Bin Hasan, M., *Current based condition monitoring of electromechanical systems. Model-free drive system current monitoring: faults detection and diagnosis through statistical features extraction and support vector machines classification (PhD Thesis)*. 2013, University of Bradford.

143. Bossio, J.M., G.R. Bossio, and C.H. De Angelo. *Angular misalignment in induction motors with flexible coupling*. in *Industrial Electronics, 2009. IECON'09. 35th Annual Conference of IEEE*. 2009. IEEE.

144. Prabhakar, S., A. Sekhar, and A. Mohanty, *Vibration analysis of a misaligned rotor—coupling—bearing system passing through the critical speed.* Proceedings of the Institution of Mechanical Engineers, Part C: Journal of Mechanical Engineering Science, 2001. **215**(12): p. 1417-1428.

145. Abusaad, S., et al., *Utilizing Data from a Sensorless AC Variable Speed Drive for Detecting Mechanical Misalignments.* Key Engineering Materials, 2013. **569**(569): p. 465-472.

146. Tang, Z. and S. Li, *A review of recent developments of friction modifiers for liquid lubricants (2007–present).* Current opinion in solid state and materials science, 2014. **18**(3): p. 119-139.

147. Abusaad, S., et al., *Investigating the Effect of Water Contamination on Gearbox Lubrication based upon Motor Control Data from a Sensorless Drive.* 2014.

148. Krause, P., et al., *Analysis of electric machinery and drive systems*. Vol. 75. 2013: John Wiley & Sons.

149. Hou, Z., et al. *A current product signal analysis method for rotor fault diagnosis in induction motors*. in *Diagnostics for Electrical Machines, Power Electronics and Drives (SDEMPED), 2015 IEEE 10th International Symposium on*. 2015. IEEE.

150. Gu, F., et al. *Motor current signal analysis using a modified bispectrum for machine fault diagnosis*. in *ICCAS-SICE, 2009*. 2009. IEEE.

151. Arebi, L., et al. *Misalignment detection using a wireless sensor mounted on a rotating shaft*. 2011. COMADEM.

152. Kia, S.H., H. Henao, and G.-A. Capolino, *Gear tooth surface damage fault detection using induction machine stator current space vector analysis.* Industrial Electronics, IEEE Transactions on, 2015. **62**(3): p. 1866-1878.

153. Gu, F., et al., *A new method of accurate broken rotor bar diagnosis based on modulation signal bispectrum analysis of motor current signals.* Mechanical Systems and Signal Processing, 2015. **50**: p. 400-413.

154. Ong, C.-M.-M.O., *Dynamic simulation of electric machinery using Matlab/Simulink*. 1998: Prentice-Hall PTR.

155. Ong, C.-M., *Dynamic simulation of electric machinery: using MATLAB/SIMULINK*. Vol. 5. 1998: Prentice Hall PTR Upper Saddle River, NJ.

156. Wieczorek, M. and E. Rosolowski. *Modelling of induction motor for simulation of internal faults*. in *Modern Electric Power Systems (MEPS), 2010 Proceedings of the International Symposium*. 2010. IEEE.

157. Slemon, G.R., *Modelling of induction machines for electric drives.* Industry Applications, IEEE Transactions on, 1989. **25**(6): p. 1126-1131.

158. Thomsen, J.S. and C. Kallesoe. *Stator fault modeling in induction motors*. in *Power Electronics, Electrical Drives, Automation and Motion, 2006. SPEEDAM 2006. International Symposium on*. 2006. IEEE.

159. Matlab, *Simpower Systems User's guide.* 2015a.

160. Giri, F., *AC electric motors control: Advanced design techniques and applications*. 2013: John Wiley & Sons.

161. Abu-Rub, H., A. Iqbal, and J. Guzinski, *High Performance Control of AC Drives with Matlab -Simulink Models*. 2012: John Wiley & Sons Ltd.

162. Vas, P., *Vector control of AC machines*. Vol. 22. 1990: Oxford University Press, USA.

163. Francois, B., P. Degobert, and J.P. Hautier, *Vector Control of Induction Machines: Desensitisation and Optimisation Through Fuzzy Logic*. 2012: Springer Science & Business Media.

164. Krause, P.C., *Analysis of electric machinery*. 1986: McGraw-Hill Book Company. 564.

165. Ozpineci, B. and L.M. Tolbert. *Simulink implementation of induction machine model-a modular approach*. in *Electric Machines and Drives Conference, 2003. IEMDC'03. IEEE International*. 2003. Ieee.

166. Quang, N.P. and J.-A. Dittrich, *Vector control of three-phase AC machines: system development in the practice*. 2008: Springer Science & Business Media.

167. Le-Huy, H. *Comparison of field-oriented control and direct torque control for induction motor drives*. in *Industry Applications Conference, 1999. Thirty-Fourth IAS Annual Meeting. Conference Record of the 1999 IEEE*. 1999. IEEE.

168. Krause, P.C., et al., *Analysis of electric machinery and drive systems*. Vol. 75. 2013: John Wiley & Sons.

169. Chen, S. and R. Živanović, *Modelling and simulation of stator and rotor fault conditions in induction machines for testing fault diagnostic techniques.* European Transactions on Electrical Power, 2010. **20**(5): p. 611-629.

170. Li, M. and L. He, *The dynamics of a parallel-misaligned and unbalanced rotor system under the action of non-linear oil film forces.* Proceedings of the Institution of Mechanical Engineers, Part C: Journal of Mechanical Engineering Science, 2010. **224**(9): p. 1875-1889.

171. Zhu, J., *Online industrial lubrication oil health condition monitoring, diagnosis and prognostics(PhD Thises)*, in *Industrial Engineering and Operations Research*. 2013, University of Illinois at Chicago.

172. Perera, P.A.B.A., *Effect of lubricating oil characteristics on gear vibrations.* 1986.

173. Johnsen, E.E. and H.P. Rønningsen, *Viscosity of 'live'water-in-crude-oil emulsions: experimental work and validation of correlations.* Journal of Petroleum Science and Engineering, 2003. **38**(1): p. 23-36.

174. Jakoby, B. and M.J. Vellekoop, *Physical sensors for water-in-oil emulsions.* Sensors and Actuators A: Physical, 2004. **110**(1): p. 28-32.

175. Mehta, N.S., N.J. Parekh, and R.K. Dayatar, *Improve the thermal efficiency of gearbox using different type of gear oils.* International Journal of Engineering and Advanced Technology (IJEAT), ISSN, 2013: p. 2249-8958.

176. Michaelis, K., B.-R. Höhn, and M. Hinterstoißer, *Influence factors on gearbox power loss.* Industrial lubrication and tribology, 2011. **63**(1): p. 46-55.

177. Höhn, B.-R. and K. Michaelis, *Influence of oil temperature on gear failures.* Tribology International, 2004. **37**(2): p. 103-109.

178. Sheng, S. and P.S. Veers, *Wind Turbine Drivetrain Condition Monitoring, an Overview*. 2011: National Renewable Energy Laboratory Golden, Colo, USA.

179. de Almeida, R.G. and L.R. Padovese. *Characterization of oil viscosity alterations in a gearbox through vibration signal analysis*. in *17th International Congress of Mechanical Engineering (COBEM2003)*. 2003.

180. Gonçalves, D.E., et al., *Torque loss in a gearbox lubricated with wind turbine gear oils.* Lubrication Science, 2013. **25**(4): p. 297-311.

181. Gorla, C., et al., *CFD simulations of splash losses of a gearbox.* Advances in Tribology, 2012. **2012**.

182. Agoston, A., C. Ötsch, and B. Jakoby, *Viscosity sensors for engine oil condition monitoring—Application and interpretation of results.* Sensors and Actuators A: Physical, 2005. **121**(2): p. 327-332.

183. Abusaad, S., et al. *The detection of lubricating oil viscosity changes in gearbox transmission systems driven by sensorless variable speed drives using electrical supply parameters*. in *Journal of Physics: Conference Series*. 2015. IOP Publishing.

184. Martins, R., et al., *Friction coefficient in FZG gears lubricated with industrial gear oils: biodegradable ester vs. mineral oil.* Tribology international, 2006. **39**(6): p. 512-521.